THE EFFECTS OF HEAT TREATMENT ON MICROSTRUCTURE, HARDNESS AND FATIGUE BEHAVIOR OF (AMS5659) 15-5 PRECIPITATION HARDENABLE STAINLESS STEEL

A THESIS SUBMITTED TO
THE GRADUATE SCHOOL OF NATURAL AND APPLIED SCIENCES
OF
MIDDLE EAST TECHNICAL UNIVERSITY

BY

ŞAHİN GÖREN

IN PARTIAL FULFILLMENT OF THE REQUIREMENTS
FOR
THE DEGREE OF MASTER OF SCIENCE
IN
METALLURGICAL AND MATERIALS ENGINEERING

OCTOBER 2018

Approval of the thesis:

THE EFFECTS OF HEAT TREATMENT ON MICROSTRUCTURE, HARDNESS AND FATIGUE BEHAVIOR OF (AMS5659) 15-5 PRECIPITATION HARDENABLE STAINLESS STEEL

submitted by **ŞAHİN GÖREN** in partial fulfillment of the requirements for the degree of **Master of Science in Metallurgical and Materials Engineering Department, Middle East Technical University** by,

Prof. Dr. Halil Kalıpçılar
Dean, Graduate School of **Natural and Applied Sciences** _____

Prof. Dr. C. Hakan Gür
Head of Department, **Metallurgical and Materials Eng.** _____

Prof. Dr. Rıza Gürbüz
Supervisor, **Metallurgical and Materials Eng. Dept., METU** _____

Examining Committee Members:

Prof. Dr. Bilgehan Ögel
Metallurgical and Materials Engineering Dept., METU _____

Prof. Dr. Rıza Gürbüz
Metallurgical and Materials Engineering Dept., METU _____

Prof. Dr. C. Hakan Gür
Metallurgical and Materials Engineering Dept., METU _____

Assist. Prof. Dr. Mert Efe
Metallurgical and Materials Engineering Dept., METU _____

Assist. Prof. Dr. Kazım Tur
Metallurgical and Materials Engineering Dept., Atılım Uni. _____

Date: 09.10.2018

I hereby declare that all information in this document has been obtained and presented in accordance with academic rules and ethical conduct. I also declare that, as required by these rules and conduct, I have fully cited and referenced all material and results that are not original to this work.

Name, Last name: Şahin Gören

Signature :

ABSTRACT

THE EFFECTS OF HEAT TREATMENT ON MICROSTRUCTURE, HARDNESS AND FATIGUE BEHAVIOR OF (AMS5659) 15-5 PRECIPITATION HARDENABLE STAINLESS STEEL

Gören, Şahin
M.Sc., Department of Metallurgical and Materials Engineering
Supervisor: Prof. Dr. Rıza Gürbüz

October 2018, 123 pages

In this study, effects of heat treatment parameters on microstructure, hardness and fatigue behavior of 15-5 precipitation hardenable stainless steels have been examined. Heat treatments have been conducted in three different steps homogenization, solutionizing and aging treatment at different temperatures and times. Microstructural analysis in terms of grain size and chemical composition analysis have been performed by optical and scanning electron microscope (SEM). Then, hardness measurements were applied for all heat treated specimens. Fatigue tests have been conducted at negative stress ratio (R) equal to -1 under constant amplitude cyclic loading for selected group of heat treated specimens. Fatigue test results have been evaluated according to AGARD-AG-292 and ISO 12107 standards in order to see the effect of heat treatment parameters on fatigue limit of the 15-5 precipitation hardenable stainless steels. Fatigue limit was determined as stress level at 10^7 cycles on stress vs. cycle (S-N) curve. It was also calculated by using staircase method in order to verify the fatigue limit that was found as stress level at 10^7 cycles on S-N curve. Higher hardness and fatigue limit were achieved for aging treatment at 480^0C for 1h and 400^0C for 70h compared to aging treatment at 550^0C for 4h. The measurements and test results show that by changing heat treatment parameters,

hardness and fatigue limit of 15-5 precipitation hardenable stainless steel can be increased.

Keywords: Precipitation Hardenable (PH) Stainless Steels, Heat Treatment, Hardness, Microstructure, Fatigue, S-N Curves.

ÖZ

ISIL İŞLEMİN (AMS5659) 15-5 ÇÖKELİMLİ SERTLEŞEBİLİR PASLANMAZ ÇELIK ALAŞIMININ MİKROYAPI, SERTLİK VE YORULMA DAVRANIŞI ÜZERİNDEKİ ETKİSİNİN İNCELENMESİ

Gören, Şahin
Yüksek Lisans, Metalurji ve Malzeme Mühendisliği Bölümü
Tez Yöneticisi: Prof. Dr. Rıza Gürbüz

Ekim 2018, 123 sayfa

Bu çalışmada, ısıl işlem parametrelerinin 15-5 çökelimli sertleştirilebilir paslanmaz çelik alışımının mikroyapı, sertlik ve yorulma davranışı üzerindeki etkileri incelenmiştir. Isıl işlem homojenleştirme, çözündürme ve yaşlandırma olarak üç faklı aşamada farklı sıcaklık değerlerinde ve farklı sürelerde uygulanmıştır. Mikroyapı analizi, tane boyutu ve kimyasal bileşim, optik ve taramalı elektron mikroskobu kullanılarak gerçekleştirildi. Sonrasında, ısıl işlem görmüş tüm numuneler için sertlik ölçümü alındı. Yorulma testleri sabit genlikli çevrimsel yük altında, negatif gerilme oranı R=-1'de ısıl işlem görmüş numunelerden seçilen grup için uygulandı. Yorulma testi sonuçları, ısıl işlem parametrelerinin 15-5 çökelimli sertleştirilebilir paslanmaz çelik alaşımının yorulma limiti üzerindeki etkisini görmek için AGARD-AG-292 ve ISO 12107 standartlarına göre değerlendirilmiştir. Yorulma limiti değeri gerilme-çevrim (S-N) eğrisi üzerindeki 10^7 çevrim değerine karşılık gelen gerilme olarak belirlenmiştir. Yorulma limiti değeri, gerilme-çevrim (S-N) eğrisi üzerinde buluanan gerilme değerini doğrulamak amacıyla merdiven yöntemi kullanılarak da hesaplanmıştır. 480^0C'de 1 saat ve 400^0C'de 70 saat olarak uygulanan yaşlandırma işlemlerinde 550^0C'de 4 saat uygulanan yaşlandırma işlemine kıyasla daha yüksek sertlik ve yorulma mukavemetine ulaşıldı. Ölçümler ve test sonuçları, ısıl işlem

parametreleri değiştirilerek, 15-5 çökelimli sertleştirilebilir paslanmaz çeliklerin sertlik ve yorulma davranışlarının arttırılabildiğini göstermektedir.

Anahtar Kelimeler: Çökelimli sertleşebilir paslanmaz çelikler, Isıl işlem, Mikroyapı, Sertlik, Yorulma, Gerilme- Çevrim Eğrisi.

To My Precious Parents

ACKNOWLEDGEMENTS

I wish to express my sincere thanks to my advisor Prof. Dr. Rıza Gürbüz for his great support, encouragement and guidance throughout the whole time on this study.

I am deeply thankful to deliver thankfulness to Turkish Aerospace Industry (TAI) for great support and permission to perform tests in its premises and equipment.

I am deeply thankful to heat treatment laboratory technician Yusuf Yıldırım for his infinite support and patience.

I wish to express my sincere thanks to Alp Aykut Kibar for his great support and patience for Scanning Electron Microscope (SEM) analyses.

My special thanks reserve to Mr. Ömer Duman, Mr. Mustafa Yavuz and Mr. Mesut Talha Güven for their great support on specimen manufacturing.

Finally, I would like to express my indebtedness to my parents to present me exceptional life and unrequited love.

TABLE OF CONTENTS

LIST OF TABLES

TABLES

LIST OF FIGURES

FIGURES

CHAPTER 1

INTRODUCTION

Steels are important structural materials that are widely used in areas such as automotive, construction, transportation, energy, defense and many other for long years. Thanks to its wide usage areas, many researchers have been focused on steel structures. In the previous, classical types of steels that is not carrying significant load in structural applications are manufactured. In the succeeding years, many contemporary structures of steels are manufactured that bring out high mechanical properties and long-life usage with low cost requirements for steel manufacturing industries. As a result; the steel improvement studies take substantial part of materials science and engineering. Mechanical properties of steels are basically modified by change in composition and heat treatments steps during or after manufacturing. Today, there exist a wide range of steels which allows safety and improved mechanical properties for various application and design.

During World War II, the need for high strength, corrosion resistant steels with reasonable production cost, that would provide significant mechanical properties especially fatigue strength at moderately elevated temperatures lead to development of precipitation hardenable stainless steels. These alloys were firstly introduced in 1946. [1] In the following twenty years, a number of stainless steels, which are hardened by precipitation reaction, have been used in manufacturing of high performance aircrafts, missiles and other military structures. Since the mechanical

properties of precipitation hardenable stainless steels are affected by heat treatment during manufacturing, determination of heat treatment parameters according to desired mechanical properties has been important issue and research areas. When the usage areas of precipitation hardenable stainless steels are considered, failure of these steels has been becoming another important research topic. Since the failure of critical components of aircrafts and some other military structures may cause catastrophic damages, thus life time prediction becomes quite important both in terms of users and system.

The fatigue life determination of a component is quite critical, in 1988 the Aloha B737 and in 2006 the Los Angeles B767 accidents are some memorable disasters caused by fatigue failure of a components. Over the last few decades, many scientists and companies focus on steel and fatigue studies in order to eliminate these disastrous failures.

Figure 1 Queen Liliuokalani, Aloha Airlines' Boeing 737-297 N73711, at Kahalui Airport (OGG), Maui, Hawaii, following the accident on April 28, 1988.[2]

1.1. MOTIVATION

Selection of suitable materials for aircraft structure is quite critical due to mechanical property requirements. Since most of the aircraft component is subjected to cyclic loading case, fatigue performance of aircraft material are becomes one of the

important requirements for aircraft industry. Fatigue failures often occur suddenly that may cause disastrous results for a system. Fatigue failures show brittle failure characteristics even in ductile materials. Therefore, there is almost never plastic deformation occurs prior to fracture. Fatigue failures comprise the initiation of some microcracks and propagation of these cracks up to final fracture.

AMS5659 15-5 precipitation hardenable stainless steel is one of the important structural materials for aircraft structure. The fatigue properties of these steels can be improved by the changing of heat treatment cycle during manufacturing. By changing heat treatment parameters mechanical properties of the steels may be improved as a result of some changes in microstructure. It is used in aircraft parts such as landing gear, some engine fitting parts and actuator parts for modern fighter aircrafts.

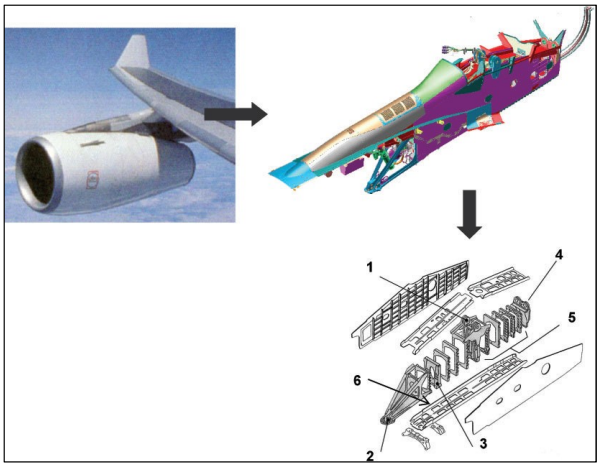

Figure 2 Components with AMS5659 15-5 PH stainless steels 1: out fit rib; 2: engine front suspension; 3: rib; 4: engine back suspension; 5: plain ribs; 6: lower spar.[3]

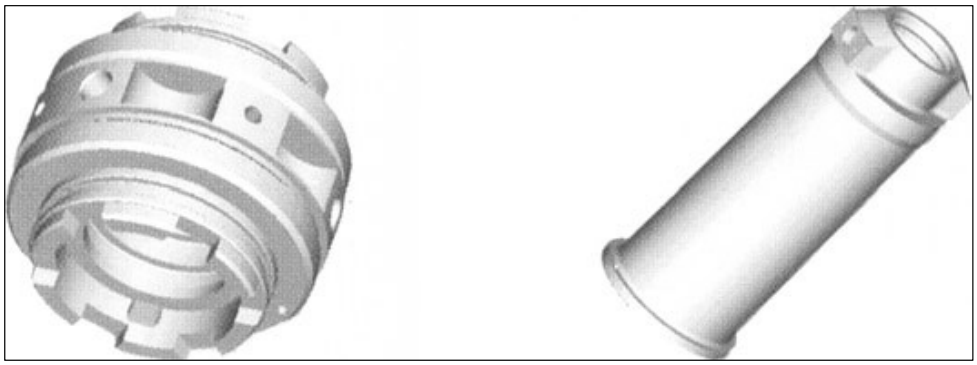

Figure 3 Actuator system components for an Indian aircraft.[4]

The aircraft industry requests determination and improving of the fatigue behavior of AMS5659 15-5 precipitation hardenable stainless steels by the application of different heat treatment cycles.

1.2. AIM OF THE WORK AND MAIN CONTRIBUTION

The scope of this study is to investigate the mechanical properties of the AMS5659 15-5 precipitation hardenable stainless steels and analyze the effect of heat treatment parameters on microstructure, hardness, tensile and fatigue strength. In order to achieve this, AMS5659 15-5 steel specimens were heat treated with different temperature and time periods during heat treatment cycles. Hardness tests were conducted by hardness testing machine. Tensile tests were carried out by using universal electro-mechanic tensile test machine. In addition, fatigue tests were conducted by servo-hydraulic and resonant fatigue testing machine in order to see effects of heat treatment parameters on these properties.

Changing heat treatments parameters, the hardness, tensile strength and fatigue strength of AMS5659 15-5 precipitation hardenable stainless steels can be increased positively. Thus, life of aircraft components can be improved under static and fatigue loading in service conditions.

CHAPTER 2

THEORETICAL BACKGROUND

2.1. PRECIPITATION HARDENABLE STAINLESS STEELS

Precipitation hardening stainless steels use nickel and chromium as major alloying elements and show combination both properties of martensitic and austenitic types of stainless steels. They have ability to gain high strength by application of heat treatment and very high resistance against corrosion like austenitic stainless steels. In precipitation hardening stainless steel, high strength can be achieved by heat treatment process which provides observation of precipitation reaction in martensitic or austenitic matrix. Hardening is achieved by the elements Copper, Aluminum, Titanium, Niobium, and Molybdenum which are included in the chemical composition of the precipitation hardening stainless steel.

Moreover, they have very high resistance against crack propagation, good transverse properties and high resistance to stress-corrosion cracking in marine environments. Fabrication of 15-5 PH stainless steels is easy. Therefore, it is economical and suitable to replace low alloy carbon steels. Aging treatment for 15-5 PH stainless steels is similar to other types of precipitation hardening stainlessness which includes aging treatment at low temperature with a single step. During aging treatment, ε-copper precipitates are formed in the form of spherical shape and coherent with the lath martensite matrix and principally provide strengthening in this alloy. The orientation relationship is found to be Kurdjumov–Sachs (K–S), which is common in fcc–bcc systems [4].

The advantage of precipitation hardening steels is that they can be supplied in solution treated condition, which is ready for aging treatment. Strength of these steels can be increased by the application of a single aging treatment at low temperature. This is known as aging treatment or age-hardening. In addition, there is not occurring any size distortion for these steels during aging treatment that makes application of the heat treatment easy.

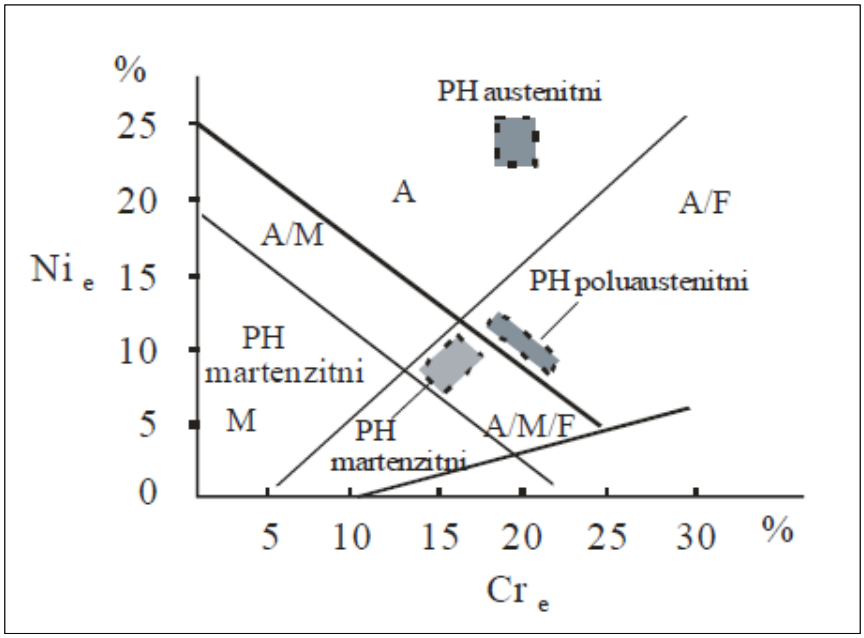

Figure 4 Position of PH steels in the Schaeffler-Delong's diagram. [5]

2.1.1. CLASSIFICATION OF PH STAINLESS STEELS

A wide range of engineering properties can be achieved by variations of heat treatment parameters during manufacturing of precipitation hardenable stainless steels. Presently, there exist three types of precipitation hardenable stainless steels. All types of these steels are essentially austenitic at their normal annealing temperatures. Precipitation hardenable stainless steels are grouped as austenitic, semi-austenitic and martensitic types. The currently available precipitation hardenable stainless steels with chemical compositions are listed in Table 1.

Table 1 Precipitation hardenable stainless steels. [1]

Alloy Type and Designation	Originator	Chemical Composition, percent[a] C	Cr	Ni	Cu	Al	Ti	Mo	Co	Cb + Ta	Si	Mn	Other
Martensitic													
17-4PH	Armco	0.07 max	15.5-17.5	3-5	3-5					0.15-0.45	1 max	1 max	
15-5PH	Armco	0.07 max	14.0-15.5	3.5-5.5	2.5-4.5					0.15-0.45	1 max	1 max	
PH13-8Mo	Armco	0.06 max	12.0-13.5	7-9		0.80-1.20		1.75-2.50			0.50 max	0.50 max	
AM362	Allegheny	0.03	14.5	6.5			0.80				0.20	0.30	
AM363	Allegheny	0.04	11.5	4.25			0.50				0.15	0.20	
Custom 455	Carpenter	0.03 max	11-13	7-10	1-3		0.90-1.40			0.25-0.50	0.50 max	0.50 max	B, 0.005 max
AFC-77	Crucible	0.15	14.5					5	13.5				V, 0.5
Semiaustenitic													
17-7PH	Armco	0.09 max	16-18	6.50-7.75		0.75-1.50					1 max	1 max	
PH15-7Mo	Armco	0.09 max	14-16	6.50-7.75		0.75-1.50		2-3			1 max	1 max	
PH14-8Mo	Armco	0.05 max	13.5-15.5	7.5-9.5		0.75-1.50		2-3			1 max	1 max	
AM350	Allegheny	0.08	16.50	4.30				2.75			0.25	0.80	N, 0.10
AM355	Allegheny	0.13	15.50	4.30				2.75			0.25	0.95	N, 0.10
Austenitic													
A286	Allegheny	0.08 max	13.5-16	24-27		0.35 max	1.9-2.3	1.0-1.75			0.4-1.0	1-2	B, 0.003-0.01 V, 0.1-0.5

(a) Composition of castings may be altered slightly from nominal.

2.1.1.1. AUSTENITIC PH STAINLESS STEELS

Austenitic precipitation hardening steels keep their austenitic structure after annealing and hardening as a result of aging treatment. Precipitation hardening phase is soluble at the annealing temperature of 1095 to 1120°C. It remains in solution during rapid cooling. When the steels are reheated to 650 to 760°C, precipitation reaction occurs in the matrix phase. Thus, hardness and strength of the material may be increased.

As it is shown in table 1, the alloy A-286 is a typical example of austenitic precipitation hardenable stainless steels. These alloys show lower mechanical properties in room-temperature conditions, Moreover; their yield strength is around 690 MPa and retains a large proportion of this yield strength up to temperature as high as 700°C.

2.1.1.2. SEMI-AUSTENITIC PH STAINLESS STEELS

Unlike martensitic types of precipitation hardening stainless steels, annealed semi-austenitic precipitation hardening steels are soft enough to be cold worked. Semi-austenitic steels retain their austenitic structure at room temperature. These steels can form martensitic structure at very low temperatures.

During solution treatment, alloy is heated to a high enough temperature in order to remove carbon atoms from solid solution and provide formation of precipitates as chromium carbide ($Cr_{23}C_6$) for semi-austenitic alloys. These reaction causes decrease in chromium content in austenite matrix. Therefore, austenite matrix becomes unstable and during cooling it transforms to martensite phase. If the solutionizing is done at higher temperature (955^{o}C) few types of carbide may be precipitated. Final stage is precipitation hardening, which is carried out in the range of 480 to 650^{o}C. During this step, aluminum in the martensite combines with the some of the nickel in the matrix phase to form intermetallic precipitates of NiAl and Ni_3Al.

As it is shown in table 1, the semi-austenitic precipitation hardenable stainless steels are 17-7 PH, PH 15-7 Mo, PH 14-8 Mo, AM 350 and AM 355. These alloys are manufactured primarily as sheet since the austenitic structure obtained during annealing provides superior formability. The transformation to martensite prior to precipitation hardening may be accomplished by some mechanical or thermal processes. Yield strength for these steels is over 1380 MPa. These steels keep their mechanical properties up to temperature 480°C.

2.1.1.3. MARTENSITIC PH STAINLESS STEELS

Martensitic precipitation hardening stainless steels have a predominantly austenitic structure at annealing temperatures around 1040 to 1065°C. Upon cooling to room temperature, microstructure changes from the austenite to lath type of martensite phase. As it is shown in Table 1, the martensitic precipitation hardenable stainless steels are 17-4 PH, 15-5 PH, PH 13-8 Mo, AM 362, AM 363, AFC- 77 and Custom 455. These materials are used as bar or forged condition, although some types of these PH stainless steels are available as castings or sheet and plate form. Hardening is achieved by a single low aging treatment. This treatment provides yield strength from 1170 to 1370 MPa. These steels can be used up to temperature as high as 480°C without losing mechanical properties.

These steels are generally used in the aircraft industry. The basic usage areas for these steels are blading, bolts, nozzles, pins, landing assemblies, and ribs and

stringers which are manufactured from the martensitic precipitation hardenable stainless steels.

15-5 PH stainless steel is the one of the important martensitic precipitation hardenable stainless steel containing approximately 3-4 wt % pct Copper (Cu) and that provide main strengthening as a result of precipitation reaction in the martensite matrix. After solution heat-treatment, this alloy is generally hardened by seven standard heat treatment cycles.

2.2. HEAT TREATMENT OF PH STAINLESS STEELS

In this section general ınformation about heat treatment of PH stainless steels are given. Following section includes the information for heat treating process of the (AMS5659) 15-5 PH stainless steels, which is studied in this thesis, in detail.

Basic composition of the stainless steels is composed of elements iron, carbon and chromium. Precipitation hardenable stainless steels include significant amount of other elements in chemical composition, in order to reach a wide range of mechanical properties and formability. Each of these elements in stainless steels have two important functions, one at high temperature and the other one is during cooling from high temperature which are determining microstructures and phases.

There exist two crystallographic arrangements for stainless steels at elevated temperatures that are ferrite, a body- centered cubic (BCC) crystal structure, and austenite, a face- centered cubic (FCC) crystal structure. Each of the elements in chemical compositions helps the formation of one or other of these crystal structures. The elements chromium (Cr), molybdenum (Mo), silicon (Si), aluminum (Al), titanium (Ti), vanadium (V) and phosphorous (P) provide formation of ferrite with BCC structure. The elements, which provide austenite with FCC structure, are iron (Fe), carbon (C), nickel (Ni), manganese (Mn) copper (Cu) and cobalt (Co). The relative proportion of these elements in the composition determines crystal structure of the stainless steels at elevated temperature. In general, steels with ferritic structure at elevated temperature retain its crystal structure during cooling and non-heat treatable. However, austenitic steels at high temperature may keep its crystal

structure or may transform to martensitic, a body centered tetragonal (BCT) structure that have higher strength during cooling.

There exist two symbols, M_S and M_F, used to indicate temperatures at which transformation from austenite to martensite takes place. In austenitic steels, all of the elements other than aluminum and cobalt tend to lower M_S and M_F temperatures. The solubility of the alloying element in the austenite increases by increasing temperature. This makes possible to control the M_S and M_F temperatures for stainless steels for intermediate alloying elements content. The effect of the alloying element content on the M_S and M_F transformation temperatures can be seen in Figure 5.

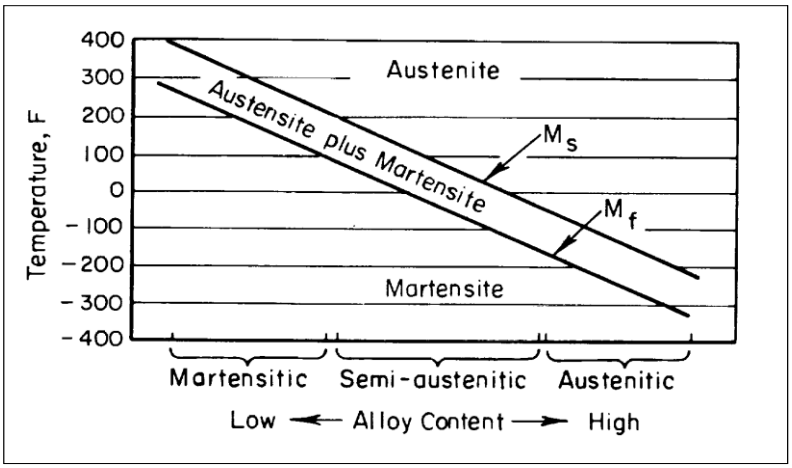

Figure 5 Effect of alloy contents on transformation temperatures of precipitation hardenable stainless steels. [1]

There exist three important steps for heat treatment cycle of precipitation hardenable stainless steels. The first step is solution treatment. In this step, steels are exposed to high temperature in order to dissolve all alloying elements to reach supersaturated solid solution at high temperature. Temperature and time values for this step may be determined according to chemical composition of steels and desired mechanical properties. The second step of heat treating cycle is formation of a supersaturated solid solution as a result of very rapid cooling or quenching. Since solubility of most elements at room temperature is lower than at elevated temperature, supersaturated solid solution is formed at room temperature.

The last and the most important step to reach desired mechanical properties is precipitation hardening or aging treatment. The primary requirement of an alloy for precipitation hardening is that the solubility of an element B in the phase A decreases with decreasing temperature. At room temperature precipitation reaction does not take place since rate of diffusion is almost zero. However, elevated temperature provides easy atomic immigration thus some intermetallics and precipitates are formed by alloying elements.

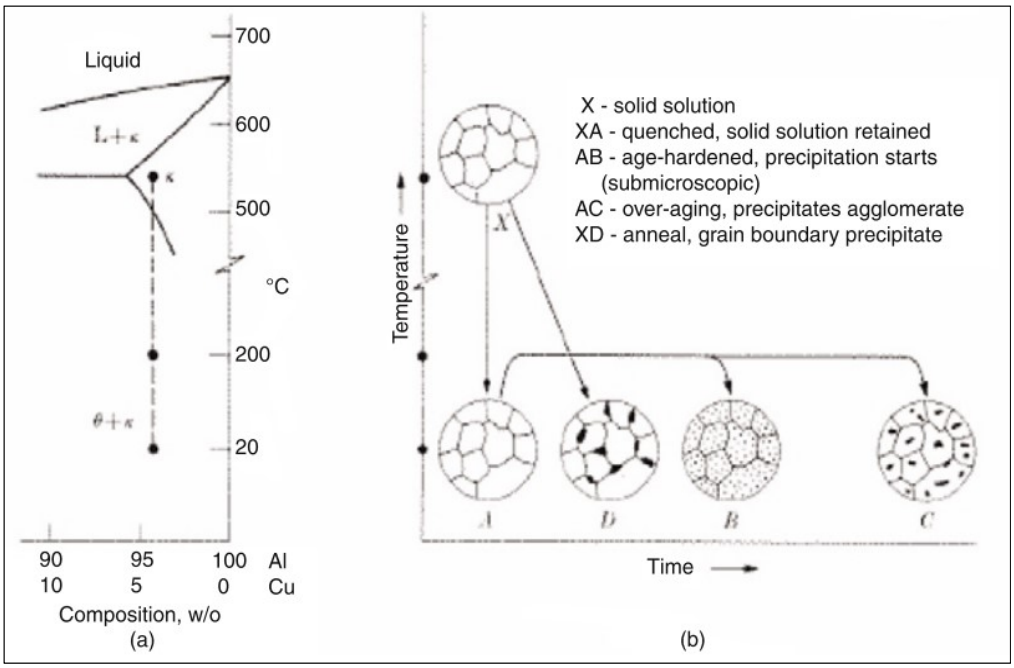

Figure 6 Precipitation hardening sequence. [6]

Initially, formed sub-microscopic precipitates are observed along the crystallographic planes of the matrix phase. Due to difference in lattice dimension between the matrix phase and precipitates, some straining is created in the matrix. Strengthening of precipitation hardenable stainless steels is defined development of this straining in the matrix phase as a result of precipitation reaction.

Size and distribution of these precipitates can be controlled by changing the aging temperature and time periods. Most effective strengthening can be reached by small and uniformly distributed precipitates. When temperatures is increased to intermediate range, the precipitate particles become larger and are not so effective so

maximum hardening is usually achieved in shorter time. At high temperature in precipitation range, precipitates may also grow to even larger size that cause shearing between precipitates and matrix phase. This condition cause reliving of the strain in the matrix phase and called overaged.

2.2.1. HEAT TREATMENT OF (AMS5659) 15-5 PH STAINLESS STEEL

Mechanical properties of (AMS5659) 15-5 PH stainless steels are reached basically by two mechanisms during heat treatment. The first one is transformation of austenite to martensite phase by cooling from solution treatment (annealing) temperature. The second one is precipitation of the hardening elements during aging treatment. At annealing temperature, 15-5 PH stainless steels have composed of mainly austenitic structure with some dissolved alloying elements in chemical composition.

There exist three most critical factors in thermal processing of 15-5 PH stainless steels which are solution treatment temperature, cooling conditions and temperature for precipitation hardening reactions.

2.2.1.1. SOLUTION TREATMENT OF 15-5 PH STAINLESS STEEL

The solution treatment temperature is selected to reach the optimum combination of austenite composition for martensitic transformation and solubility of hardening elements. Higher or lower annealing temperature may affect the mechanical properties and microstructure of the 15-5 PH stainless steels. Lower annealing temperature may cause decrease in both yield and ultimate tensile strength for 15-5 PH stainless steels when the material is aged. The reason for decrease in strength can be explained by lesser amount of hardening elements that goes into solution thus; softer martensite is formed. Higher annealing temperature causes increase in ultimate strength but decrease in yield strength for 15-5 PH stainless steels. At higher solution treatment temperature, amount of alloying elements in solution will be more that causes less transformation during cooling. As a result of this, there may be more retained austenite which decreases the yield strength. When the yield strength is

exceeded by deformation process, austenite phase may transform to stronger martensitic phase that provides higher ultimate tensile strength.

2.2.1.2. COOLING AND TRANSFORMATION FOR 15-5 PH STAINLESS STEEL

15-5 PH stainless steels are cooled continuously from their solution treatment temperature to room temperature. This cooling provides formation of supersaturated solid solution since solubility of alloying elements becomes less at room temperature condition. Moreover, transformation of austenite to martensite phase may cause increase in volume, so cooling rate should be controlled in order to prevent cracking phenomena due to mechanical strains which is caused by expansion. It is also important that martensite finish (M_f) temperature is reached during cooling to ensure complete martensitic transformation.

2.2.1.3. PRECIPITATION HARDENING OF 15-5 PH STAINLESS STEEL

After cooling, the structure of martensitic phase is supersaturated by alloying elements. The final heating step for 15-5 PH stainless steels includes reheating of material for a temperature range between 450 to 620^0C. This operation improves the both ultimate and yield strength as a results of precipitation reaction and formation of intermetallic compounds.

Size and distribution of the precipitates may be controlled by changing the time and temperature during aging treatment that provide wide range of desired mechanical properties. Highest strength is obtained by uniformly distributed small precipitates by keeping at low temperature in aging treatment range for a long times. Higher aging temperature causes larger and fewer precipitates. Moreover, higher aging temperature may cause reformation of austenite phase which cause decrease on hardness and strength of 15-5 PH stainless steel.

There exist seven (7) standard heat treatments process that are H 900, H 925, H 1025, H 1075, H 1100, H 1150, H 1150-M, Application of this heat treatment processes may be referred to MIL-H-6875 handbook [7].

Table 2 Standard heat treatment conditions for 15- 5 PH stainless steels. [8]

	Condition	Heat To ± 15°F (8.4°C)	Time at Temperature, hours	Type of Cooling
Condition A Solution Treated 1900°F ± 25°F (1038°C ± 14°C) Air cool below 90°F (32°C)	H 900	900°F (482°C)	1	Air
	H 925	925°F (496°C)	4	Air
	H 1025	1025°F (551°C)	4	Air
	H 1075	1075°F (580°C)	4	Air
	H 1100	1100°F (593°C)	4	Air
	H 1150	1150°F (621°C)	4	Air
	H 1150-M	1400°F (760°C)	2	Air
			followed by	
		1150°F (621°C)	4	Air

2.3. MANUFACTURING METHOD OF 15- 5 PH STAINLESS STEEL

AMS5659 15-5 precipitation hardenable stainless is manufactured by consumable electrode by vacuum arc remelted process that provides high ductility and toughness. Initially, primary melt of the alloy is formed as a result of melting of raw materials in the electric arc furnaces. After addition of the suitable element, melted alloy is casted in the form of electrodes. After that, these electrodes are remelted in Vacuum Arc Remelting (VAR) furnace in order to achieve homogenous ingot without the any internal segregation and defects. A systematic flow chart for manufacturing of 15–5 precipitation hardenable stainless steel may be seen in Figure 7.

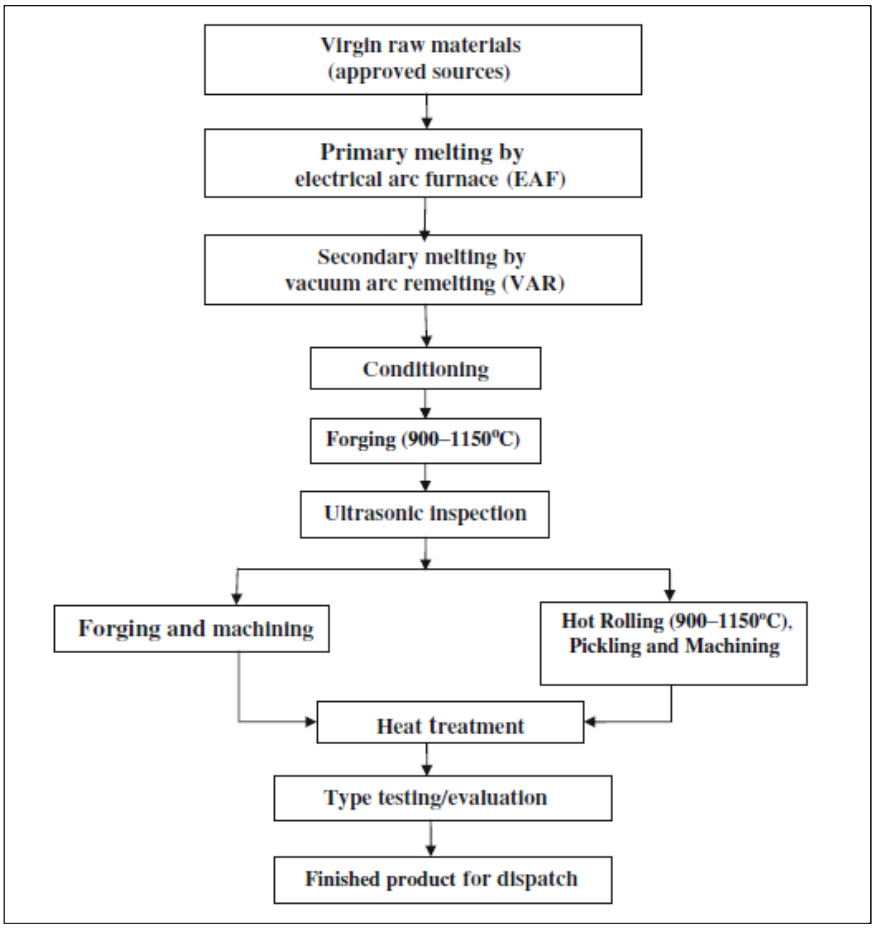

Figure 7 Manufacturing process flow of 15–5 PH martensitic stainless steels. [4]

2.4. MICROSTRUCTURE OF 15- 5 PH STAINLESS STEEL

As it mentioned before, 15-5 precipitation hardenable stainless steels include chromium and nickel as the major alloying elements. They also comprise copper that plays significant role in precipitation reaction during aging treatment. There may exist some other elements such as niobium and molybdenum which may cause formation of some carbide during heat treatment.

Precipitation hardened stainless steels have complex microstructure that is developed during a sequence of solution treatment. The resulting microstructure of 15-5 PH stainless steels includes lath martensite, Cu precipitates, retained austenite depending aging time and temperatures. When the material is heated to annealing temperature, all alloying elements in chemical compositions are dissolved and austenite phase is

formed. After air cooling supersaturated solid solution is formed with lath martensite matrix which includes high density of dislocations in the microstructure.

Aging treatment provides precipitation of ε-copper precipitates that are spherical in shape and incoherent with the lath martensite matrix. These precipitates provide main strengthening for 15-5 PH stainless steel. The precipitation reaction is occurred in a sequence. Initially coherent body centered cubic (BCC) Cu-rich clusters form in the martensite matrix phase. Then, these clusters transform into intermediate 9R structure and finally transforming into the incoherent face centered cubic (FCC) precipitates. The typical size of these Cu precipitates in the coherent state is of the order of 2–5nm [9].

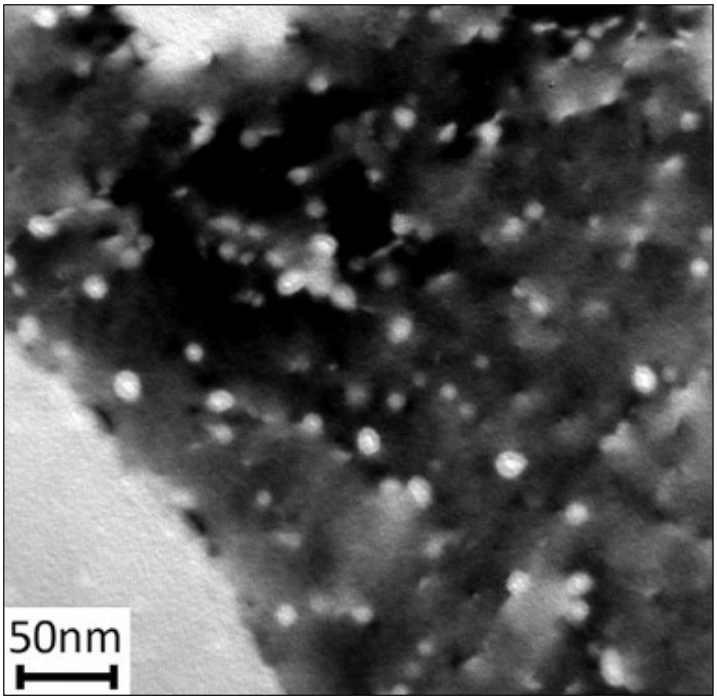

Figure 8 Bright field TEM micrograph of the aged material showing the distribution of the Cu precipitates (in white) in one martensite lath (in black). [10]

Size and amount of the ε-copper precipitates are affected temperature and time for aging treatment. Cu precipitates, which were dispersed in the martensite matrix, were larger in size for higher aging treatment temperature. Moreover, at high aging

temperature, shape of the Cu precipitates transformed from spherical to elliptical with a diagonal axis about 15 nm that can be seen in Figure 9. [11]

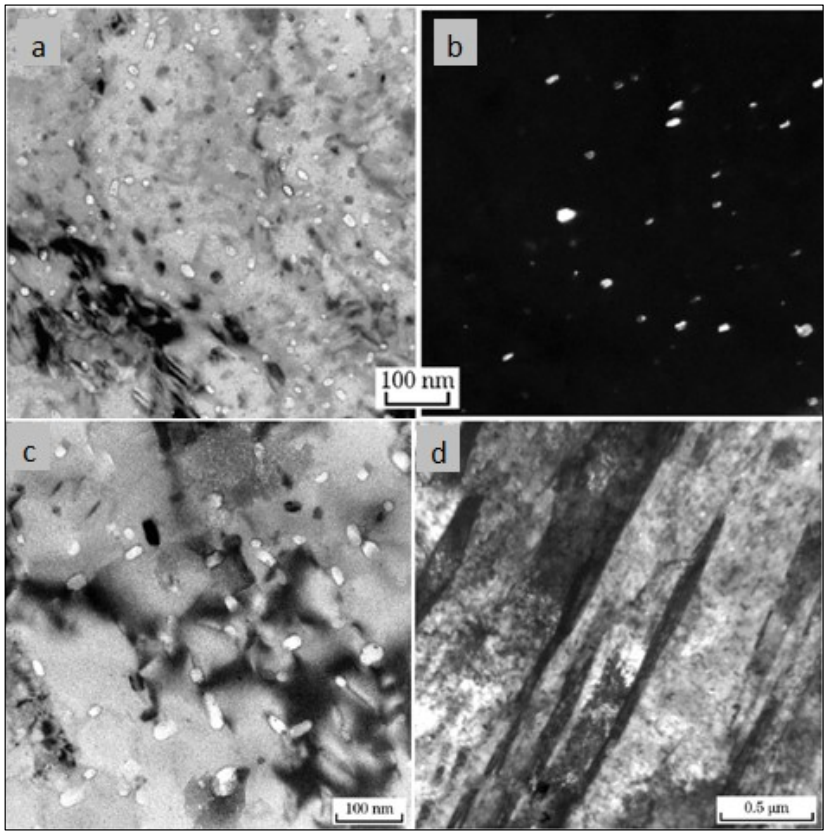

Figure 9 TEM and HRTEM micrographs of Cu precipitates and reversed austenite obtained from specimen aged at 580^0C for 4 h (a-b) aged at 620^0C for 4 h (c-d). [11]

In addition to this, for the same aging time, increase in aging temperature cause reformation of austenite phase in the microstructure. Since both copper and austenite have the same FCC structure with the similar lattice parameter, copper particles behave favorable nucleation sites for reversed austenite phase. After precipitation of Cu, Ni and C atoms start to segregate around copper precipitate from lath martensite matrix which is shown in Figure 10. The reversed austenite formation reaction is also affected by this phenomenon. Since the segregation of Ni and C reduce the austenite stabilizing temperature, reversed austenite formation may become possible around the Cu precipitates.

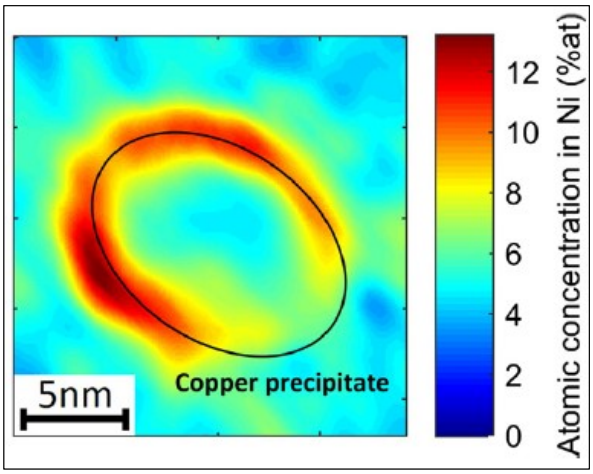

Figure 10 Concentration of Ni on a cross section of a copper precipitate in an APT volume obtained on the aged material. [10]

In 15- 5 PH stainless steels, niobium is also included in the chemical composition in order to decrease amount of carbon into carbides. Therefore, it is also possible to observe some niobium carbide particles in the microstructure. Size of these particles is around 300 nm in diameter that is shown in Figure 11. However, observation of precipitates, carbides and reversed austenite are not possible under optical microscope

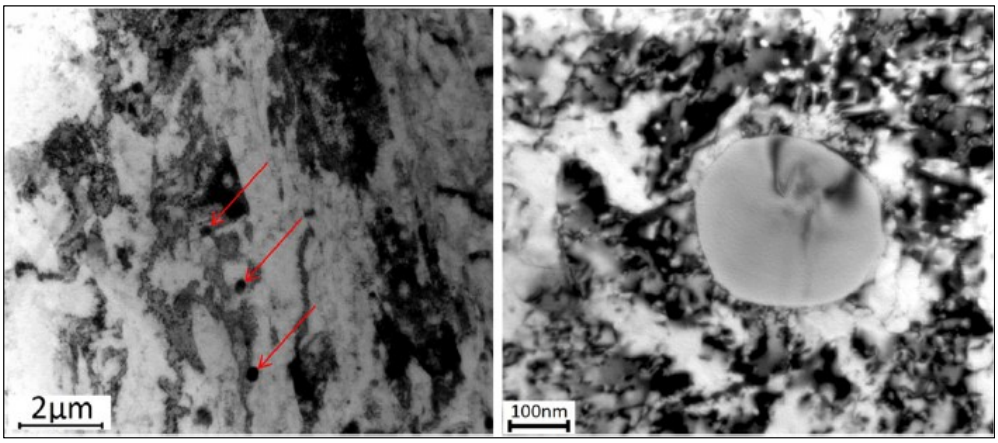

Figure 11 Bright field TEM micrographs showing spherical niobium carbides (arrows). Right hand side figure shows a larger magnification image of carbide. [10]

According to optical microstructural image of 15-5 PH stainless steels, the material that is annealed condition showed well-defined grain boundaries. However, ıncrease ın aging treatment temperature from 480 to 620^0C lead to change phase morphology martensite phase form lath to the needle type of martensite phase which is seen in Figure 12.

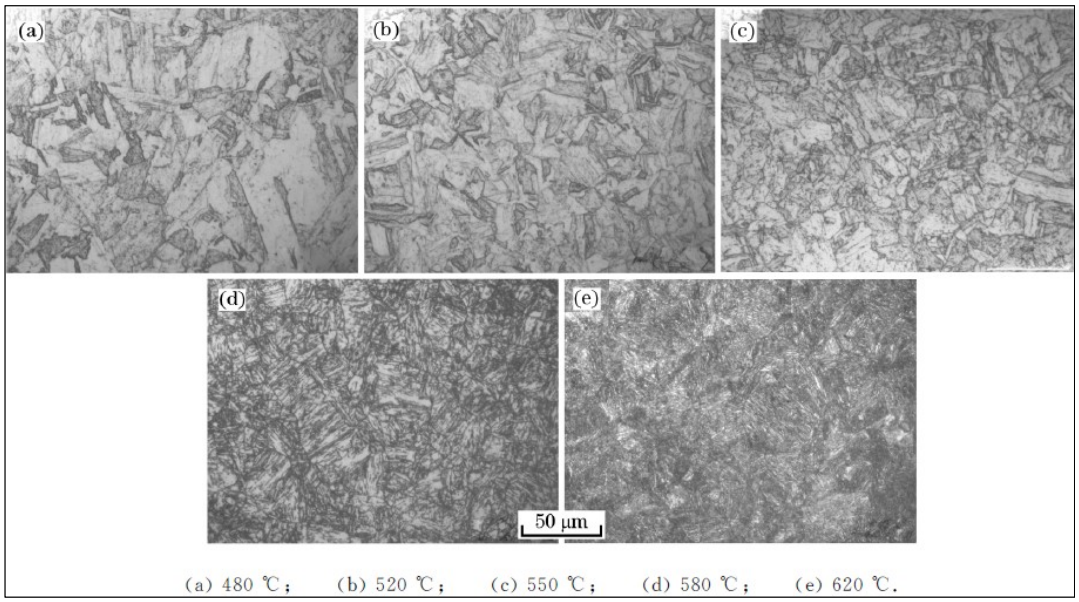

Figure 12 Optical micrographs of 15-5 PH aged at various temperatures for 4h. [11]

This transformation of the martensite phase may be explained by tempering phenomenon. Tempering causes diffusion of some carbon and other alloying elements to from precipitates and some other intermetallics. As a result of diffusion of these elements, tetragonality of the lath martensite phase is disintegrated that cause formation of needle type of martensite. In addition increase on aging temperature, tempering phenomenon is also affected by time for aging. For the same aging temperature, increase in time for aging treatment lead to increase the amount of the tempered martensite phase that may be seen in Figure 13.

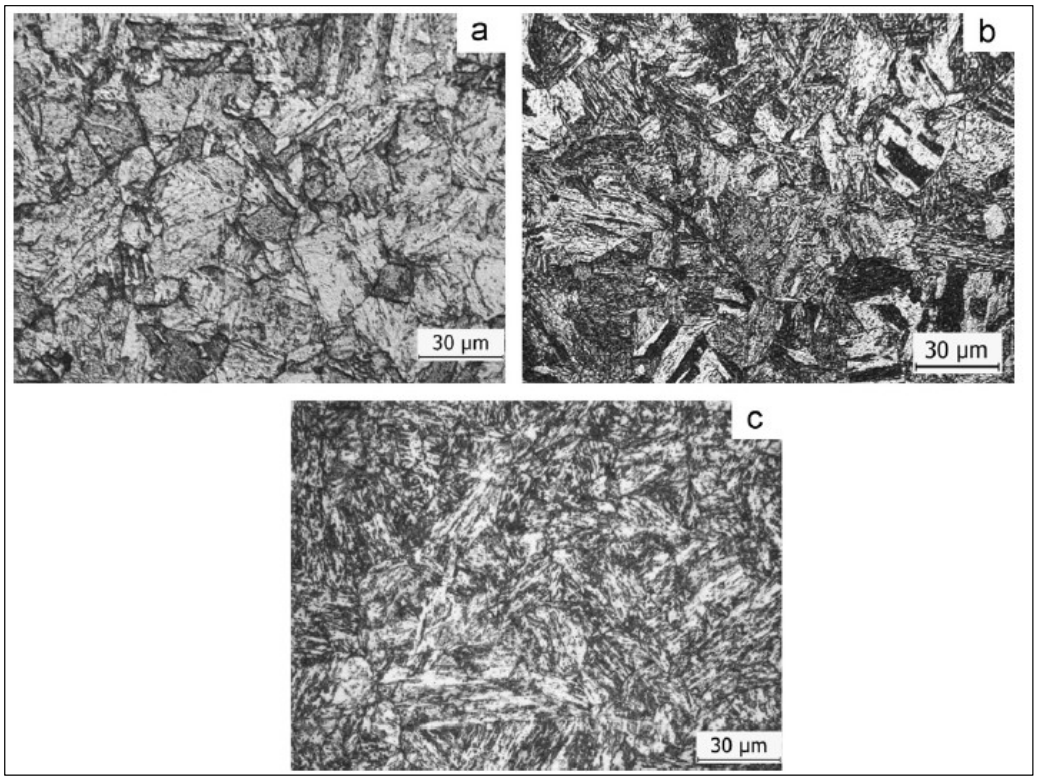

Figure 13 Optical micrographs of the material in different metallurgical conditions: (a) solution annealed, (b) aged at 580^0C for 0.25h, (c) aged at 580^0C for 4h. [9]

2.5. HARDNESS VALUES OF 15-5 PH STAINLESS STEEL

Hardness is an important mechanical property of the materials which is defined a measure of material resistance against localized plastic deformation or resistance to a wear. Hardness of 15-5 PH stainless steel that is affected by heat treatment process. As it mentioned before there exist seven (7) standard heat treatments process that are H 900, H 925, H 1025, H 1075, H 1150, H 1100, H 1150-M for these steels. According to different aging temperature and time period, different hardness values can be achieved that is shown in Table 3.

Table 3 Hardness values for different aging condition. [12]

Heat Treatment Condition	Hardness in HRC
Solution annealed	36 HRC
H900 Condition	38 HRC
H925 Condition	38 HRC
H1025 Condition	39 HRC
H1075 Condition	37 HRC
H1100 Condition	33 HRC
H1150 Condition	35 HRC

As it mentioned before, heat treatment was conducted in three steps that were homogenization, solutionizing and aging treatment for 15-5 PH stainless steels in this study. Hardness of the 15-5 PH stainless steels is affected by temperature and time period of each heat treatment steps. The effect of homogenization time on hardness of the 15-5 PH stainless is examined by Yoo et al. (2006). Increasing in time for homogenization from 1 to 5 hours, initially leads to decrease on hardness. However, after two hours, increase in time for homogenization causes increase on the hardness of the 15-5 PH stainless steels. This increase on hardness is explained according to composition of the supersaturation solid solution. As the time for homogenization increases, solubility of the alloying element in the austenite matrix increases at high temperature. During cooling, driving force become much higher to form some intermetallic and other second phase particles which cause increase on hardness. Variation of the hardness of 15-5 PH stainless steels with homogenization time is presented in Figure 14.

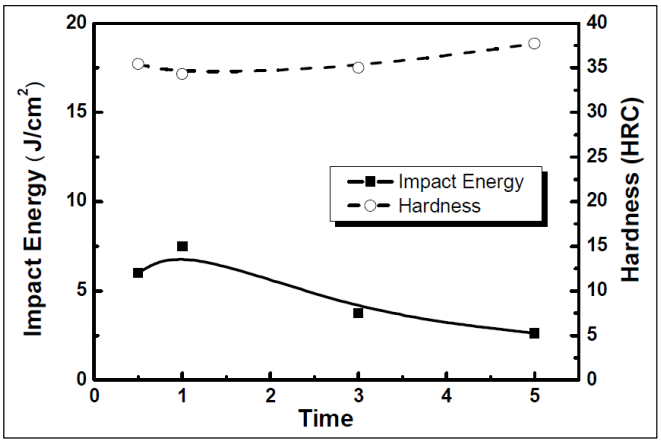

Figure 14 Variation of hardness & impact energy as a function of homogenizing heat treatment time. [26]

Hardness of 15-5 PH stainless steels is mostly affected by temperature and time period for aging step since main hardening is provided by aging treatment. The effect of the time and temperature on hardness is conducted by Mirzadeh et al. (2009). This investigation is applied for 17-4 PH stainless steels which has nearly the same chemical composition and show almost the same mechanical properties as 15-5 PH stainless steel. The effect of aging temperature and time on percent hardening is exhibited in Figure 15.

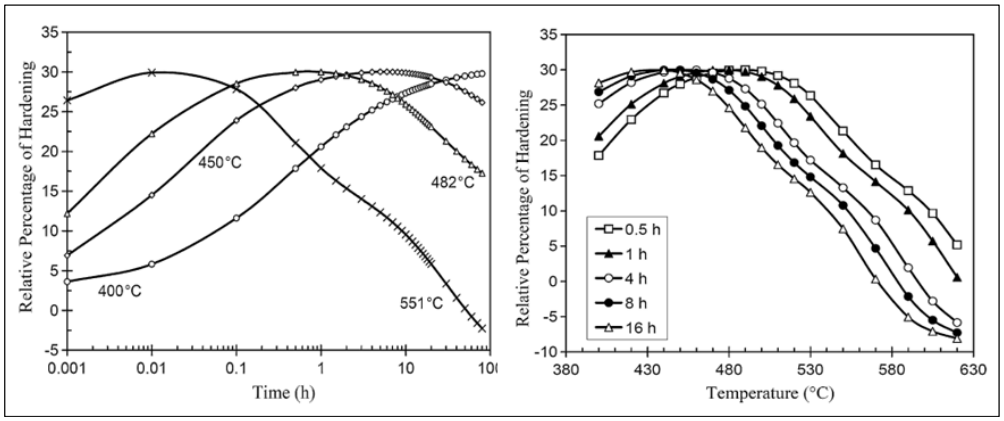

Figure 15 Temperature and time effect on the hardening behavior at different aging condition for 17-4 PH stainless steel. [14]

As it mentioned before, main hardening is provided by precipitation of the copper element as a ε- copper precipitates, which prevent motion of dislocations in the martensite matrix. Change in temperature and time period of aging treatment affects size and distribution of these precipitates. At lower aging temperatures, hardness value increases slowly compared to higher aging temperature which increases rapidly. It can be also said that at lower aging temperature, time needed to achieve peak hardness is generally high while for higher aging temperature, it is low that may be seen in Figure 16.

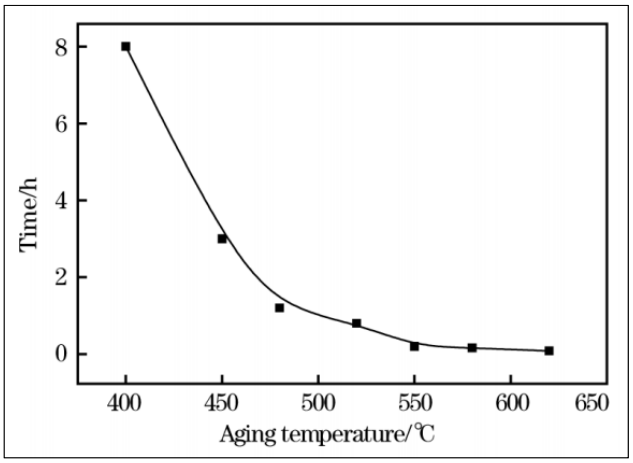

Figure 16 Required time to achieve peak hardness according to aging temperature for 15-5 PH stainless steels. [11]

Increase on aging temperature leads to decrease relative percent of hardening. This decrease is explained by coarsening of the ε- copper precipitates, recovery and re-transformation of the martensite to austenite phase. When the size of precipitates increases, probability of inhibiting the motion of the dislocation decreases that causes decrease on hardness of the 15-5 PH stainless steels.

In addition, it is difficult to keep peak hardness value at higher aging temperature, since after reaching peak value hardness becomes very sensitive against time. Hsiao et al. (2002) studied development of microstructure and aging reaction for 17-4 PH stainless steels. Accordingly, the steel reached peak hardness value at aging temperature 480^0C after 1 h, however by keeping the material for a prolonged time

for 8 hours was not observed any significant decrease on hardness value. However, at aging temperatures between 565 to 620^0C after 0.5 hour a remarkable decrease in hardness was observed compared to initial rise that is seen in Figure 17. Material that was aged at temperature 565^0C shows higher hardness value than materials which were aged at temperature 620^0C.

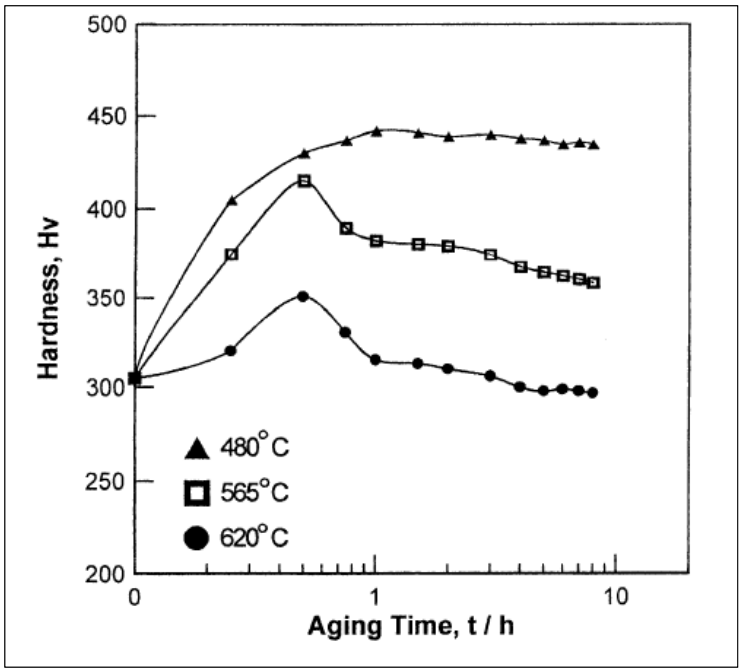

Figure 17 Effect of aging time on hardness of the solution-treated specimens. [31]

2.6. TENSILE PROPERTIES OF 15-5 PH STAINLESS STEEL

Strength and ductility are two important mechanical properties of 15-5 PH stainless steel that are affected by heat treatment parameters. According to different heat treatment condition, yield strength, tensile strength and elongation values can be changed for 15-5 PH stainless steels. Rhyim et al. (2002) studied the effect of homogenization time on the tensile strength of the 17-4 PH. Accordingly, as the homogenization time increased from 0.5 to 1 hour elongation and yield strength increase and maximum tensile strength value is reached after 3 hours homogenization treatment. However, increase in time from 1 to 3 hours leads to decrease the yield strength of the material that is seen in Figure 18.

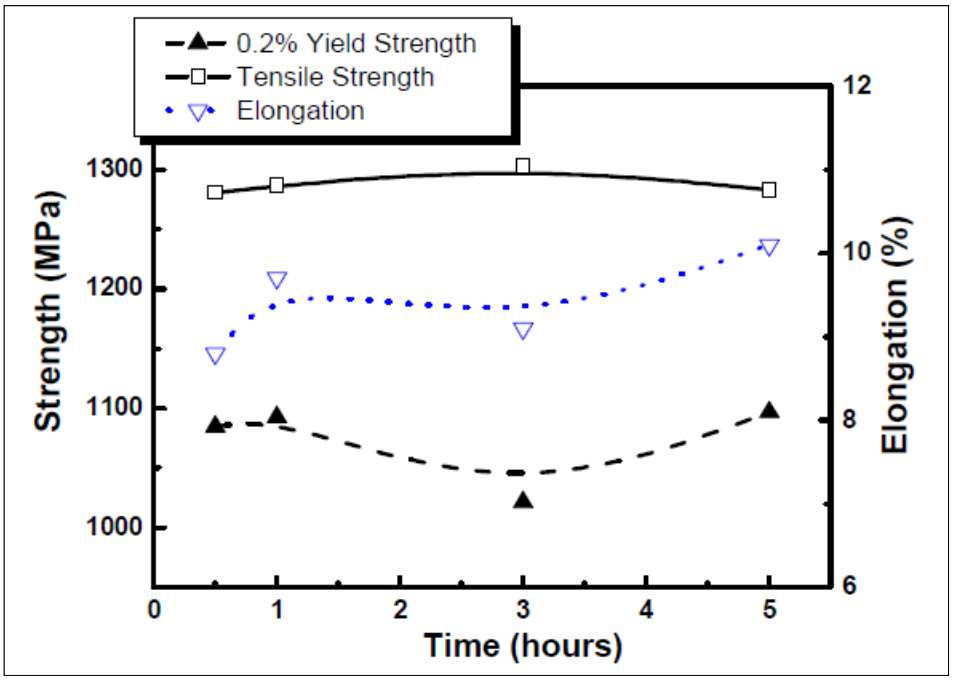

Figure 18 Deviation of the yield, tensile strength and elongation according to homogenization time. [26]

Aging temperature also has important effect on yield and tensile strength of the 15-5 PH stainless steels. Bhambroo et al. (2013) studied effects of solution annealing and aging treatment on mechanical properties of the 15-5 PH stainless steels. Tensile properties of the materials were evaluated for different aging and solution annealed conditions at room temperature at a strain rate of $1x10^{-4}$/s. Consequently, aging at 580^{0}C cause a sharp increase in the yield and tensile strength of the material in the initial stage while on prolong time for aging, the yield and tensile strength of the material reduced and fixed around 1020 MPa that is seen in Figure 19.

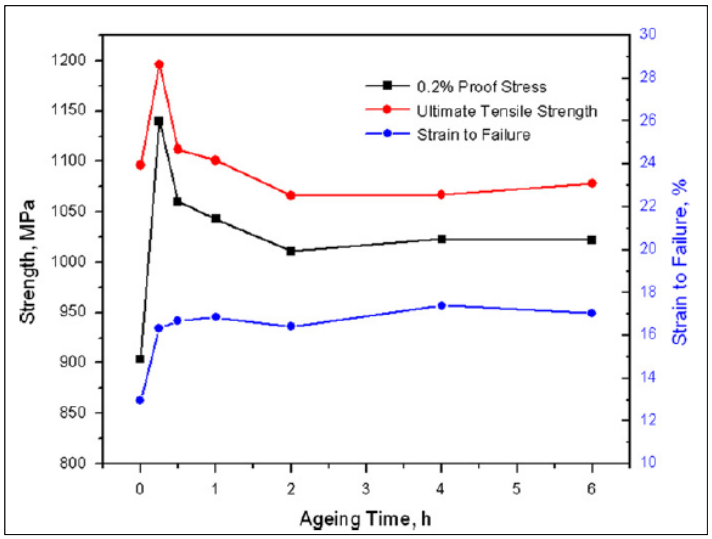

Figure 19 Effect of ageing time at 580^{0}C on the tensile behavior of 17-4 PH at room temperature. [9]

As it mentioned before, there exist seven standard heat treatment processes for 15-5 PH stainless steels which provide different mechanical properties. Tensile and elongation properties of the 15-5 PH stainless steel may be seen in Table 4. H900 heat treatment condition provides highest tensile and yield strength for 15-5 PH stainless steel while values for H1150-M condition is lowest. This decrease may also be explained the coarsening of the ε-copper precipitates and re-formation of the austenite phase at high aging temperature.

Table 4 Mechanical properties of 15-5 PH stainless steel. [8].

Property	Condition A	H 900	H 925	H 1025	H 1075	H 1150	H 1150-M
UTS, ksi (MPa)							
Longitudinal	161 (1110)	209 (1438)	181 (1249)	174 (1200)	162 (1114)	150 (1035)	136 (938)
Transverse	162 (1116)	213 (1466)	184 (1272)	175 (1204)	162 (1114)	152 (1050)	137 (944)
0.2% YS, ksi (MPa)							
Longitudinal	140 (963)	201 (1385)	175 (1208)	171 (1176)	160 (1102)	140 (967)	111 (765)
Transverse	143 (988)	202 (1393)	177 (1222)	171 (1176)	161 (1112)	146 (1009)	111 (765)
Elongation, % in 2" (50.8 mm)							
Longitudinal	8.4	10.1	12.2	12.2	12.8	14.6	18.8
Transverse	7.6	9.4	9.8	9.3	11.4	13.1	17.8

In most design case, stress versus strain curves were used in handling of the tensile behavior of 15-5 PH stainless steels that is presented in Figure 20.

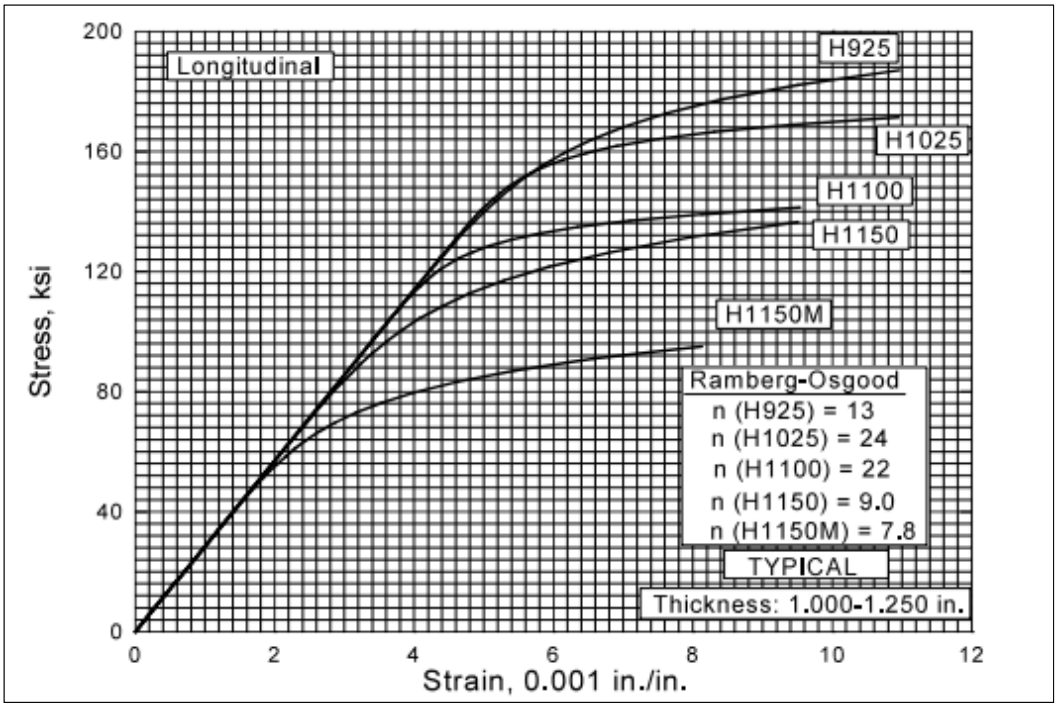

Figure 20 Typical tensile behavior for various heat treatment conditions for 15-5 PH stainless steel bar, at room temperature condition. [16]

2.7. FATIGUE PROPERTIES

Fatigue is a form of the failure that is observed in structures and components when subjected to dynamic and fluctuating stresses that may be shown on bridges, aircraft, railways and some machine components. Fatigue failures in metallic structures may cause significant problems. Several serious fatigue failures were studied and reported by August Wöhler in the 19th century. He recognized that, when a material is exposed to a single static load far below the static strength of the materials, no damage observed on the structures and components. However, ıf the same load is exposed in many times it may cause failure of the components. Therefore, the term fatigue is explained by the type of failure that occurs after a long period of applied cyclic stress or strains.

Fatigue failure is observed in brittle nature even in ductile metals, but there may be very little plastic deformation during failure. Repeated cyclic load in fatigue mechanism causes initiation of small microcracks that are followed by growth up to complete failure. In addition, fracture surface of the fatigue failure is directly perpendicular to direction of applied tensile stress.

There exist three basic factors which are necessary for fatigue failures:

- There should be a maximum tensile stress with a sufficiently high value.
- There should be an enough variation and fluctuation on applied load.
- Applied load should expose sufficiently large number of cycles.

2.7.1. DEFINITIONS AND TERMS FOR FATIGUE

The applied cyclic load may be in the form of axial (tension-compression), bending, or torsional (twisting). In fatigue concept, there exist three different cyclic stress vs. time diagrams. The first one is where the maximum and minimum applied stress (load) levels are equal that is called fully reversed stress vs. time diagram. The second type is where applied stress (load) are asymmetrical that is known as repeated stress vs. time diagram. Stresses (loads) may be in the form of compression-compression, tension- tension and tension- compression. The final stress vs. cycle diagram is where stress (load) level varies randomly in frequency and amplitude. That is named as irregular stress vs. cycle diagram.

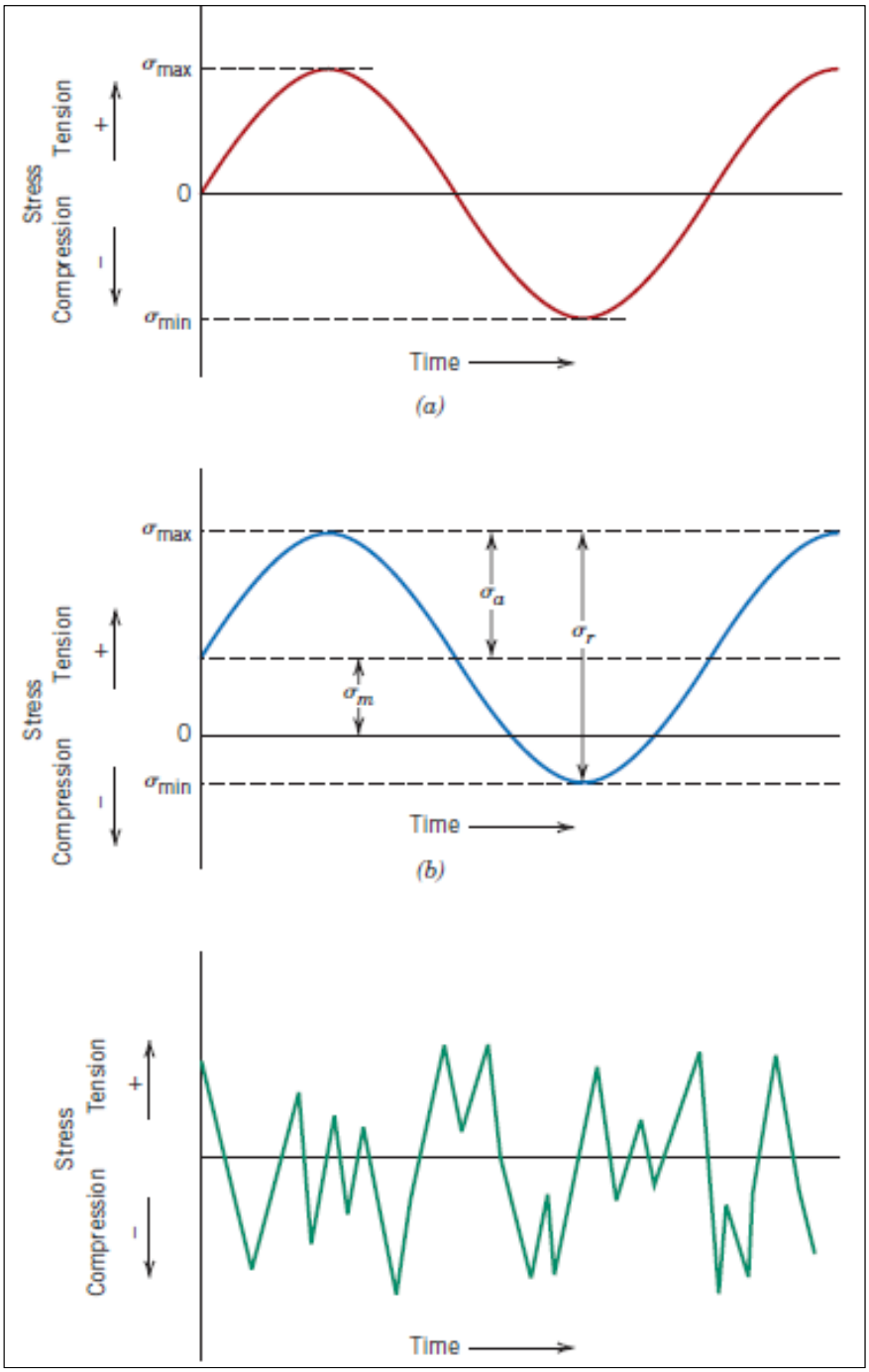

Figure 21 Schematic exhibition of loading types. [17]

There exist several parameters that are cyclic stress (load) range, cyclic stress (load) amplitude, mean stress (load) and stress (load) ratio used to fluctuating stress (load) vs. cycle diagrams.

Stress (load) range is the algebraic difference between the consecutive peak forces and valley in fatigue loading:

$$\sigma_r = \sigma_{max} - \sigma_{min} \tag{2.1}$$

Stress (load) amplitude is the one half of the range of cycle:

$$\sigma_a = \left(\frac{\sigma_r}{2}\right) = \frac{\sigma_{max} - \sigma_{min}}{2} \tag{2.2}$$

Mean stress (load) is the algebraic average of the maximum and minimum stresses in constant amplitude fatigue loading:

$$\sigma_m = \frac{\sigma_{max} - \sigma_{min}}{2} \tag{2.3}$$

Stress (force) ratio is the ratio of minimum stress (load) over maximum stress (load):

$$R = \frac{\sigma_{min}}{\sigma_{max}} \tag{2.4}$$

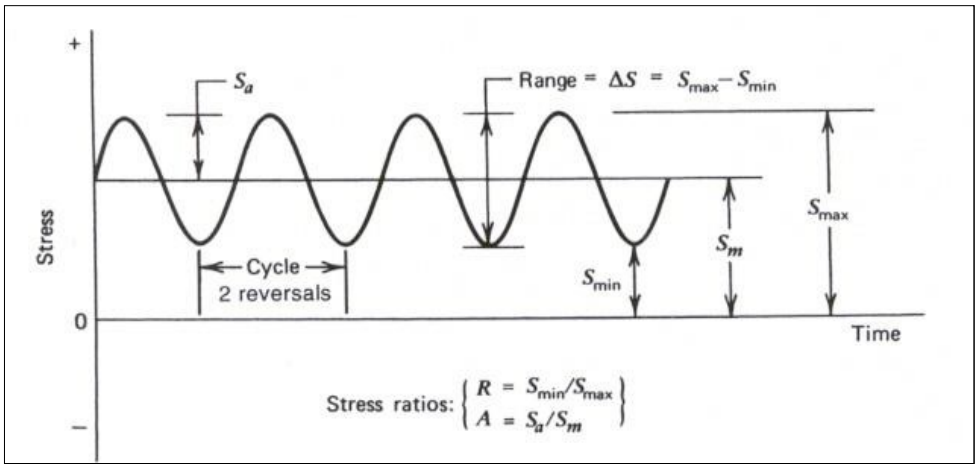

Figure 22 Schematic exhibition of basic terms on sinusoidal fatigue loading. [18]

2.7.2. NUCLEATION AND GROWTH OF FATIGUE CRACK

According to some microscopic investigation in the initial period of the 20th century, nucleation of fatigue crack starts as invisible microcracks in slip bands. Nucleation of these microcracks generally takes place very early period in the fatigue life when a cyclic stress just above the fatigue limit is applied. In addition, these microcracks generally remain invisible during significant part of the total fatigue life. Therefore, it can be said that when these cracks become visible, there will be small percentage of total fatigue life for a laboratory specimen. On the other hand for real structure, the remaining percentage of the total fatigue life will be much larger even if cracks become visible.

When a microcrack has been reached, crack exhibit a low growth rate due to some microstructural effects such as grain boundary. However, crack away from the nucleation site show more regular growth rate. This situation can be named as a real crack growth period. Therefore, until the failure, fatigue life is consisted by two periods which are crack initiation period and crack growth period.

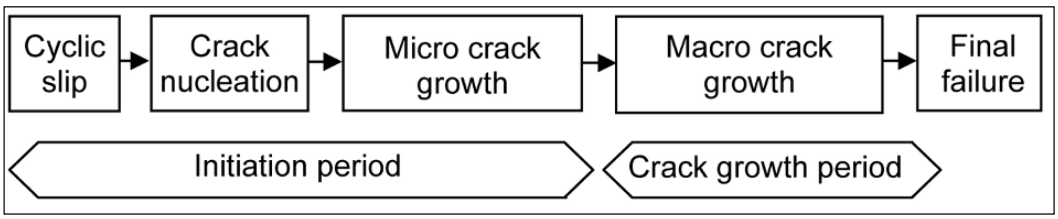

Figure 23 Different phases of the fatigue life. [19]

2.7.2.1. CRACK INITIATION PERIOD

Cyclic slips are enabled by cyclic shear stress. In the microscopic point of view, these shear stresses are not distributed homogenously on the material. This inhomogeneity is affected by shape and size of the grains, crystallographic orientation of the grains and anisotropy of the materials which cause variation of the shear stress from one grain to another. Some surface grains for the materials are usually more favorable for cyclic slip mechanism than others. When a cyclic slip

occurs, a slip step is formed at the surface of the material. When load is increased, some strain hardening is formed on these slip bands. During unloading, this hardening causes formation of the shear stress in the same slip but in reversed direction that causes formation of a reversed slip band in parallel. Cyclic loading provides back and forth movement for the slip bands that leads to the formation of intrusions and extrusions on the surface of the materials. These intrusions and extrusions provide formation of a microcrack on the surface of the materials. These cracks are initially propagated in parallel with slip bands with a very small growth rate like 1 nm in each cycle. When crack reached sufficient length, becomes dominant to overcome the stress field at the tip of the slip bands. Thus, crack growth plane changes to perpendicular direction to the principal stress.

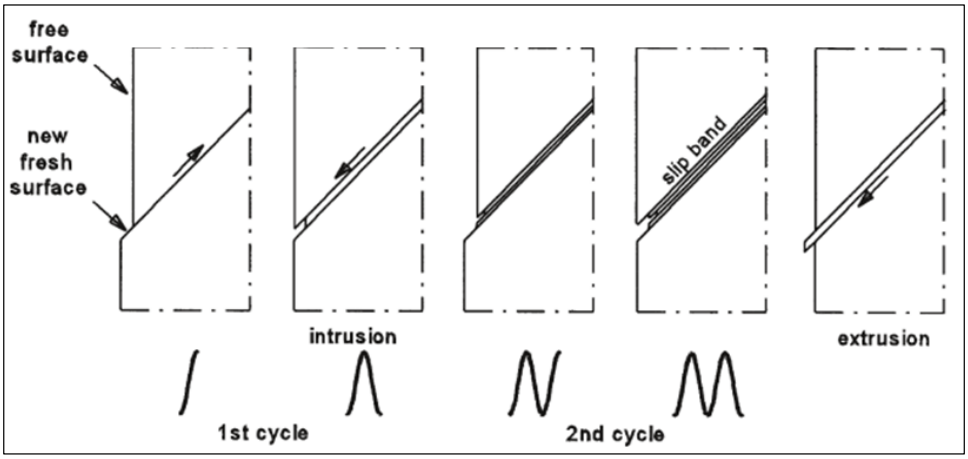

Figure 24 Effect of the cycle slip on the crack nucleation. [19]

2.7.2.2. CRACK GROWTH PERİOD

If a microcrack grows through adjacent grains, restrain on the cyclic slip mechanism increases due to effect of the neighboring grains. Therefore, it may become difficult to continue the cyclic slip only by one slip plane that provides observation of the more slip planes. As a result, the growth direction of the microcracks deviates from slip band orientation. There exists usually a tendency to grow perpendicular direction normal to applied stress that is shown in Figure 25.

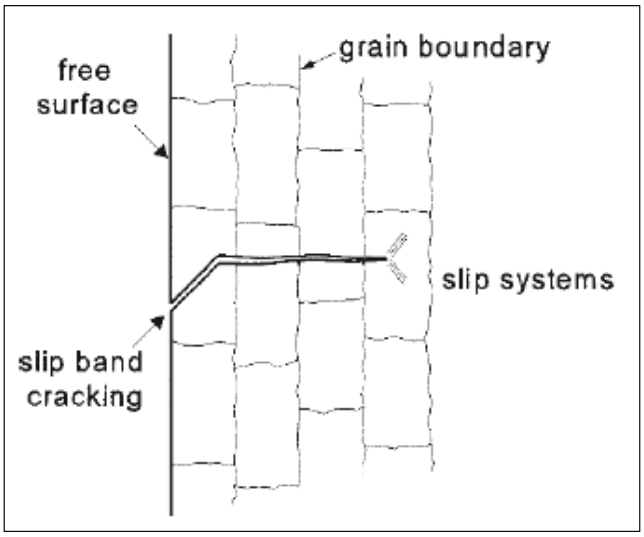

Figure 25 Cross section of microcrack. [19]

Growth of the microcrack depends on cyclic plasticity so barriers in the microstructure can behave a threshold for crack growth. Crack growth rate is expressed by increase in crack length per cycle and decreases when tip of the crack confront the grain boundaries. After penetrating to other neighboring grain, crack growth rate again increases. The effect of the grain boundaries on the crack growth rate may be seen in Figure 26.

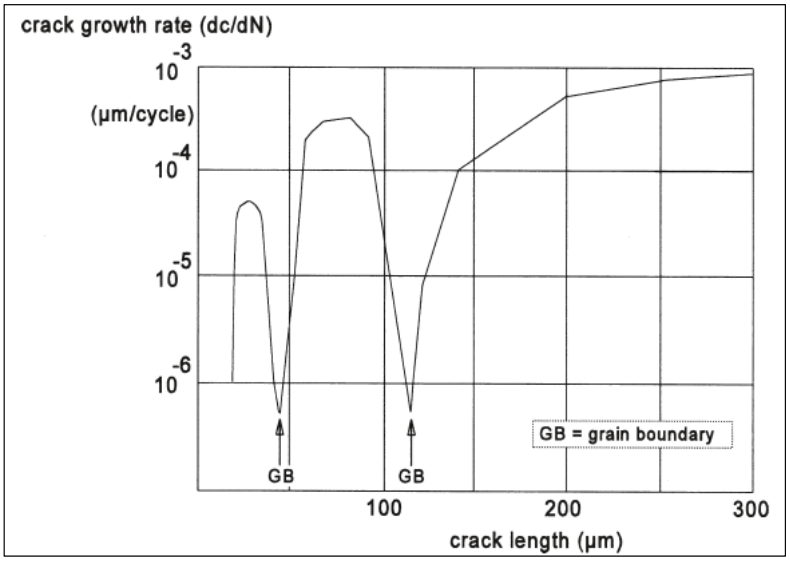

Figure 26 Effect of the grain boundary on crack growth period for an Al-alloy. [19]

During the crack growth period, there is not large gradients in the crack growth since crack cannot grow in the random direction through the grains. Therefore, crack front generally remains coherent which may be seen in Figure 277.

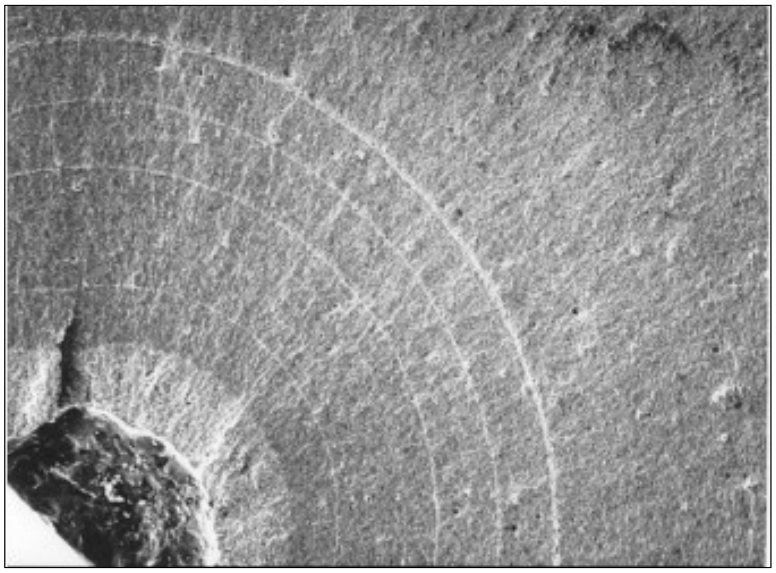

Figure 27 Evolution of the fatigue crack front. [20]

2.7.3. STRESS- LIFE DIAGRAMS (S-N CURVES)

Similar to other mechanical properties, fatigue characteristics of the materials can also be derived by laboratory tests. Test apparatus provide service conditions with respect to stress level, time and frequency. In general, two different fatigue testing systems are used with different loading condition. These systems are axial and rotating bending fatigue testing systems.

A range of tests may be performed by subjecting specimens to cycling stress at different stress levels and the number of cycles up to failure is recorded. Results of the fatigue tests are plotted as stress versus number of cycles to failure for all tested specimens. This plot is called S-N curves that provide information for fatigue behaviors of materials. The bases of the stress-life diagrams are known as Wohler S-N diagrams which can be seen in Figure 28. S-N diagrams represent the mean of the data from several fatigue tests.

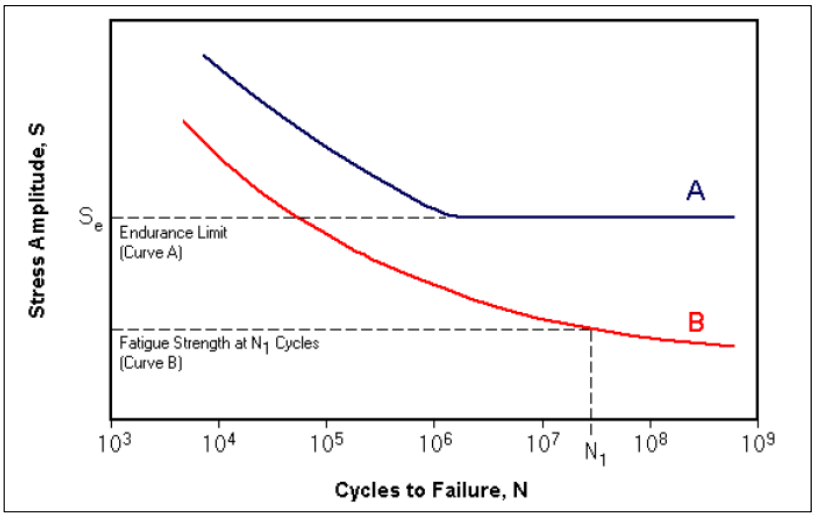

Figure 28 Typical S-N curves. [21]

Stress versus number of cycles to failure data (S-N) may also be plotted on a log-log plots that is seen in Figure 29. These diagrams are generally called as idealized S-N curve.

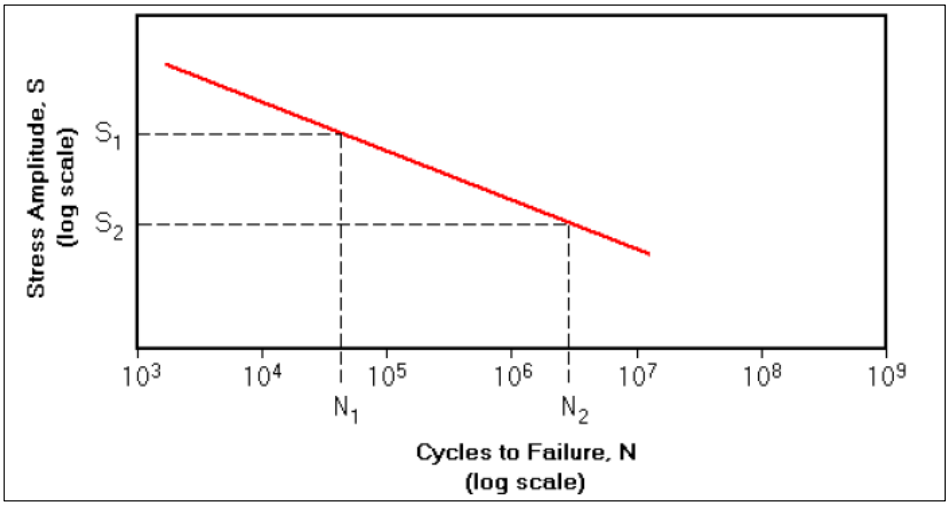

Figure 29 Idealized S-N curve. [21]

S–N curves for some ferrous materials (iron base) and some titanium alloys become horizontal at large number of cycles, or it can be said there exist a limiting stress level. This stress level is called by fatigue limit or sometimes endurance limit and below this stress level, fatigue failure will not occur. In other words, fatigue limit

represents the maximum stress level that will not cause failure for an infinite number of cycles. For many high strength steels, fatigue limits are generally ranged between 30% and 60% of the ultimate tensile strength. Typical trend of S-N curve for those types of materials can be shown curve A in Figure 28.

Most of nonferrous alloys such as aluminum, copper, magnesium do not show endurance limit. S-N diagrams for these alloys shows a downward trend through relatively large number of cycles. For these types of materials, fatigue behavior is specified as fatigue strength that is defined as stress levels at which failure will occur for some determined number of cycles. Typical trend of S-N curve for those types of materials can be shown curve B in Figure 28.

2.7.4. FATIGUE BEHAVIOR AND STRESS- LIFE DIAGRAMS FOR 15-5 PH STAINLESS STEEL.

15-5 PH stainless steels are preferred in aerospace and defense industries thanks to its high fatigue performance. Fatigue performance of the 15-5 PH stainless steel is much affected by heat treatment condition. Increase in aging temperature from 480^0C to 550^0C causes decrease on fatigue limit of the 15-5 PH stainless steel of 5 to 10 percent [22]. Fatigue test results (R=0.1) for two different heat treatment conditions may be seen in Table 5.

Table 5 Fatigue test results for 15-5 PH stainless steels for H-900 and H-1050 conditions. [22]

FATIGUE RESULTS, 15-5 PH, H-1050 CONDITION

Stress Ksi	Cycles to Failure	Specimen No.
130	.052 x 10^6	46
120	.074 x 10^6	37
110	.161 x 10^6	48
100	1.506 x 10^6	39
98	.711 x 10^6	45
98	.967 x 10^6	40
95	.846 x 10^6	38
94	.964 x 10^6	42
94	16.339 x 10^6 Runout	43
92.5	.667 x 10^6	47
92.5	39.000 x 10^6 Runout	41
90	10.916 x 10^6 Runout	44

FATIGUE RESULTS, 15-5 PH, H-900 CONDITION

Stress Ksi	Cycles to Failure	Specimen No.
130	.089 x 10^6	23
120	.098 x 10^6	16
115	.236 x 10^6	14
110	.419 x 10^6	24
105	.357 x 10^6	13
102	.318 x 10^6	20
100	1.246 x 10^6	18
100	11.500 x 10^6 Runout	23
99	.241 x 10^6	22
97	11.037 x 10^6 Runout	19

Constructed Stress (S) vs. Life (N) according to these fatigue test results, which are given in Table 5, may be seen in Figure 30. S-N curve was constructed and fatigue limit was calculated according to AGARD-AG-292 international standard which is explained in detail in following topics.

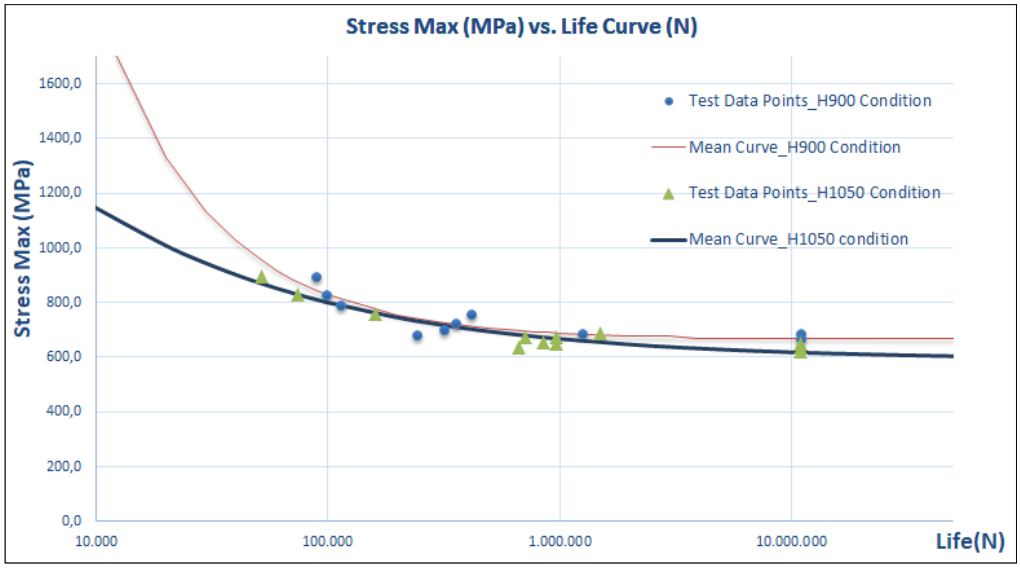

Figure 30 Stress vs. Life curve of 15-5 PH stainless steels for H900 and H1150 conditions. [22]

Fatigue test results (R=-1) for H1025 heat treatment condition for two different surface condition may also be seen in Table 6.

Table 6 High cycle fatigue behavior of 15–5 PH martensitic stainless steel. [4]

Stress range (MPa)	As per AMS 5659 H specified minimum number of cycles	Type test schedule specified minimum number of cycles	Experimentally obtained values in three melts (number of cycles)	
			Forged bars	Hot rolled bars
Axial fatigue (smooth) $R = -1.0$; $K_t = 1$; $F = 30$ Hz (H1025)				
1048	1×10^5	1×10^5	$(1.05–4.77) \times 10^5$	$(1.04–1.10) \times 10^5$
985	1×10^6	1×10^6	$(1.03–1.13) \times 10^6$	$(1.03–1.10) \times 10^6$
935	1×10^7	1×10^7	$(1.01–1.07) \times 10^7$	$(1.0–1.10) \times 10^7$
Axial fatigue (notch) $R = -1.0$; $K_t = 3$; $F = 30$ Hz (H1025)				
345	1×10^4	1×10^4	$(1.0–1.16) \times 10^4$	$(1.10–1.18) \times 10^4$
276	1×10^5	1×10^5	$(1.01–1.10) \times 10^5$	$(1.08–1.11) \times 10^5$
240	1×10^6	1×10^6	$(1.0–1.11) \times 10^6$	$(1.02–1.37) \times 10^6$
205	1×10^7	1×10^7	$(1.01–1.53) \times 10^7$	$(1.0–1.10) \times 10^7$

2.8. STATISTICAL ANALYSIS OF FATIGUE TEST DATA

By its nature, fatigue test results for a material is a random process, so there is always scatter in test results, although controlling of fatigue testing conditions carefully. This scatter in fatigue data causes analysis of fatigue test results and application of these to real problems much difficult. Therefore, some statistical methods are needed to handle these scatter in fatigue test results. Statistical methods generally provide information on the limited number of tested specimens and finding a specified degree of confidence level on test results. The construction of S-N can be basically described to the individual data points. The one of the common function that provides an adequate fitting for certain data is known as normal distribution (Gaussian distribution) and defined with equation 2.5.

$$p\ (S) = \left(\frac{1}{\sigma\sqrt{2\pi}}\right) exp\left(\frac{-S^2}{2S\sigma^2}\right) \tag{2.5}$$

A normal distribution p(S) shows variation with variable (S), mean (μ) and variance (σ^2) of these all values of S. The function p(S) is also known as probability density function. This shows a measure of a width of the scatter band. In most cases, normal distribution gives a good approximation for distribution of fatigue lives of metallic specimens in logarithmic scale.

Parameters related to population can only be estimated from tested sample. Otherwise, ın order to obtain exact values of parameters for the population, whole population should be tested. The estimates of behavior of the population from a tested sample, and the confidence level are the essence of the statistical analysis of metal fatigue data of specimens.

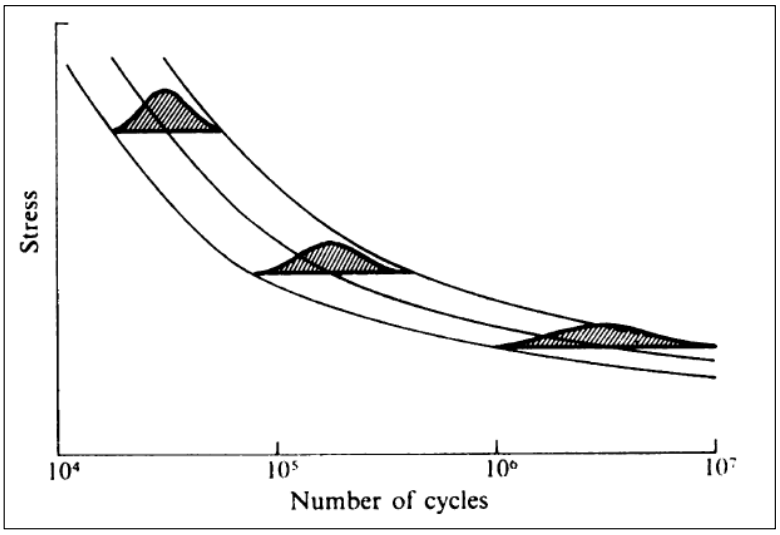

Figure 31 Schematic P-S-N diagram for three probabilities of failure and log normal distributions of lives. [23]

In general, specimens are tested at different stress levels so different probabilities of failures may exist for S-N curves. In the conventional S-N curves, fifty percent (50%) probability corresponds to median is preferred. These curves are referred to as P-S-N curves and scatter in endurance increases through the fatigue limit that can be seen in Figure 3131. According to this statistical concepts, construction of S- N curves and calculation of fatigue limit were carried according to AGARD-AG-292 HELICOPTER FATIGUE DESIGN GUIDE [24] that is explained in following section in detail.

2.8.1. AGARD-AG-292 FOUR (4) PARAMETER BEST FITTING TECHNIQUE

As it mentioned before, ın order to get representative results from fatigue tests, a large number specimens are needed for construction of S-N curves. However, for most of the cases, the number of fatigue test specimens is usually limited in practice due to cost and time consuming. Therefore, in order to get accurate results for the design, the mean fatigue strength concept is used. The mean fatigue strength can be reached by a relatively small number of specimens by using some fitting technique to

establish S-N curves. The curve shape for fatigue test results can be constructed by some regression analysis as is shown in below.

The result of a fatigue test consists of a pair of values, one of which is related to the applied load and the other is the number of cycle. The trend of test data can be interpreted by the relationship S = f (N) with S = maximum stress and N = number of cycles to failure. The type of the equation f (N) can be established by a numerical analysis of test data. For this kind of curve, the Weibull four parameters equation may be commonly used.

Determination of curve shape for S-N curves is carried out according to equation (2.6);

$$\frac{S}{Si} = H + A * (N + C)^{B} \tag{2.6}$$

Where, S is the applied maximum stress level, Si is the stress level at infinity, N is the number of cycles for a given stress level and H, A, C and B are the variables for construction of best fit for test data points. S-N curve shape can be derived from test data and exhibits % 50 probabilities.

In order to derive mean S-N curve, fatigue test data are projected to a given number of cycles through which is shown in Figure 32.

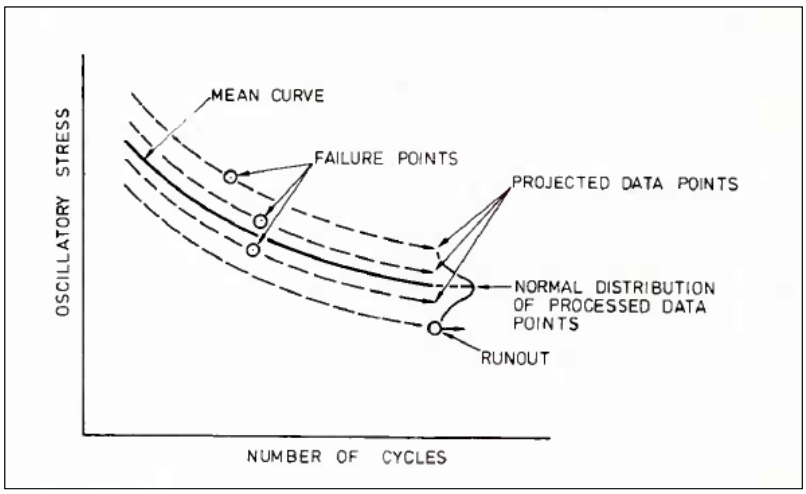

Figure 32 Extrapolation of data for statistical analysis. [24]

The extrapolation for test data is usually carried according to design criteria. In general, for ferrous materials extrapolation is carried out to 10 million cycles and 50 million cycles for nonferrous materials like aluminum alloys. Mean and standard deviations for extrapolated fatigue test data are calculated according to log normal probability distribution function by using following equations.

$$log\ \overline{S} = \frac{\sum(logS_i)}{n} \tag{2.7}$$

$$\sigma = \sqrt{\frac{\sum(logS_i - log\ \overline{S})^2}{n-1}} \tag{2.8}$$

where:

$\overline{S}$= Mean fatigue strength for fatigue test data at extrapolated number of cycles

S_i= Fatigue strength of individual specimen at extrapolated number of cycles

n= Number of specimens

σ= standard deviation

Best estimates of the unknown constants SI, H, A, B and C are obtained in fitting the equation 2.6 by applying the method of least squares to fatigue life that can be seen in Figure 33. Due to the fact that the S-N curve is practically horizontal for small and large values of N, the regression of stress on life is performed, i.e. the sum of squared deviations in the vertical direction between test data points and the best fitting curve is minimized.

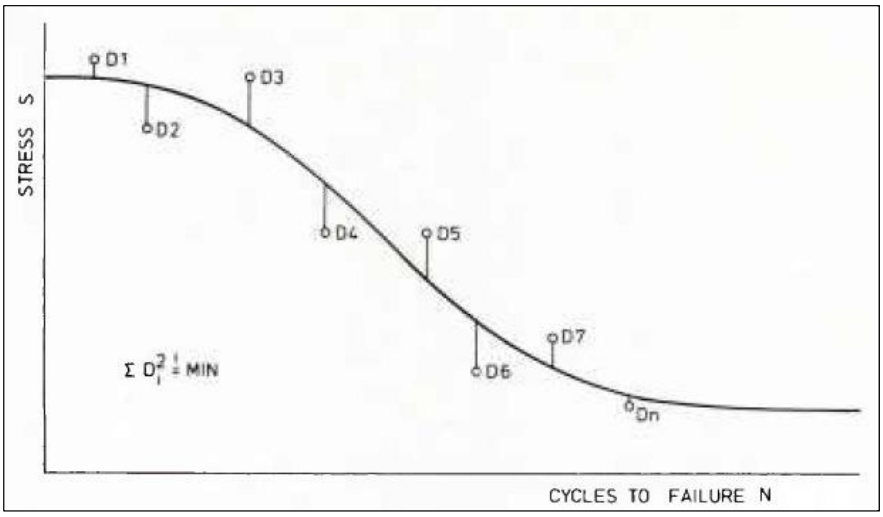

Figure 33 Least Square Fitting Concept for non-linear analysis of test data. [24]

Since equation 2.6 is nonlinear, a nonlinear regression algorithm is used according to equation 2.6 and the minimization is done according to some conditions for variables SI, H, A, B and C for those are shown in Table 7. In most of the cases H is taken as one (1) since it has less effect on curve shape.

Table 7 Conditions for parameters SI, H, A, B and C in fitting equation

Conditions for Variables				
A≥0	B≤0	C≥0	H≥0	Si≥0

2.8.2. STAIRCASE METHOD FOR FATIGUE LIMIT CALCULATION

Alternatively, fatigue limit of a materials can also be estimated according to staircase method that is given in ISO 12107 International Standard (Metallic materials — Fatigue testing — Statistical planning and analysis of data) [25]. Staircase method provides to get rough estimates for the fatigue strength for the materials to be tested.

There exist two important points in staircase method. The first one is determination of the stress level for the first specimen. The second one is the determination of the increment value between stress levels. Stress level for fist specimen can be determined according to expected average fatigue strength. On the other hand, increment value may be determined standard deviation of the stress at 10^7 million

cycles. If there is no information available for standard deviation, 5 or 10 % of the expected average fatigue strength may be used as an increment value.

After determination of the stress level for the first specimen, fatigue test is started. If the specimen does not fail until 10^7 cycles. Then, next specimen is exposed to stress level that is one increment higher than the previous one. If the specimen does not survive at this stress level before reaching 10^7 cycles, the following specimen is tested at a stress level that is lower in the degree of one increment value. An example of the staircase test data can be seen in Figure 344.

Stress S_i MPa	Sequence number of specimen														
	1				5				10						15
540								X							X
520				X			O		X		X			O	
500			O		X		O			O		X	O		
480		O*				O						O			
460	O*														

X for failure
O for non-failure
* not counted

Figure 34 Example of staircase test data. [25]

After completing the all tests, the fatigue strength can be simply calculated as the sample mean of the stress levels during the staircase sequence, where a fictitious test is added at the end of the sequence and the first run-out test is discarded. Calculation of the fatigue limit according to staircase method is shown schematically in Figure 35.

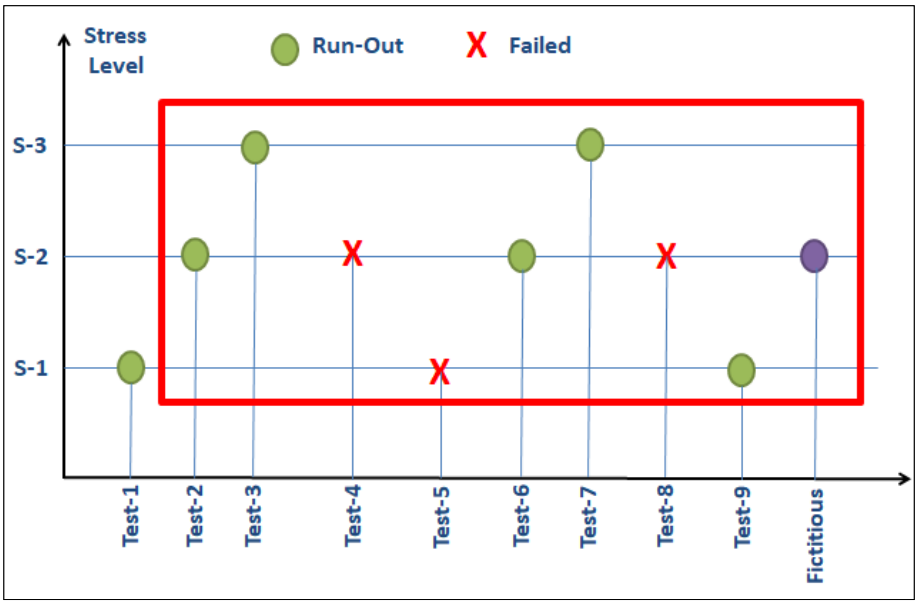

Figure 35 Schematically calculation of the fatigue limit according to staircase method.

2.8.3. NORMAL PROBABILITY PLOT FOR OUTLIERS DETERMINATION

As it mentioned before, fatigue test results for material is a random process, so there is always scatter in the test results by its nature. Therefore, in order to determine correct shape for S-N curve. Outliers should be determined according to standard deviation of fatigue test data and not be included in S-N curve construction.

The use of normal probability plot is quite common in order to see if a given physical phenomenon follows a certain kind of statistical distribution and to obtain graphically the characteristic values of the distribution. Scatter bands for outliers are determined at endurance limit by using projected fatigue test data.

First of all, all projected test data points (stress values at logarithmic scale) are sorted in ascending order from smallest to largest. Integer numbers are also sorted in ascending order like (1, 2, 3, etc.). Then cumulative probability function P(i) shall be calculated by using both data according to equation 2.13.

$$P(i) = \frac{i}{n+1} \tag{2.9}$$

where:

n= Number of all xi elements of the sample

i= Integer number corresponding to the order of xi

In order to find theoretical normal distribution according to fatigue test data, inverse cumulative distribution (ICDF) function is used by using cumulative probability function. (e.g. "NORM.S.INV" function can be used for excel). Then, theoretical stress values for projected data are calculated by using equation 2.14.

$$S(x) = \overline{X} + \text{ICDF} * \sigma \tag{2.10}$$

where:

S(x)= Projected theoretical stress on logarithmic scale

$\overline{X}$= Mean stress on logaritmic scale for projected data

σ=Standard deviation for projected stress values on logarithmic scale

After plotting theoretical value of stress and the inverse of the standard normal cumulative distribution, outliers' criteria can be determined according to value of standard deviation for projected stress values on logarithmic scale. The normal probability plot for hypothetical fatigue test data can be seen in Figure 36.

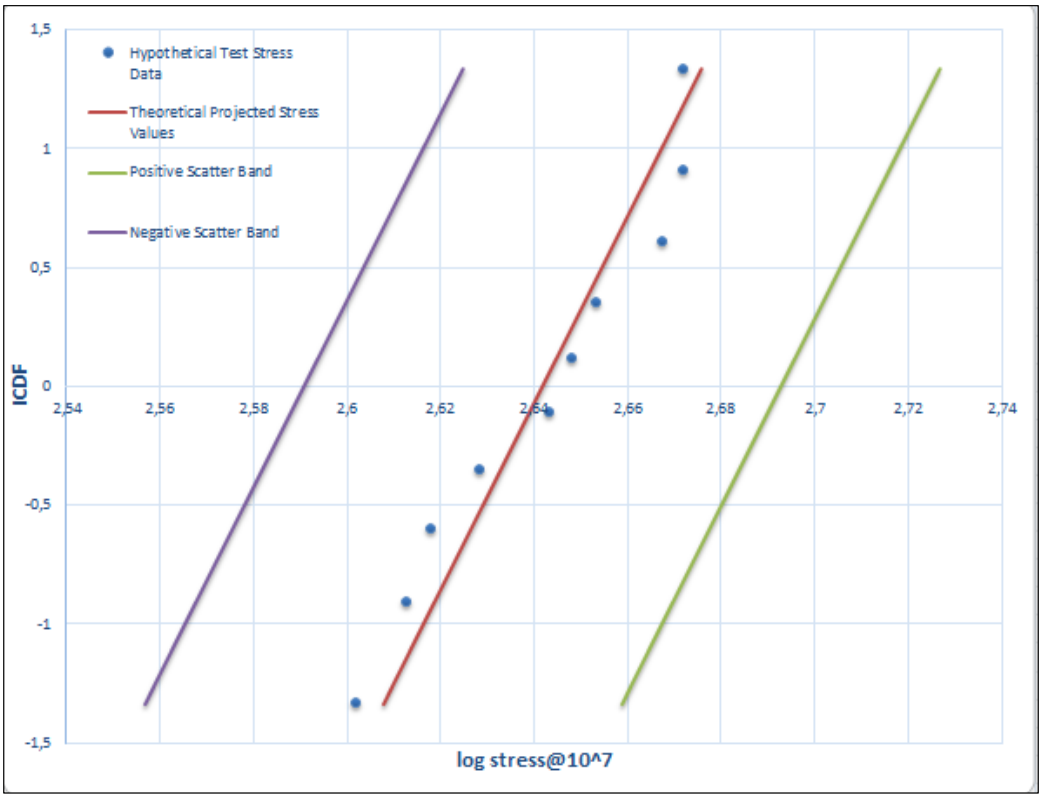

Figure 36 Normal probability plot for hypothetical fatigue test data.

2.9. FRACTURE SURFACE ANALYSIS OF 15-5 PH STAINLESS STEELS

Failure of materials may lead to huge costs so it is important to understand fracture mode and mechanism of the materials in design. Causes of failures may be improper material selection or processing, the improper component design and improper usage areas. Fracture of the metals is a form of failure where materials separate into small pieces due to some stresses at a temperature below the melting point. The applied stress on the materials may be tensile, compressive, shear or torsional. Depending of the degree of material plasticity and elongation, fracture is named as ductile or brittle fracture for engineering materials. Ductile materials usually show high amount of plastic deformation which means high energy absorption before failure. On the other hand, for brittle materials there exists little or no plastic deformation before failure due to low energy absorption. Any types of fracture take place in two steps that are crack formation and crack propagation. It can also be said that fracture mode for the materials highly dependent on crack propagation mechanism.

As it mentioned before, there exist seven standard heat treatment conditions for 15-5 PH stainless steels. These treatments provide different types of fracture modes for tensile tested specimens. Palanisamy et al. (2015) investigated the effect of aging on the fracture mode of the tensile test specimen by comparing the specimens which were exposed to solution treated (Hardness HV= 352, UTS= 1048) and H900 (Hardness HV= 486, UTS= 1466) condition. The fracture surface of the tensile tested specimens is shown in Figure 37.

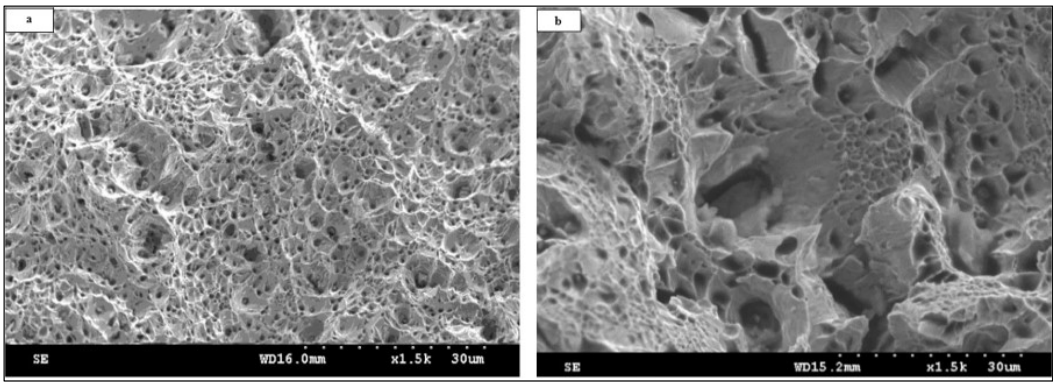

Figure 37 Fractographs of aged samples a (solution treated) b (H900) condition. [26]

The fracture surface of the specimen that is exposed to solution treated condition, shows ductile fracture mode. In addition, small equiaxed dimples are uniformly distributed on fracture surface. However, fracture surface of the specimen, which is exposed to H900 condition, is composed both cleavages/facets and dimple/voids on the fracture surface. This type of fracture mode is known as mixed mode of fracture or quasi-cleavage fracture.

High strength metallic materials are very sensitive to small defects in the microstructure which causes formation of stress concentration locally. Therefore, under cyclic loading, flaws or some none metallic inclusions with a size of a few microns may cause initiation of some micro-cracks. In 15-5 PH stainless steels, there exist ε- copper precipitates and some other non-metallic oxide inclusion in the microstructure. Although size of these particles is mostly controlled during manufacturing, it may cause initiation of cracks during cyclic loading.

Schönbaueret al. (2015) investigated the cause of crack initiation for 17-4 PH stainless steels after high cycle fatigue failure. The fatigue failure is initiated from a non-metallic inclusion in the interior part of the specimen. For these specimens, there is no any sign for the surface cracks so fatigue crack is grown in inside of the specimen until final failure. The size of the non-metallic inclusion may be seen in Figure 38.

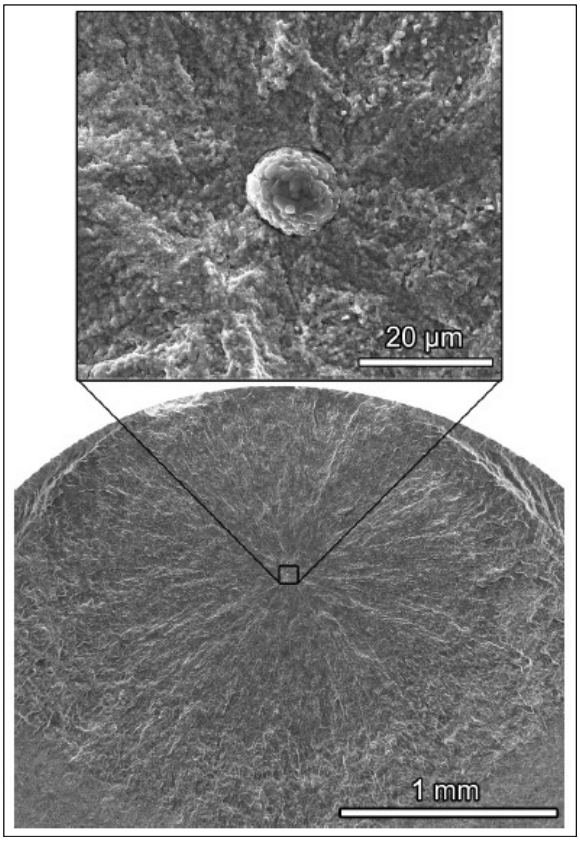

Figure 38 Observation of fatigue failure from internal inclusion [27].

There exists optically dark area (ODA) around the non-metallic inclusion that causes initiation of the fatigue failure. It is also very difficult to measure the size of this ODA area and this type of failure mode is known as fish-eye. SEM and optical micrographs for these ODA may be seen in Figure 39.

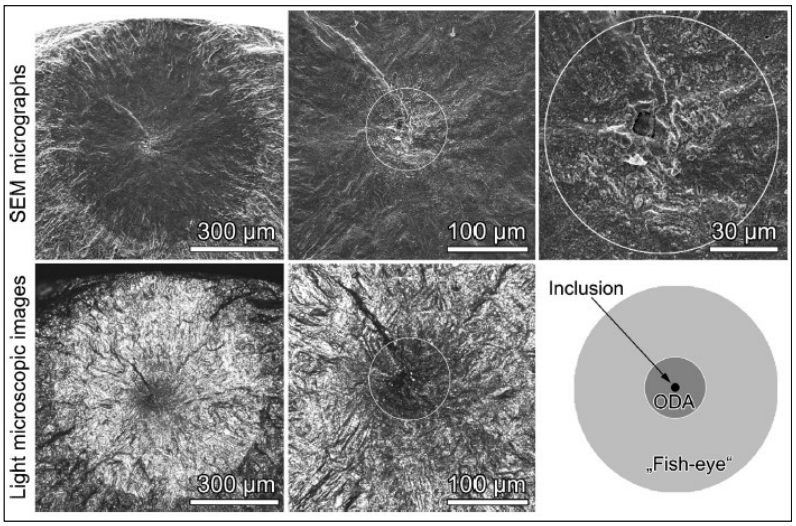

Figure 39 SEM and optical micrographs of a fish-eye fracture with ODA around a non-metallic inclusion. [28]

Murakami (2002) suggested that observation of the rough area around the fish- eye crack initiation site is higher for specimens that have exposed to higher number of cycle before failure. In addition, observation of this optically dark rough area may be caused by some environmental factor like penetration of hydrogen or oxygen during fatigue testing.

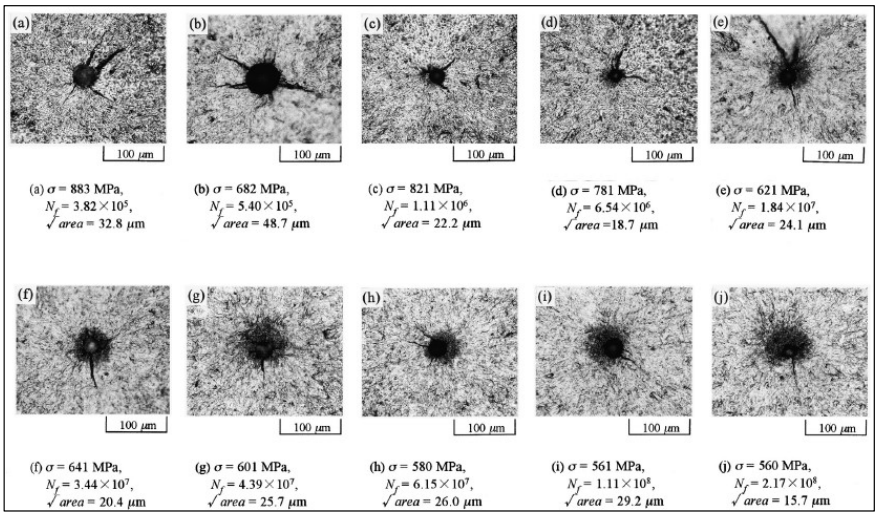

Figure 40 The size of dark areas (Optically Dark Area, ODA) in the vicinity of an inclusion at a fracture origin increases with increase in fatigue life. [29]

CHAPTER 3

EXPERIMENTAL PROCEDURE

3.1. MATERIAL

AMS5669 15-5 precipitation hardenable stainless steel was selected for the experiments. The chemical composition of the material was determined by using X-ray fluorescent (XRF) analyzers gun and presented in table 7.

Table 8 Chemical Composition for 15-5 PH Stainless Steels.

Chemical Composition	Percent % (XRF Results)
Iron	75.25
Chromium	15.37
Nickel	3.28
Copper	3.82
Manganese	0.85
Molybdenum	0.11
Niobium	0.34

3.2. SPECIMEN GEOMETRY

The material was in the form of a round bar which was manufactured by forging with a diameter of 25.4 mm. Thirty (30) disc shaped specimens with a thickness of 12 mm were cut from round bar 15-5 PH material for heat treatment experiments.

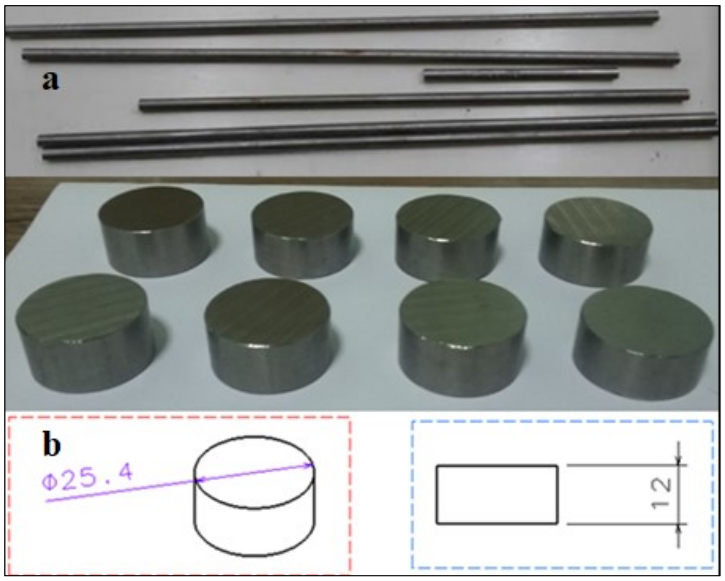

Figure 41 Round Bar 15-5 PH (a) and heat treatment specimen geometry (b).

In addition, forty six (46) specimens were manufactured for static and fatigue tests. Geometry for these specimens were determined according to ASTM E466 [30] standard that provide some design criteria for the specimen geometry to ensure observation of failure in the reduced (gage) section. Geometry for these specimens is presented in Figure 43.

Figure 42 Fatigue test specimens after machining.

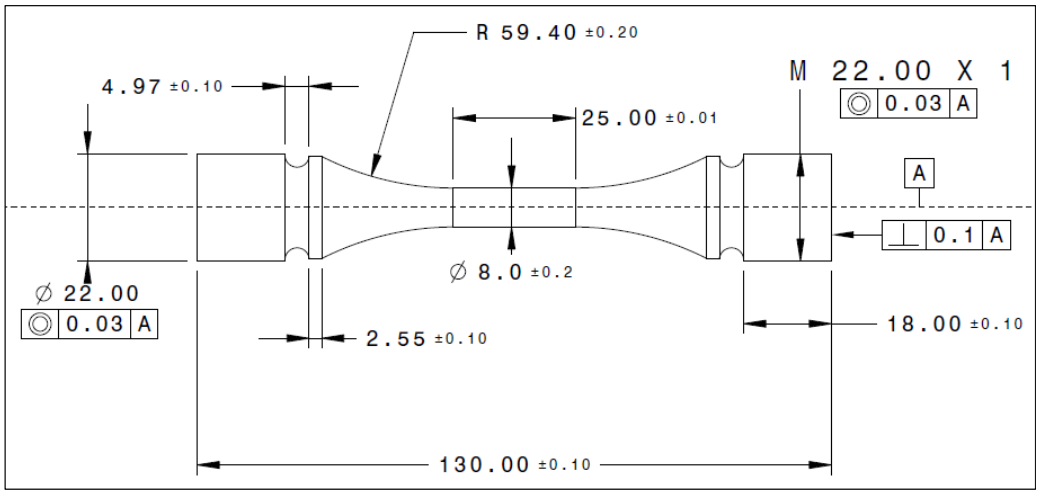

Figure 43 Technical drawing of static and fatigue test specimens.

3.3. HEAT TREATMENT PARAMETERS

Thirty (30) specimens were heat treated for determination of the parameters for homogenization, solutionizing and aging treatment steps. Heat treatment steps were consisted of homogenization, solutionizing and aging treatment that provides precipitation reaction. As it mentioned before, heat treatment was applied in six groups in order to see effect heat treatment parameters on microstructure, hardness and fatigue behavior of the 15- 5 PH stainless steel better. In brief, homogenization treatment was applied at 1150^0C for three different times 0.5, 1 and 3h. Solutionizing was applied at 1040^0C for time period 0.5h. Finally, aging treatment was applied at three different temperatures 400^0C, 480^0C and 550^0C with three different times 1, 4 and 70 hours**.** All heat treatments were performed at laboratory type of heat treating furnaces with max temperature capacity 1200^0C. After completing heat treatment all specimens were air cooled which is seen in Figure 44.

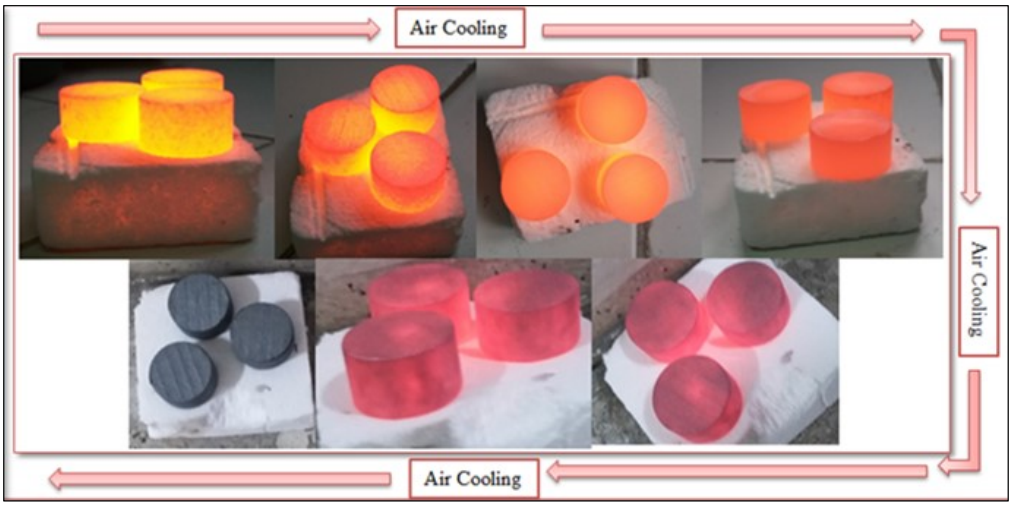

Figure 44 Heat treated specimens during air cooling.

Inıtially, specimens were separated six (6) groups before heat treatments ın order to compare results in terms of the heat treatment parameters on microstructure and hardness better. All disc shaped specimens were designated as SP-1 to SP-30 respectively before heat treatment.

3.3.1. GROUP-1 SPECIMENS

Five (5) specimens were heat treated in order to see the effects of the solutionizing and homogenization separately compared to as- received state.

Table 9 Applied heat treatment for group-1 specimens.

Specimens	As- received	Homogenization Treatment	Solution Treatment
SP-1	X	-	-
SP-2	-	-	1040^0C / 0.5h
SP-3	-	-	1040^0C / 2 h
SP-4	-	1150^0C / 0.5 h	-
SP-5	-	1150^0C / 1 h	-
SP-6	-	1150^0C / 3 h	-

3.3.2. GROUP-2 SPECIMENS

Three (3) specimens were heat treated at different homogenization time under the same solutionizing condition in order to see the effect of heat treatment time for homogenization.

Table 10 Applied heat treatment for group-2 specimens.

Specimens	Homogenization	Solution Treatment	Aging Treatment
SP-7	1150^0C / 0.5 h	1040^0C / 0.5 h	-
SP-8	1150^0C / 1 h	1040^0C / 0.5 h	-
SP-9	1150^0C / 3 h	1040^0C / 0.5 h	-

3.3.3. GROUP-3 SPECIMENS

Three (3) specimens were heat treated at different aging time under the same solutionizing condition without homogenization. These heat treatment conditions were applied to observe effect of different aging treatments for the same solutionizing condition.

Table 11 Applied heat treatment for group-3 specimens.

Specimens	Homogenizaiton	Solution Treatment	Aging Treatment
SP-10	-	1040^0C / 0.5 h	480^0C / 1 h
SP-11	-	1040^0C / 0.5 h	550^0C / 4 h
SP-12	-	1040^0C / 0.5 h	400^0C / 70 h

3.3.4. GROUP-4 SPECIMENS

Three (3) specimens were heat treated at the same solutionizing and homogenization time under different aging condition. This heat treatment group was determined in order to examine the effect of different aging treatments for the same solutionizing and homogenization condition.

Table 12 Applied heat treatment for group-4 specimens.

Specimens	Homogenization	Solution Treatment	Aging Treatment
SP-13	1150^0C / 0.5 h	1040^0C / 0.5 h	480^0C / 1 h
SP-14	1150^0C / 0.5 h	1040^0C / 0.5 h	550^0C / 4 h
SP-15	1150^0C / 0.5 h	1040^0C / 0.5 h	400^0C / 70 h

3.3.5. GROUP-5 SPECIMENS

Three (3) specimens were heat treated at the same solutionizing and homogenization times under different aging condition. The difference between these groups with group-4 is the time for homogenization.

Table 13 Applied heat treatment for group-5 specimens.

Specimens	Homogenization	Solution Treatment	Aging Treatment
SP-16	1150^0C / 1 h	1040^0C / 0.5 h	480^0C / 1 h
SP-17	1150^0C / 1 h	1040^0C / 0.5 h	550^0C / 4 h
SP-18	1150^0C / 1 h	1040^0C / 0.5 h	400^0C / 70 h

3.3.6. GROUP-6 SPECIMENS

Three (3) specimens were heat treated at the same solutionizing and homogenization time under different aging condition. Homogenization time for this group was selected as 3 hours in order to see the effect of homogenization time for the same solutionizing and aging conditions.

Table 14 Applied heat treatment for group-6 specimens.

Specimens	Homogenization	Solution Treatment	Aging Treatment
SP-19	1150^0C / 3 h	1040^0C / 0.5 h	480^0C / 1 h
SP-20	1150^0C / 3 h	1040^0C / 0.5 h	550^0C / 4 h
SP-21	1150^0C / 3 h	1040^0C / 0.5 h	400^0C / 70 h

3.4. METALLOGRAPHY

3.4.1. SPECIMEN PREPARATION

Specimens' surfaces were oxidized during heat treatments since there was no inert atmosphere for heating furnace. Specimens were ground by finer grits of emery paper (up to 2000grit) and then polished using a diamond paste of 3 µm particle size on a lapping wheel. Oxide layer that is formed during heat treatment was removed completely by grinding and polishing. Buehler trade grinding and polishing machine and emery papers were used during preparation of the metallographic specimens.

3.4.2. SPECIMEN ETCHING

Specimens were etched by using two different etchants which were Marble's and Kalling's with a composition given in ASTM E407 – 07 [31] standard in order to determine the more suitable etchant for examination of the microstructure and to reveal grain boundaries better.

Kalling's Etchant 5 gr CuCl2 100 ml Hydrochloric Acid 100 ml Ethanol	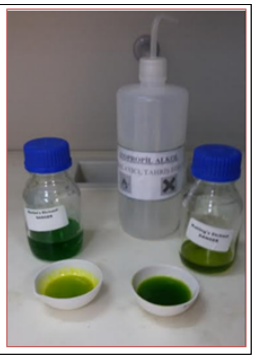
Marble's Etchant 10 gr CuSO4 50 ml Hydrochloric Acid 50 ml Distilled Water	

Figure 45 Etchants with chemical compositions.

3.5. GRAIN SIZE MEASUREMENT

Grain size analysis was performed according to ASTM E 112 [32] standard by using horizontal line approach for all heat treated specimens. Initially, grain size measurements were conducted automatically by the Lieca optical microstructure analysis tool. However, microstructures were so complex for too in order to identify grain boundaries correctly. Therefore, all measurements were done manually.

3.6. HARDNESS TEST

In order to determine the hardness, disc shaped specimens were used after microstructural analysis. Wizhard trade HR-521 (L) Series 810-Rockwell Type Hardness Testing Machines [33] was used and measurement carried out according to ASTM E18 – (16) [34] standard. 150 kgf load was applied through spheroconical diamond indenter at four different points on the specimen surface for 15 sec. Average of four measurements was taken as hardness value of specimens. Indenter surface was also examined under optical microscope in order to find diameter of spheroconical diamond indenter. According to Figure 46, it can be said that diameter was almost 600 µm.

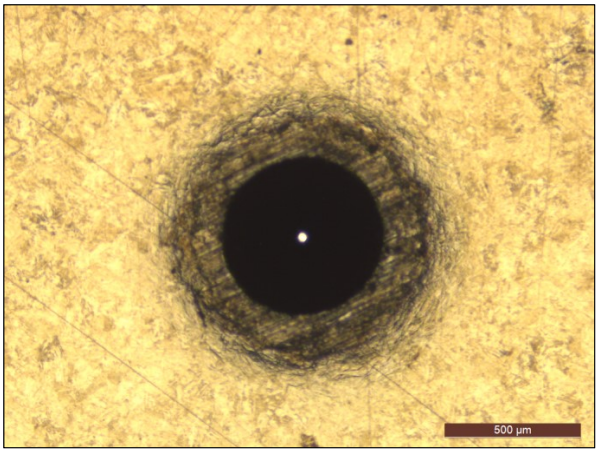

Figure 46 Optical microscope image for indented surface.

3.7. ROUGHNESS MEASUREMENT

Roughness is the important parameters that affect the fatigue test results of high strength steels. Before testing, surface roughness of the all fatigue test specimens were measured by Marsurf PS 10 mobile roughness measuring instrument [35]. Surface roughness values were measured by needle on the head of the movable part. This needle scans the surface of the specimen ± 5 mm on the specimen surface. Roughness measurement was done in Ra scale at three times and average of three measurements was taken as roughness value of specimens.

3.8. STATIC AND FATIGUE TESTS

Electromechanic universal tensile testing machine was used for static tests while magnetic resonant and servo-hydraulic fatigue testing machines were used for fatigue tests.

3.8.1. TENSILE TEST

Tensile tests were performed for one specimen of each selected heat treatment group in order to find ultimate tensile strength (UTS) value of the material. UTS value was used in construction of S-N curve. Tensile tests were performed on the INSTRON 5985 universal testing machine with 250 kN [38] loading capacity. Specimen was placed into the machine grips that apply 120 bar pressure to the specimen in order to prevent sliding during loading. Tensile loading was applied to the specimen with a constant crosshead speed 0.5 and 0.15 mm/min.

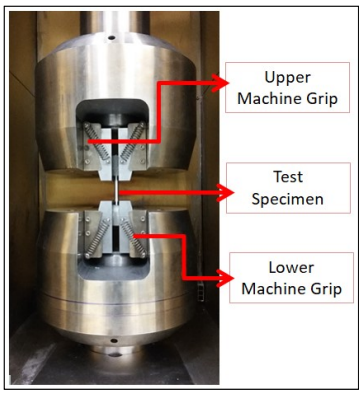

Figure 47 General view of INSTRON 5985 machine grips with tensile test specimen.

3.8.2. FATIGUE TEST

Fatigue tests were performed for selected specimen of heat treatment groups in order to construct S-N curve. All fatigue tests were carried under constant amplitude cyclic loading with a stress ratio (R) equal to –1 that is known as fully reversed fatigue loading. Fatigue test were conducted according to ASTM E-466 standard [30]. Applied cyclic load was in the form of sinusoidal wave. Fatigue tests were carried out by magnetic resonant and servo-hydraulic testing machines. INSTRON 8802

Servo-hydraulic testing machine was preferred for high loading condition in other words low cycle region (LCF) tests. These tests were conducted at 1 Hz frequency. On the other hand, RUMUL magnetic resonant fatigue testing machine [37] was preferred for the tests which were conducted at moderate testing loads in other words high cycle region (HCF) tests. Fatigue tests were carried at 140- 160 Hz frequency in magnetic resonant machine. Frequency was changing with testing loads and machine configuration. Loading capacity was 100kN for both servo-hydraulic and magnetic resonant testing machines.

In servo-hydraulic systems, specimen was placed into the machine grips similar to tensile test mentioned above then 120 bar pressure was applied to the specimen in order to prevent sliding during cyclic loading. On the other hand for magnetic resonant testing systems, specimen was placed in inserts then clamped. Clamps were screwed by hand torque to prevent formation of any gaps that negatively affect cyclic loading condition of testing systems.

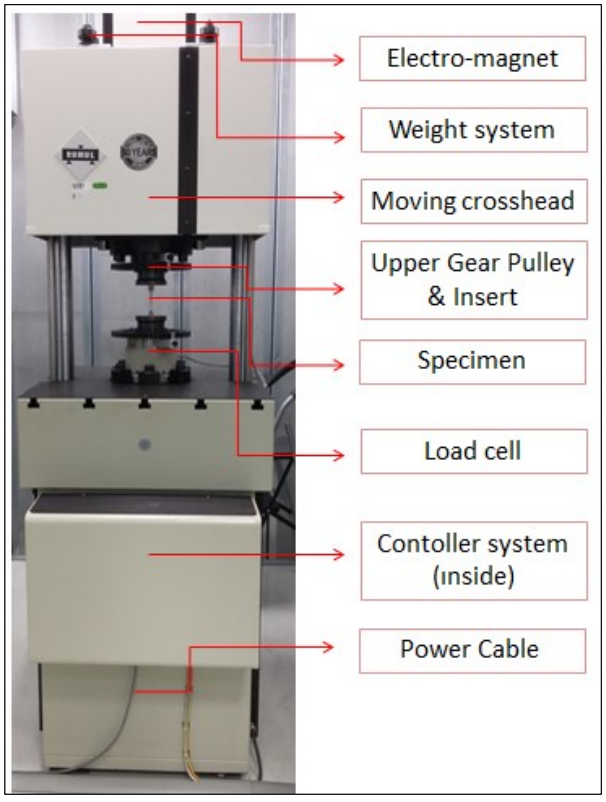

Figure 48 General view for RUMUL magnetic resonant testing machine grips. [37]

Magnetic resonant fatigue testing machine works at material natural resonant condition. Before, application of cyclic loading static mean load was applied by a spindle system that is actuated by a servo gearmotor then force is coupled by springs to the system. Dynamic loading of the specimens is done by a mechanical oscillating system. Oscillating system can be described by activated masses, elasticities and test specimen. There exists an electromagnet that activates the oscillating system. Test frequency can be changed by activating and deactivating masses in the system.

CHAPTER 4

RESULTS AND DISCUSSIONS

4.1. MICROSTRUCTURE OF THE SAMPLE

After heat treatment, microstructure of all specimens was examined under optical microscope and grain size measurement was conducted for all heat treated specimens. In order to determine more suitable etchant with optimum etching time, specimen, which is exposed to homogenization treatment at 1150^0C for 1h, was immersed in the Marble's and Kalling's etchants. Microstructures were examined after etching in every twenty (20) seconds under optical microscopes. Microstructures of the specimen may be seen in Figure 49 and Figure 50. According to microstructural image Marble's was selected as a suitable etchant since it revealed microstructure especially grain boundaries better compared to Kalling's etchant. Then all heat treated sample was etched by Marble's then examined under optical microscope for grain size analysis. Although lath martensite matrix was reached after cooling from homogenization and solution treatment, observed grain boundaries refer to prior austenite phase. Lath martensite phase becomes observable after aging treatment that provides observation of the lath martensite matrix phase. Therefore, all grain size measurements belong to prior austenite phase.

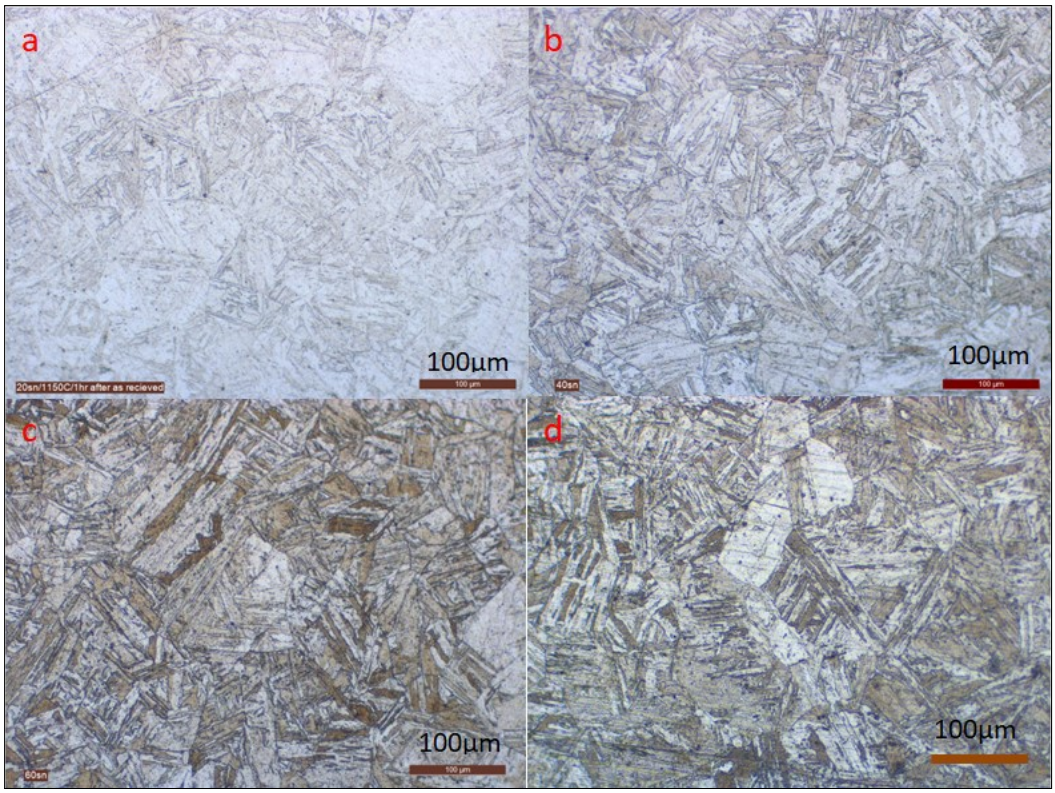

Figure 49 Optical microscope image for specimen As-received+ Homogenization at 1150^0C for 1 hour as a result of Marble's Etching with time a (20 seconds), b (40 seconds), c (60 seconds), d (80 seconds).

It can be said that sixty (60) seconds can be taken as the optimum etching time for these etchants to examine microstructure and reveal grain boundaries of the 15-5 PH stainless steels better under the optical microscope.

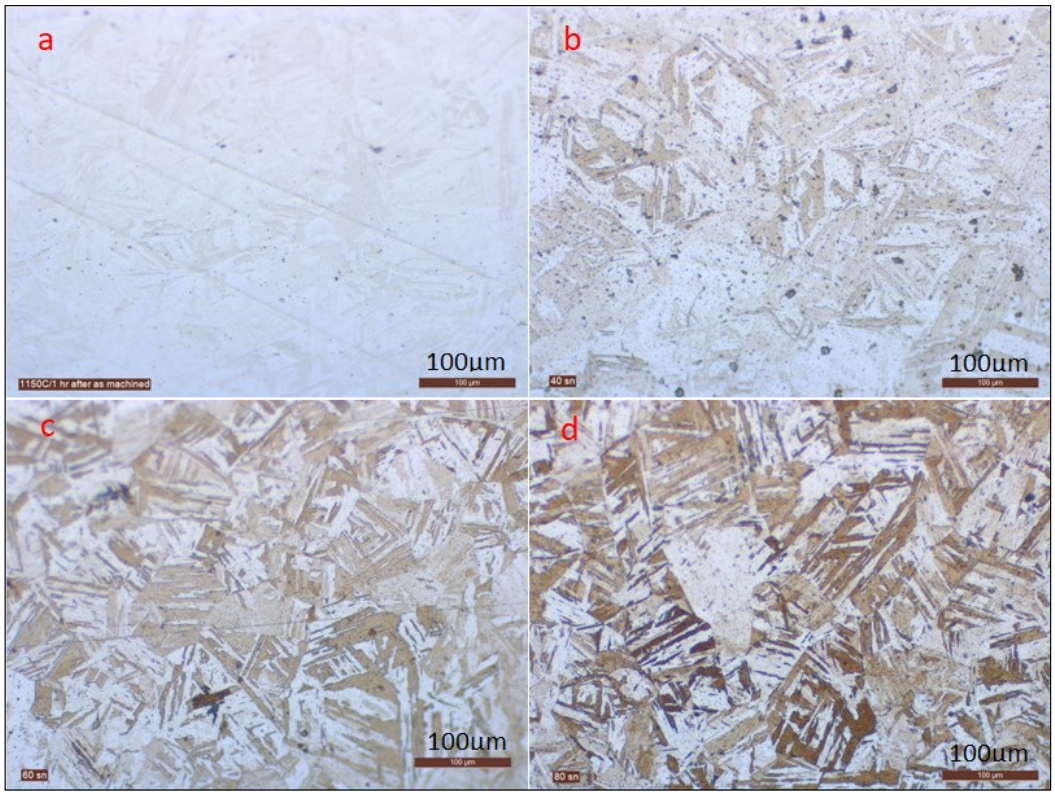

Figure 50 Optical microscope image for specimen As-received+ Homogenization at 1150^0C for 1 hour as a result of Kalling's Etching with time a (20 seconds), b (40 seconds), c (60 seconds), d (80 seconds)

Microstructure of 15-5 PH stainless steel was consisted lath martensite phase after homogenization and solution treatment followed by air cooling. However, after aging treatment microstructure was transformed to needle type of martensite which can be seen in Figure 51. This transformation can be explained by tempering of the lath martensite matrix during aging treatment. Increase of aging time leads to enhance fineness of the needle type of martensite structure. This transformation is explained by continuous rejection of carbon and other alloying elements from the martensite matrix that causes reduction of the tetragonality of the crystal structure as a result of tempering.

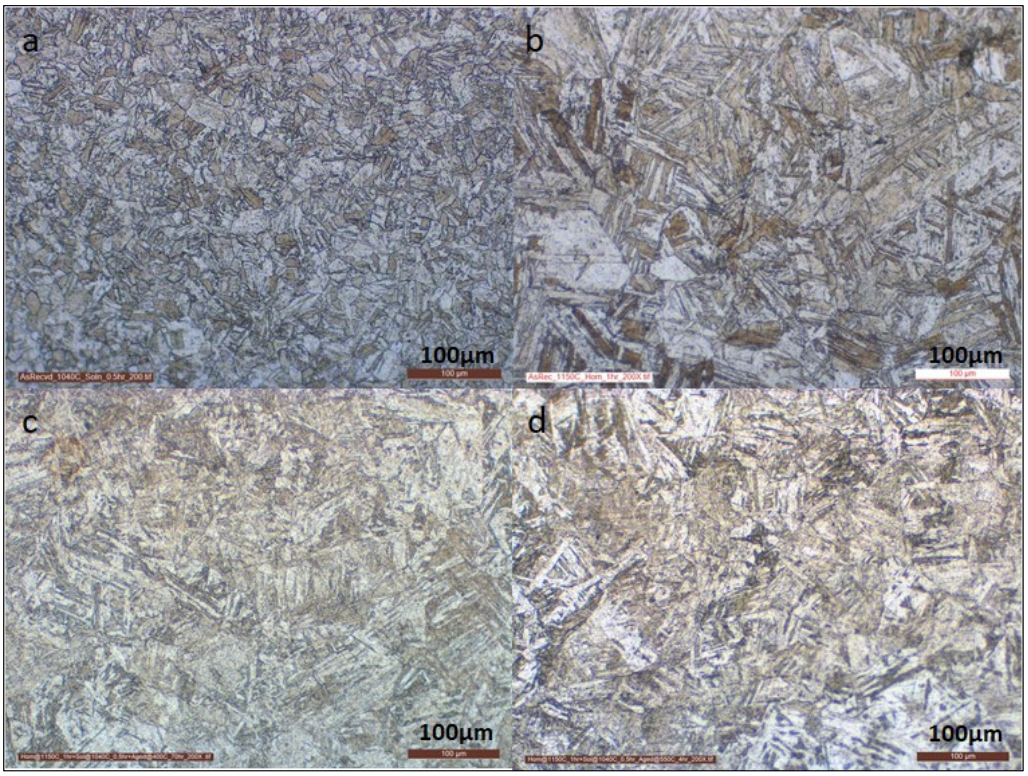

Figure 51 Optical microscope image for specimen (a) Sol. at 1040^0C/0.5h (b) Hom. at 1150^0C/1h (c) Hom. at 1150^0C/1h+ Sol. at 1040^0C/0.5h +Aged at 400^0C/70h (d) Hom. at 1150^0C/1h+ Sol. at 1040^0C/0.5h +Aged at 550^0C/4h

4.1.1. GRAIN SIZE MEASUREMENT RESULTS

After etching of the specimens, all heat treated samples were examined under optical microscope to measure the grain size. Grain size measurement was done in order to examine the relation between heat treatment parameters and grain size. All grain size measurements were performed by Lieca optical microstructure analysis tool according to ASTM E112 [32]. As it mentioned before identification of grain boundaries correctly was so difficult for optical microscope analysis tool. Therefore, all measurements were done manually according to procedure given below.

Average grain size measurement was conducted according to following steps [38];

Step-1: Several arbitrary test lines with specific length were drawn on the micrograph

Step-2: If grains were fully included on the line, it is counted as 1. If not, it is counted as 0.5.

Step-3: This counting process was conducted for eleven lines.

Step-4: Then, all counted data were summed and divided into number of test lines in order to determine average count for one test line.

Step-5: Test lines with specific length were divided number of average counts per line.

Step-6: Calculated length for one count was firstly converted to meter then divided by magnification of the micrograph in order to determine average grain size.

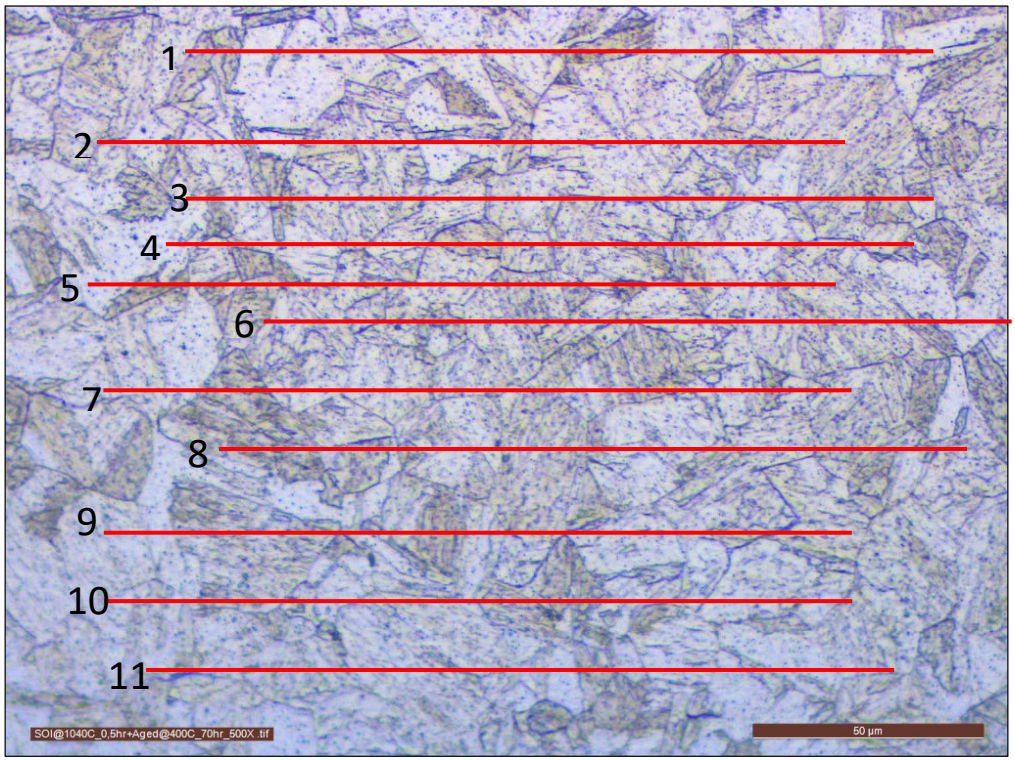

Figure 52 Optical microscope image for specimen which is solutionized at 1040^0C/0.5h +Aged at 400^0C/70h with arbitrary test lines with specific length

Step-1: Eleven lines were drawn with a 10 cm length.

Step-2& 3: Number of counts per line was calculated and shown in table Table 15.

Table 15 Calculation of total counts for grain size measurement analysis.

Number of Lines	Counts
1	0.5+1+1+1+1+1+1+1+1+0.5=10
2	0.5+1+1+1+1+1+1+1+1+1+0.5=11
3	0.5+1+1+1+1+1+1+1+1+1+1=11.5
4	0.5+1+1+1+1+1+1+1+1+1+0.5=11
5	0.5+1+1+1+1+1+1+1+1+1+0.5=11
6	0.5+1+1+1+1+1+1+1+1+1+0.5=11
7	0.5+1+1+1+1+1+1+1+0.5=9
8	0.5+1+1+1+1+1+1+1+1+1=10.5
9	0.5+1+1+1+1+1+1+1+0.5=9
10	0.5+1+1+1+1+1+1+1+1+1+0.5=11
11	0.5+1+1+1+1+1+1+1+1+0.5=10
Total Counts	115 counts in eleven (11) lines

Step-4: Number of average counts for one test line was calculated.

$$\text{Average Counts} = \frac{115}{11} = 10.45 \tag{4.1}$$

Step-5: Length of test line was divided number of average counts per line.

$$\frac{10cm}{10.45} = 0.96cm \tag{4.2}$$

Step-6: 0.96 cm was converted to meter $0.96*10^{-2}$ m. Then, it was divided to magnification.

$$\frac{0.96*10\text{^}(-2)\ \text{m}}{500} = 19.2 * 10^{-6}\text{m} = 19\mu\text{m} \tag{4.3}$$

These calculations were conducted for all heat treated specimens and results were presented in table 16.

Table 16 Grain size measurement results.

Heat Treatment Groups		Homogenization Treatment	Solution Treatment	Aging Treatment	Average Grain Size (μm)
Group-1	SP-1	As-Received Condition			26
	SP-2		1040^0C / 0.5h		23
	SP-3		1040^0C / 2h		19
	SP-4	1150^0C / 0.5h	-	-	28
	SP-5	1150^0C / 1h	-	-	36
	SP-6	1150^0C / 3h	-	-	30
Group-2	SP-1	1150^0C / 0.5h	1040^0C / 0.5h	-	26
	SP-2	1150^0C / 1h	1040^0C / 0.5h	-	29
	SP-3	1150^0C / 3h	1040^0C / 0.5h	-	28
Group-3	SP-1	-	1040^0C / 0.5h	480^0C / 1h	24
	SP-2	-	1040^0C / 0.5h	550^0C / 4h	22
	SP-3	-	1040^0C / 0.5h	400^0C / 70h	19
Group-4	SP-1	1150^0C / 0.5h	1040^0C / 0.5h	480^0C / 1h	25
	SP-2	1150^0C / 0.5h	1040^0C / 0.5h	550^0C / 4h	24
	SP-3	1150^0C / 0.5h	1040^0C / 0.5h	400^0C / 70h	28
Group-5	SP-1	1150^0C / 1h	1040^0C / 0.5h	480^0C / 1h	26
	SP-2	1150^0C / 1h	1040^0C / 0.5h	550^0C / 4h	29
	SP-3	1150^0C / 1h	1040^0C / 0.5h	400^0C / 70h	28
Group-6	SP-1	1150^0C / 3h	1040^0C / 0.5h	480^0C / 1h	32
	SP-2	1150^0C / 3h	1040^0C / 0.5h	550^0C / 4h	24
	SP-3	1150^0C / 3h	1040^0C / 0.5h	400^0C / 70h	23

As it mentioned before, measured grain size values belong to prior austenite grains that was formed during homogenization and solution treatment. There was no significant difference between the grain size values for different heat treatment conditions. All heat treatment steps which were homogenization, solutionizing and aging treatments provide nearly the same grain size value for 15-5 PH stainless steels. Grain size values changes between 20 to 35 μm for 15-5 PH stainless steels. These values are consistent with the values given in the literature that is presented in chapter 2.

4.2. HARDNESS TEST RESULTS

As it mentioned before, ın 15-5 PH stainless steels, mechanism of strengthening is provided by some precipitates and carbide which are formed during heat treatment. The main element is copper that provides formation of the precipitates during aging. Aging treatment provides precipitation of ε-copper precipitates that are spherical in shape and coherent with the matrix and principally provide strengthening in this alloy. Precipitation sequence is described as formation of coherent body centered cubic (BCC) Cu-rich clusters initially then transform into intermediate 9R structure before finally transforming into the incoherent face centered cubic (FCC) precipitates. The typical size of these Cu precipitates in the coherent state is of the order of 2–5nm [9].

In order to examine effect of heat treatment parameters on the hardness of the 15-5 PH stainless steel, hardness tests were conducted for all specimens after completing grain size measurements. Hardness measurement provided very consistent results in terms of effect the heat treatment parameters for 15-5 PH stainless steel compared to grain size analysis results. Hardness measurement results are presented in Table 17 with standard deviation errors.

Table 17 Hardness test results

Heat Treatment Groups		Homogenization Treatment	Solution Treatment	Aging Treatment	Hardness (HRC)
Group-1	SP-1	As-Received Condition			34.3± 0.4
	SP-2		1040^0C / 0.5h		29.8± 0.1
	SP-3		1040^0C / 2h		28.4± 0.1
	SP-4	1150^0C / 0.5h	-	-	31.1± 0.4
	SP-5	1150^0C / 1h	-	-	31.4± 0.2
	SP-6	1150^0C / 3h	-	-	31.7± 0.2
Group-2	SP-1	1150^0C / 0.5h	1040^0C / 0.5h	-	28.3± 0.6
	SP-2	1150^0C / 1h	1040^0C / 0.5h	-	28.9± 0.7
	SP-3	1150^0C / 3h	1040^0C / 0.5h	-	31.1± 0.5
Group-3	SP-1	-	1040^0C / 0.5h	480^0C / 1h	41.3± 0.3
	SP-2	-	1040^0C / 0.5h	550^0C / 4h	36.7± 0.1
	SP-3	-	1040^0C / 0.5h	400^0C / 70h	46.4± 0.3
Group-4	SP-1	1150^0C / 0.5h	1040^0C / 0.5h	480^0C / 1h	43.6± 0.3
	SP-2	1150^0C / 0.5h	1040^0C / 0.5h	550^0C / 4h	35.6± 0.2
	SP-3	1150^0C / 0.5h	1040^0C / 0.5h	400^0C / 70h	46.2± 0.3
Group-5	SP-1	1150^0C / 1h	1040^0C / 0.5h	480^0C / 1h	43.7± 0.3
	SP-2	1150^0C / 1h	1040^0C / 0.5h	550^0C / 4h	35.8± 0.6
	SP-3	1150^0C / 1h	1040^0C / 0.5h	400^0C / 70h	46.5± 0.6
Group-6	SP-1	1150^0C / 3h	1040^0C / 0.5h	480^0C / 1h	43.8± 0.1
	SP-2	1150^0C / 3h	1040^0C / 0.5h	550^0C / 4h	36.8± 0.6
	SP-3	1150^0C / 3h	1040^0C / 0.5h	400^0C / 70h	47.1± 0.1

Initially, heat treatment material condition was not known for as-received material. However, as- received materials may be exposed to H-1100 (Solutionzed at 1040^0C for 0.5 hour + Aged at 593^0C for 4 hour) which provides 33- 34 HRC hardness for 15-5 PH stainless steel according to table 3.

Homogenization and solution treatment process consists of a relatively high-temperature treatment that provides dissolving of precipitates and alloying elements by forming a supersaturated solid solution. When we compare the hardness value for solutionized or homogenized specimens with as received condition, there is a

decrease in the hardness value. As it mentioned before, hardening phenomena for precipitation hardenable stainless steels directly related to strain field around ε-Cu precipitations that obstruct the motion of the dislocations. At high temperature, all precipitates and other intermetallic dissolve in the solid solution. Then, lath martensitic microstructure is formed after homogenization and solutionizing followed by air cooling. Although there exist very high density of the dislocations in the lath martensitic microstructure, hardness value is generally low since after homogenization or solutionizing, there are no strengthening phase in the matrix.

It can be also said that increase in time for homogenization and solution treatment for the same temperature does not lead to significant change on hardness of the 15-5 PH stainless steel. However, it may be expected that increase in time keeping for these treatment, more precipitates and other hardening elements dissolve so hardness may decrease more. According to hardness test results of group-2, it can be said that application of the homogenization before solution treatments does not have more effects on hardness. 15-5 PH stainless steels may include some δ-delta ferrite phase that has detrimental effect on mechanical properties. Increase in time for homogenization decreases the volume fraction of the delta ferrite phase and change of the phase morphology from elongated to spherical [13]. Therefore, three different time period for homogenization treatment was applied during heat treatment condition.

According to hardness test results it can be said that, main hardening for 15-5 PH stainless steels was provided by aging treatment. When aging treatment is applied, supersaturated solid solution allows formation of the ε-copper precipitates. When we compared to aging treatment at 480^0C with 550^0C for 4h, there is very high number of ε-copper precipitates with smaller size. At lower aging temperature and time period, there is not enough driving force solute atoms for diffusion and to form precipitates. This phenomenon causes formation of high number of precipitates with smaller size. Therefore, motion of the dislocation becomes much difficult due to more strain field formed around the precipitate in lath martensite matrix. Thus, hardness increase more compared to aging treatment 550^0C for 4h.

The decrease of hardness may be explained by growth of ε-copper precipitates and reformation of the austenite in the microstructures. Growth of size of precipitates cause decrease on the probability of the pinning of dislocations that leads to decrease on hardness. On the other hand, areas around copper precipitates may contain some austenite forming elements like Ni and Fe. Segregation of these elements on the surround of ε-copper precipitates provides formation of austenite stable region. These regions behave nucleation sites for austenite phases since they have the same fcc structure with the similar lattice parameter. It is s also known that solubility of the Cu in austenite is higher than lath martensite matrix so increase in temperature drive solubility of the precipitates on the reformed austenite region thus hardness of 15-5 PH stainless steels decreases more.

According to hardness test results, aging treatment at 400^0C for 70h provide peak hardness value for 15-5 PH stainless steels. As it mentioned before, it may be formed some delta ferrite phase in the microstructure that is formed during manufacturing. Aging treatment at 400^0C for 70h provides another precipitation reaction which takes place on the δ-delta ferrite phase thus provide more increase on hardness of the 15-5 PH stainless steels.

4.3. TENSILE TEST RESULTS

In order to see the effect of heat treatment parameters on tensile and fatigue strength, group-5 specimens were selected. As it mentioned before, forty six (46) specimens were manufactured for three different groups of group-5 specimens. Detail number of specimens for static and fatigue test can be seen in Table 18.

After heat treatment, tensile tests were applied ın order to see the effect of heat treatment parameters on ultimate tensile strength. The main reason for performing tensile test was determination of UTS that was used for stress value at fırst cycle in S-N curve construction step for 15-5 PH stainless steel. Locating of the UTS value on S-N curve provides more accurate curve shape especially at low cycle region.

Table 18 Hardness, types and number of specimens for static and fatigue tests

Specimen Group	Heat Treatment Conditions	# of Static Specimen	# of Fatigue Specimen	Hardness (HRC)
Group-1	Hom. at 1150^{0}C for 1hr + Sol. at 1040^{0}C for 0.5hr + Aged at 550^{0}C for 4hr	1	20	35.8± 0.6
Group-2	Hom. at 1150^{0}C for 1hr + Sol. at 1040^{0}C for 0.5hr + Aged at 480^{0}C for 1hr	1	11	43.7± 0.3
Group-3	Hom. at 1150^{0}C for 1hr + Sol. at 1040^{0}C for 0.5hr + Aged at 400^{0}C for 70hr	1	12	46.5± 0.6

Tensile tests were conducted for one specimen of each group. Stress versus strain curves is exhibited in Figure 53.

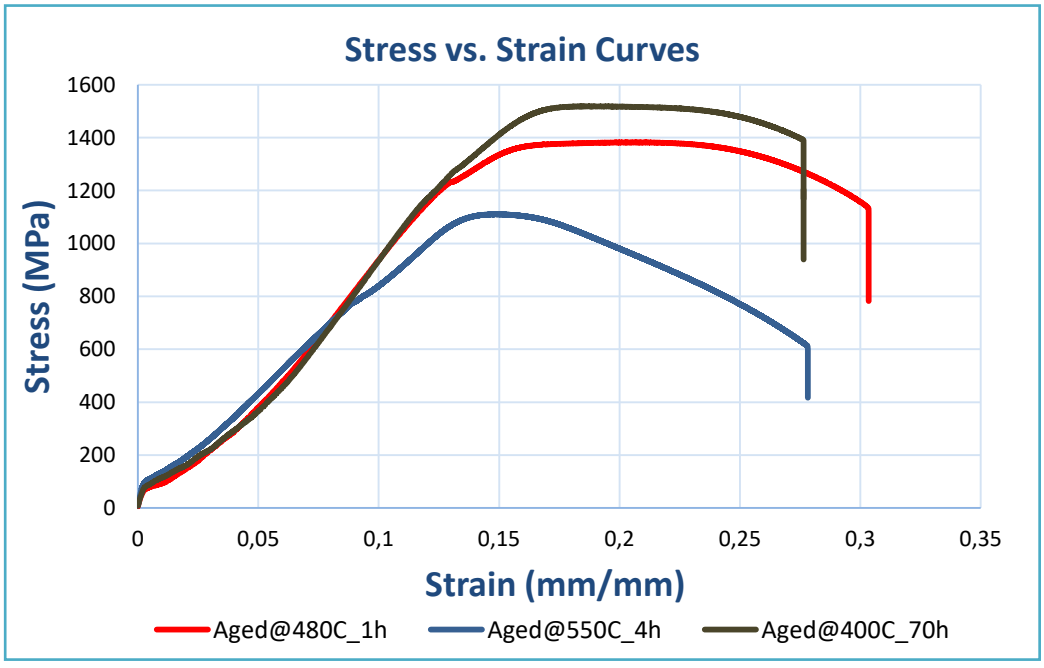

Figure 53 Stress vs. strain curve for group-5 tensile test specimens.

During tensile tests, crosshead speed for specimen which was exposed to aging treatment at temperature 550^{0}C for one hour was 0.15 mm/min while for others tensile loading was applied with a constant crosshead speed 0.50 mm/min. Therefore,

there exists difference in curve shape of stress vs. strain curves. As it mentioned before, the main purpose of tensile test application was finding ultimate tensile strength value of the 15-5 stainless steels after different heat treatment condition. Ultimate tensile strength values were used in S-N curve construction.

Table 19 Tensile test and hardness results.

Specimen Group	Hardness (HRC)	Max Load (kN)	UTS (MPa)	Strain at Max Load (mm/mm)	Strain at Failure (mm/mm)
Group-1	35.8± 0.6	55.8	1110	0.149	0.278
Group-2	43.7± 0.3	69.4	1381	0.199	0.303
Group-3	46.5± 0.6	76.3	1517	0.183	0.276

Moreover, increase in UTS causes decrease on the extension value according to comparison of results of group-2 and group-3. Tensile test results for specimens which are exposed to aging treatment at 550^0C for 4h and 480^0C for 1h are almost the same with the results given literature in chapter 2. Therefore, it can be said that, suitable heat treatment conditions were applied in terms of temperature and time period. In addition, tensile test result for specimen that is exposed to aging treatment at 400^0C for 1h is highest compared to other. This value can be explained by precipitation reaction in the delta ferrite phase which provides more strengthening for 15-5 PH stainless steels. According to tensile test results, it can be also said that there exist direct relation between hardness and ultimate tensile strength of the material. Therefore, the effect of heat treatment parameters on tensile strength of the 15-5 PH stainless steels is almost the same with effect on hardness in terms of time and temperature period for homogenization, solutionizing and aging treatment.

There exist also an approximate relationship between the hardness and the tensile strength of the high strength steels that were given in below equation (4.4). The relation between hardness and ultimate tensile strength for the specimens can also be corrected by the equation below.

$$\mathrm{UTS(MPa)} = (3.38 * \mathrm{HB}, \langle \mathrm{HB} > 175 \rangle) \text{ [39]} \quad (4.4)$$

where:

HB= Hardness of the materials in Brinnell Scale,

According to equation 4.4, hardness and tensile strength values were compared for tensile tested specimens in order to show results which are compatible with this approximation.

Table 20 Actual and approximated UTS values

Specimen Group	Hardness (HRC)	Hardness (HB)	Actual Ultimate Tensile Strength [MPa]	Approximated Ultimate Tensile Strength [MPa]
Group-1	35.8± 0.6	335	1110	1132
Group-2	43.7± 0.3	410	1381	1386
Group-3	46.5± 0.6	442	1517	1494

It can be said that, the approximation that is given in equation 4.4 is almost accurate for hardness and tensile test results for 15-5 PH stainless steel used in experiments.

4.4. SURFACE ROUGHNESS MEASUREMENT RESULTS

It is known that fatigue test results were much affected by manufacturing and surface condition of the test specimens. Therefore, the same machining parameters were used for specimen manufacturing to reach similar surface roughness vales that has more effects on fatigue behavior for high strength steels.

After manufacturing surface roughness values in Ra scale were measured for all three groups of specimens ın order to prevent formation of the scatter due to surface condition before fatigue test.

4.4.1. SURFACE ROUGHNESS RESULTS FOR GROUP-1 SPECIMEN

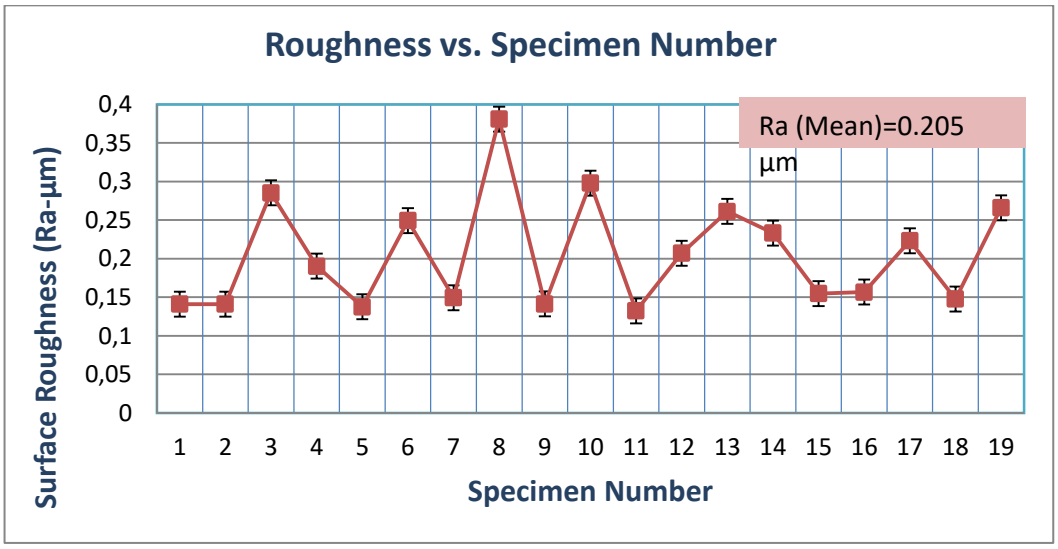

Surface roughness value was changing between 0.132 to 0.381 µm for group-1 specimens.

4.4.2. SURFACE ROUGHNESS RESULTS FOR GROUP-1 SPECIMEN

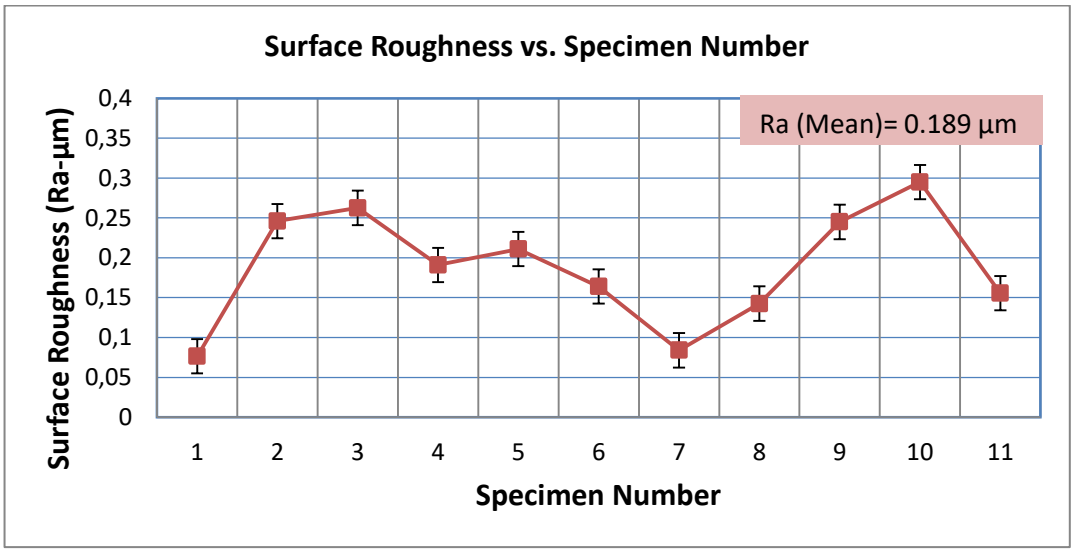

Surface roughness value was changing between 0.076 to 0.295 µm for group-2 specimens.

4.4.3. SURFACE ROUGHNESS RESULTS FOR GROUP-1 SPECIMEN

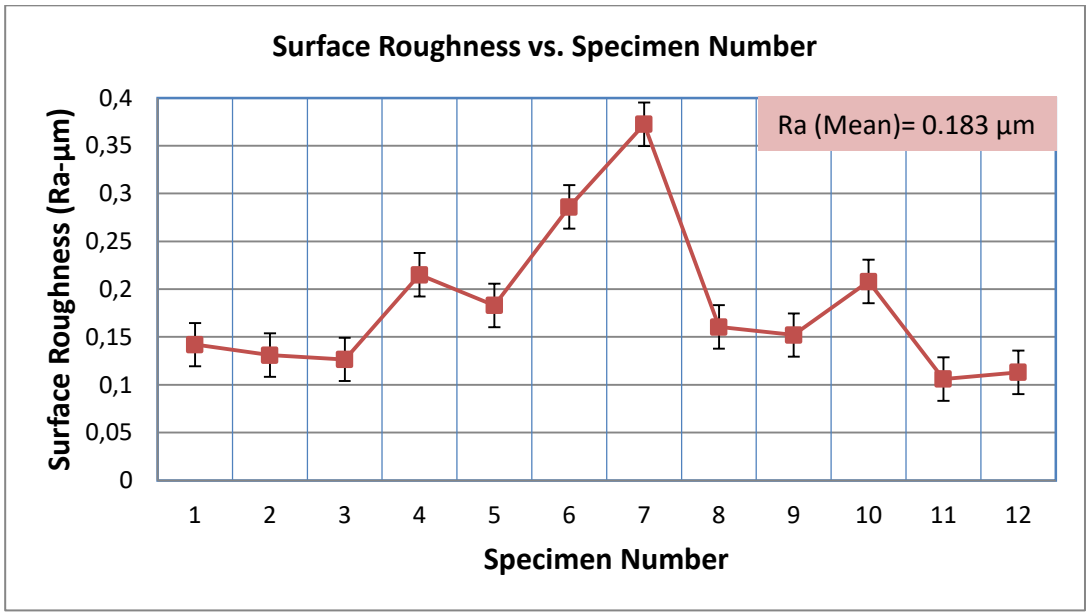

Surface roughness value was changing between 0.106 to 0.373 µm for group-3 specimens.

When the average values for surface roughness are compared, there is not much difference between surface roughness values that cause formation of the scatter on fatigue test results. The effect of the surface roughness on fatigue strength of high strength steels as a reduction factor may be shown in Figure 54. According to Figure 54, if the surface roughness value is lower than 0.25 micron there is no reduction on fatigue strength of high strength steels. According to our surface roughness measurement results, it can be said that there is no effect of surface roughness on fatigue behavior of 15-5 PH stainless steels for this study. However, there exist some deviations in surface roughness of specimens in the same group. This may cause formation of some scatter in fatigue test results.

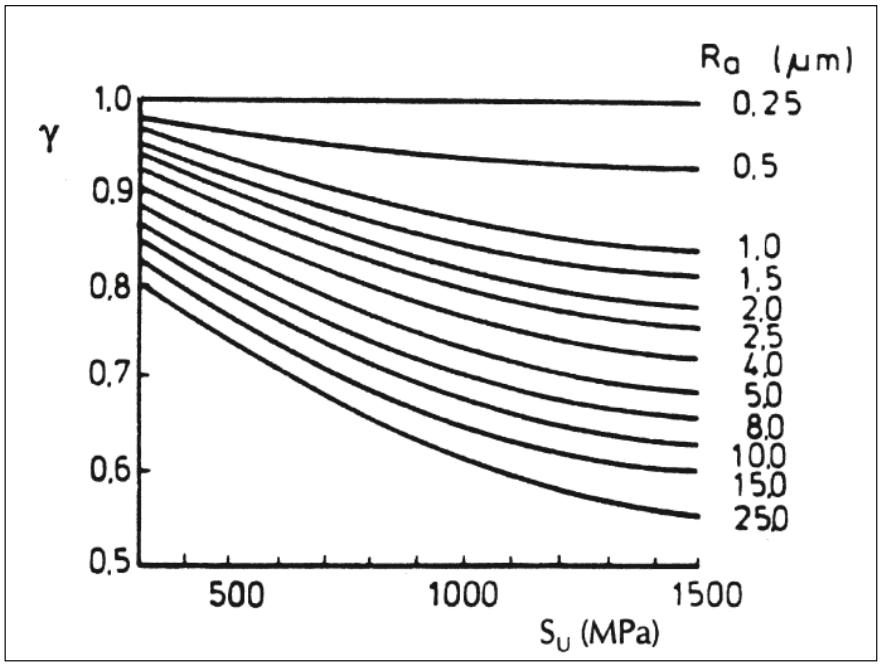

Figure 54 Surface roughness reduction factor γ for high strength steels as a function of Ra (average surface roughness) and the tensile strength. [19]

4.5. FATIGUE TEST RESULTS

Fatigue behavior for 15-5 PH stainless steels was examined for three different groups of group-5 specimens that were presented in table 18. Fatigue behavior for these three groups is considered according to S-N curve construction by calculating fatigue limits.

All the specimens were executed with the same procedure constant amplitude cyclic loading according to ASTM E466 – 15 testing standard [30]. The run-out criteria was chosen as 1.0 E+07 cycles. In addition, test was terminated according to observation of the visible cracks on specimen surface or 1.0 E+07 cycles for run-out specimens.

As it mentioned before S-N curve was constructed according to AGARD-AG-292 HELICOPTER FATIGUE DESIGN GUIDE [24]. In addition fatigue limit was also calculated according to staircase method that is given in ISO 12107 International Standard (Metallic materials — Fatigue testing — Statistical planning and analysis of data) [25].

4.5.1. FATIGUE TEST RESULTS FOR GROUP-1 SPECIMENS

Twenty (20) specimens were tested in order to construct S-N curves according to procedure that was defined in section 2.8.1.

Table 21 Fatigue test results for group-1 specimens (15-5 PH Stainless Steels exposed to Hom.@1150^{0}C /1h + Sol.@1040^{0}C /0.5h + Aged 550^{0}C /4h)

Specimen No	Stress [Mpa]	Life [cycle]	Frequency [Hz]	log (Std. Dev. At) $1.0x10^7$	Stress at $1.0x10^7$ [Mpa]	R^2
SP-1	760	13.251	156	0.034	441	0.954
SP-2	760	12.192	155			
SP-3	710	46.276	158			
SP-4	710	57.783	158			
SP-5	610	120.019	157			
SP-6	510	135.921	159			
SP-7	510	713.442	158			
SP-8	460	867.472	159			
SP-9	440	11.000.000	159			
SP-10	440	11.000.000	159			
SP-11	460	135921	159	**Std. Dev. of Stress @1.0x10^7**		
SP-12	440	11.000.000	158	33		
SP-13	460	10.000.065	159			
SP-14	440	11.000.000	145			
SP-15	840	18.458	1			
SP-16	840	10.049	1			
SP-17	940	6.347	1			
SP-18	940	7.161	1			
SP-19	610	181.943	159			
SP-20	440	11.000.000	159			
SP-21 (Static)	1110	1	-			

According to fatigue test results, fatigue limit ($1.0x10^7$) was determined as 441MPa for the specimens that were exposed to heat treatment (Hom.@1150^{0}C /1h +

Sol.@1040^{0}C /0.5h + Aged 550^{0}C /4h). It is needed to define outliers before construction of S-N curve.

As it mentioned before outlier criteria was determined according to normal probability plot that was mentioned in detail in section 2.8.3.

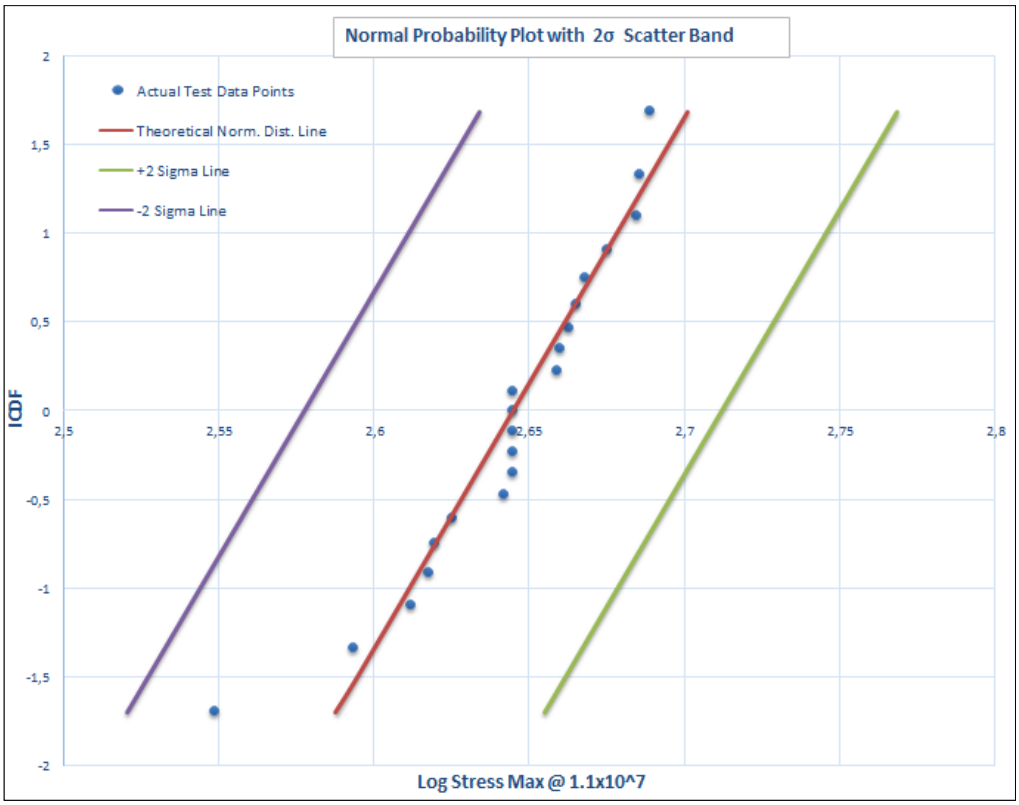

Figure 55 Normal probability plot for group-1 specimens (15-5 PH Stainless Steels exposed to Hom.@1150^{0}C /1h + Sol.@1040^{0}C /0.5h + Aged 550^{0}C /4h)

Normal probability plot was drawn according to 2σ (St. Dev. of log Stress @1.0x10^7). It can be seen that all test data remain in defined scatter band therefore all results were used in S-N curve construction.

4.5.1.1. FATIGUE LIMIT CALCULATION BY STAIRCASE METHOD FOR GROUP-1 SPECIMENS

It is also possible to calculate fatigue limit by staircase method that was explained in detail in section 2.8.2. This calculation usually provides the double check on fatigue

limit value that was found according to four (4) parameter best fitting technique. The increment value is generally taken between 5 to 10 percent of the fatigue limit that is found after 4 parameter best fitting techniques or standard deviation. 20 MPa was determined as increment value in staircase sequence.

First Run-Out Data	Staircase Stress Squence						Fictious Data	Stress Level [MPa]	Fatigue Limit
	460		460		460		460	460	451
440		440		440		440		440	

Figure 56 Fatigue limit calculation by staircase method for group-1 specimens (15-5 PH Stainless Steels exposed to Hom.@1150^{0}C /1h + Sol.@1040^{0}C /0.5h + Aged 550^{0}C /4h)

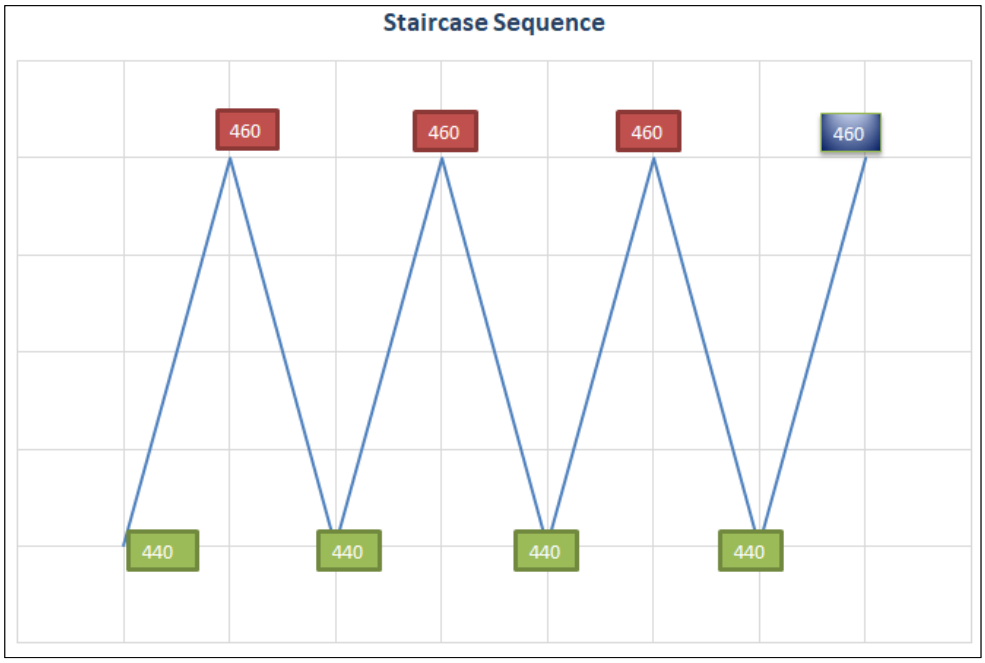

Figure 57 Staircase sequence for group-1 specimens (15-5 PH Stainless Steels exposed to Hom.@1150^{0}C /1h + Sol.@1040^{0}C /0.5h + Aged 550^{0}C /4h)

Fatigue limit value that was calculated according to staircase method is 451MPa. This value is very close to fatigue limit value which was calculated according to four parameter best fitting technique.

4.5.2. FATIGUE TEST RESULTS FOR GROUP-2 SPECIMENS

Eleven (11) specimens were tested in order to construct S-N curves according to procedure that was defined in section 2.7.

Table 22 Fatigue test results for group-2 specimens (15-5 PH Stainless Steels exposed to Hom.@1150^{0}C /1h + Sol.@1040^{0}C /0.5h + Aged 480^{0}C /1h)

Specimen No	Stress [Mpa]	Life [cycle]	Frequency [Hz]	Std. Dev. of log Stress @1.0x10^7	Stress @1.0x10^7 [Mpa]	R^2
SP-1	710	280.082	161	0.057	519	0.903
SP-2	1160	3.397	1			
SP-3 (Static)	1381	1	-			
SP-4	610	1.729.986	161			
SP-5	560	10.087.227	161			
SP-6	860	12.561	159	**Std. Dev. of Stress @10^7**		
SP-7	760	183.800	161	61		
SP-8	560	99.152	161			
SP-9	510	4.604.306	161			
SP-10	460	11000000	162			
SP-11	510	437761	161			
SP-12	860	40534	160			

According to fatigue test results, fatigue limit (1.0x10^7) was determined as 519MPa for the specimens that were exposed to heat treatment (Hom.@1150^{0}C /1h + Sol.@1040^{0}C /0.5h + Aged 480^{0}C /1h). It is needed to define outliers before construction of S-N curve the same procedure was applied for group-2 specimens.

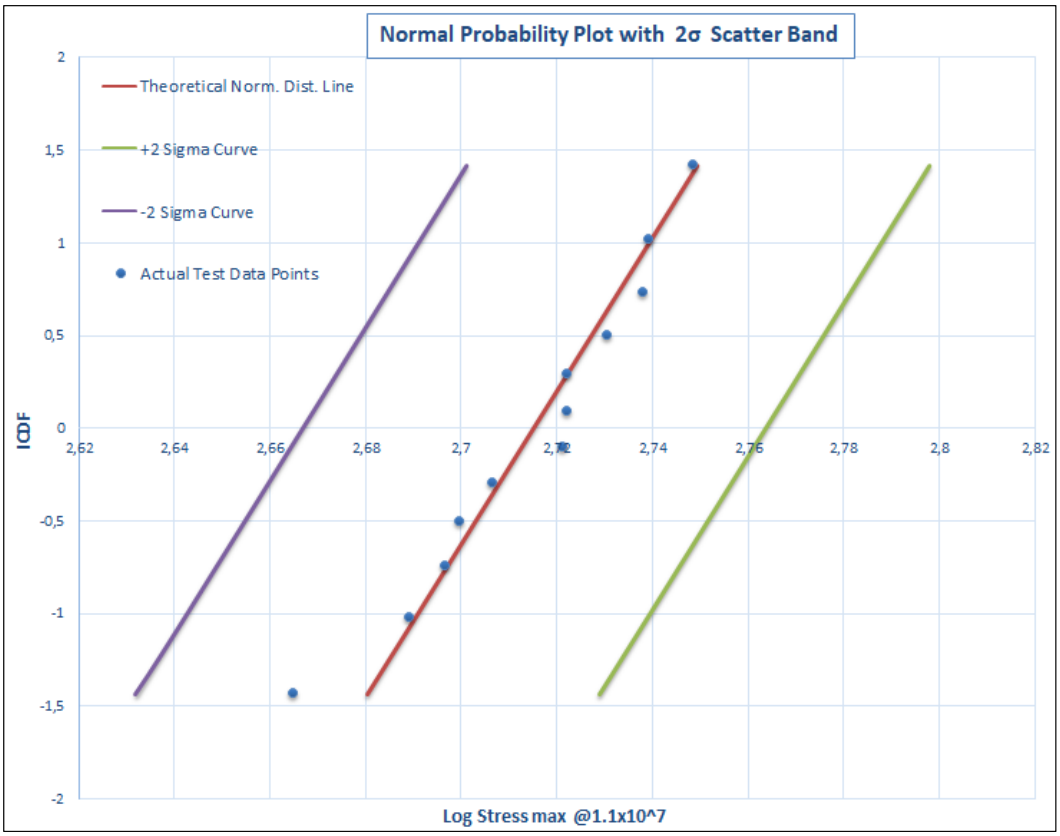

Figure 58 Normal probability plot for group-2 specimens (15-5 PH Stainless Steels exposed to Hom.@1150^{0}C /1h + Sol.@1040^{0}C /0.5h + Aged 480^{0}C /1h)

It can be seen that all test data remain in defined scatter band therefore all results were used in S-N curve construction.

4.5.2.1. FATIGUE LIMIT CALCULATION BY STAIRCASE METHOD FOR GROUP-2 SPECIMENS

Fifty (50) MPa was determined as increment value in staircase sequence according to fatigue limit that was found according to four parameter best fitting technique.

First Run-Out Data	Staircase Stress Squence					Fictious Data	Stress Level [MPa]	Fatigue Limit
	610						610	
		560					560	
560			510		510		510	518
				460		460	460	

Figure 59 Fatigue limit calculation by staircase method for group-2 specimens (15-5 PH Stainless Steels exposed to Hom.@1150^{0}C /1h + Sol.@1040^{0}C /0.5h + Aged 480^{0}C /1h)

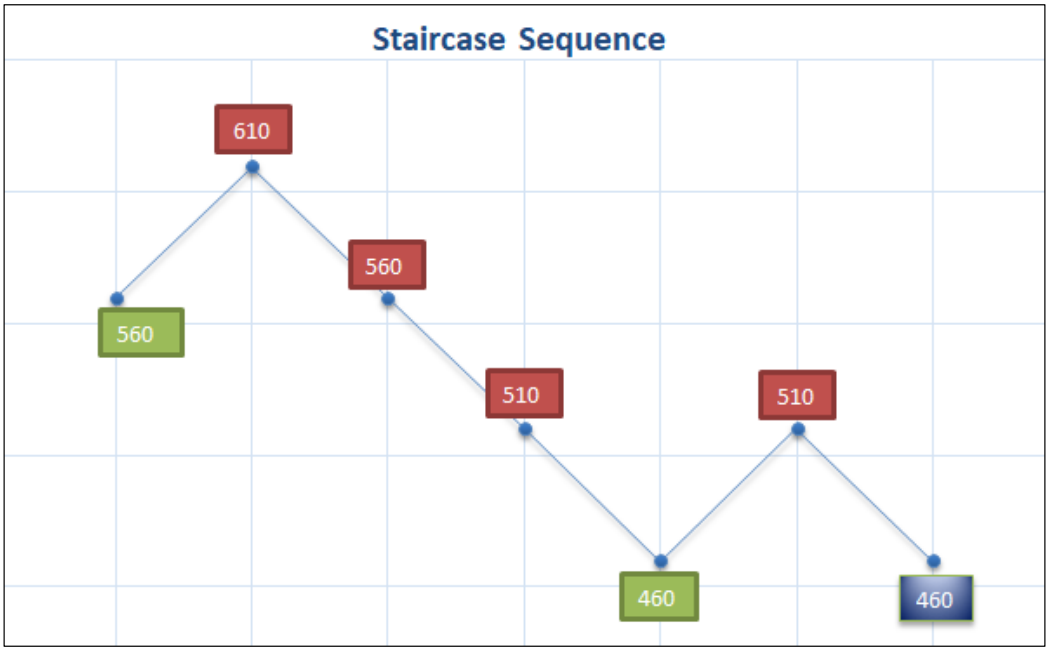

Figure 60 Staircase sequence for group-2 specimens (15-5 PH Stainless Steels exposed to Hom.@1150^{0}C /1h + Sol.@1040^{0}C /0.5h + Aged 550^{0}C /4h)

Fatigue limit value that was calculated according to staircase method is 519 MPa. This value is the same as the fatigue limit which was calculated according to four parameter best fitting technique.

4.5.3. FATIGUE TEST RESULTS FOR GROUP-3 SPECIMENS

Twelve (12) specimens were tested in order to construct S-N curves according to procedure that was defined in section 2.7

Table 23 Fatigue test results for group-3 specimens (15-5 PH Stainless Steels exposed to Hom.@1150^{0}C /1h + Sol.@1040^{0}C /0.5h + Aged 400^{0}C /70h)

Specimen No	**Stress [Mpa]**	**Life [cycle]**	**Frequency [Hz]**	**Std. Dev. of log Stress @1.0x10^7**	**Stress @1.0x10^7 [Mpa]**	**R^2**
SP-1	860	51.206	156	0.054	493	0.958
SP-2	760	113.644	161			
SP-3	610	1.759.600	159			
SP-4	560	7.433.969	162			
SP-5	510	113.197	162			
SP-6	460	11.000.000	160			
SP-7	510	1.009.078	161	**Std. Dev. of Stress @10^7**		
SP-8	460	11.000.000	160	54		
SP-9	460	11.000.000	162			
SP-10	510	11.000.000	161			
SP-11	1360	1032	1			
SP-12	1160	3976	1			
SP-13 (static)	1517	1	-			

According to fatigue test results, fatigue limit (1.0x10^7) was determined as 493 MPa for the specimens that were exposed to heat treatment (Hom.@1150^{0}C /1h + Sol.@1040^{0}C /0.5h + Aged 400^{0}C /70h). It is needed to define outliers before construction of S-N curve the same procedure was applied for group-3 specimens.

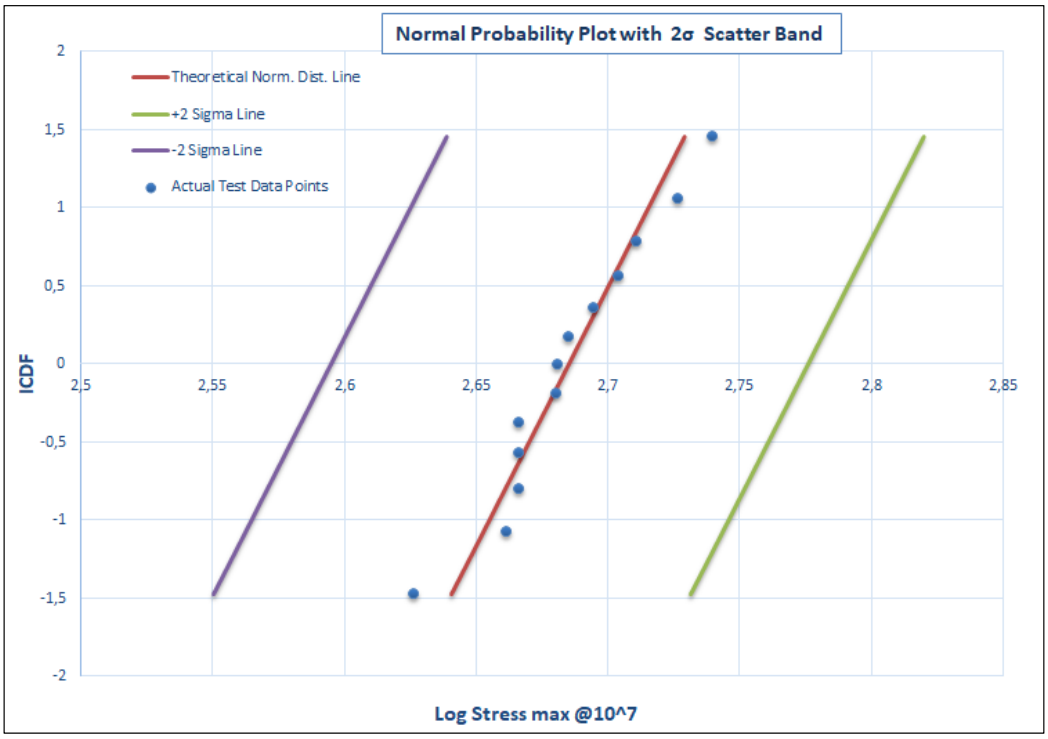

Figure 61 Normal probability plot for group-3 specimens (15-5 PH Stainless Steels exposed to Hom.@1150^{0}C /1h + Sol.@1040^{0}C /0.5h + Aged 400^{0}C /70h)

It can be seen that all test data remain in defined 2σ (St. Dev. of log Stress @1.0x10^7) scatter band therefore all results were used in S-N curve construction.

4.5.3.1 FATIGUE LIMIT CALCULATION BY STAIRCASE METHOD FOR GROUP-3 SPECIMENS

Fifty (50) MPa was determined as increment value in staircase sequence according to fatigue limit.

First Run-Out Data	Staircase Stress Squence						Fictious Data	Stress Level [MPa]	Fatigue Limit
						560	510	560	503
460	510		510		510			510	
		460		460				460	

Figure 62 Fatigue limit calculation by staircase method for group-3 specimens (15-5 PH Stainless Steels exposed to Hom.@1150^{0}C /1h +Sol.@1040^{0}C /0.5h +Aged 400^{0}C /70h)

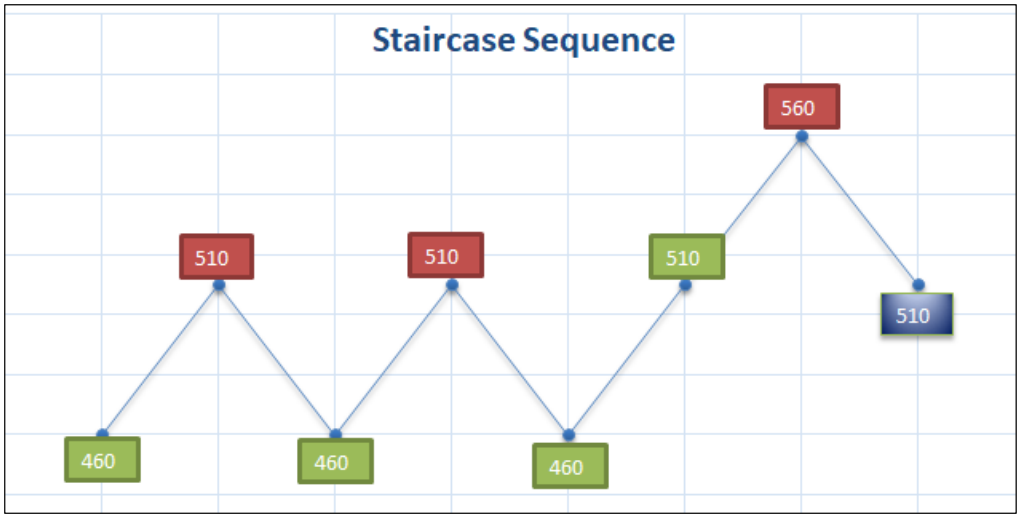

Figure 63 Staircase sequence for group-3 specimens (15-5 PH Stainless Steels exposed to Hom.@1150^{0}C /1h + Sol.@1040^{0}C /0.5h + Aged 400^{0}C /70h)

Fatigue limit value that was calculated according to staircase method is 503 MPa. This value is very close to fatigue limit value which was calculated according to four parameter best fitting technique.

4.5.4. COMPARISON OF S-N CURVES

Stress versus life (S-N) curves were constructed according to the same procedure that was given is section 2.8.1.

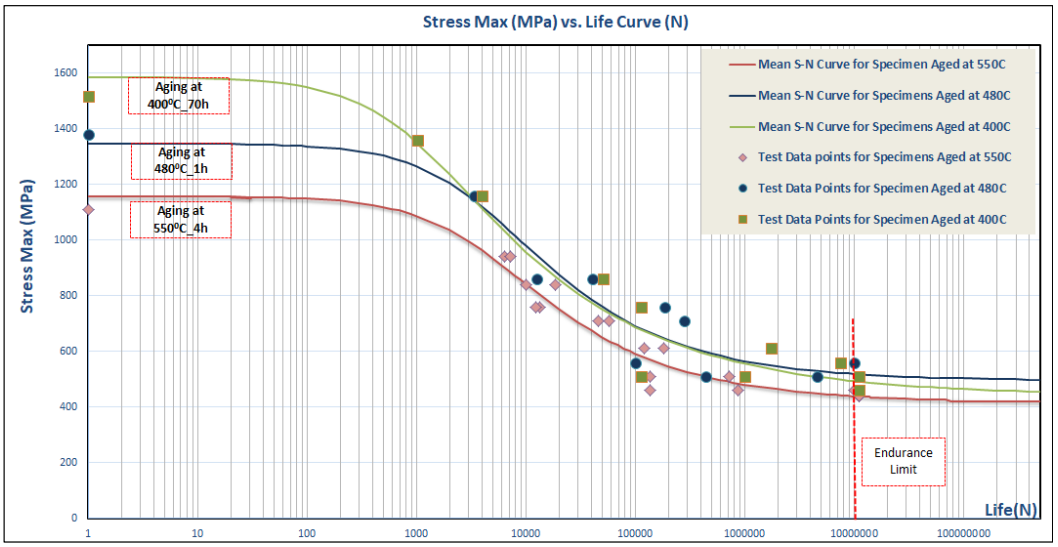

Figure 64 Stress versus life (S-N) curves for three groups of group-5 specimens.

According to fatigue test results of three groups of group-5 specimens, heat treatment parameters have significant effects on fatigue behavior of 15-5 precipitation hardenable stainless steels. Fatigue limit value for aging treatment at temperature 480^0C for 1h has higher fatigue limit compared to aging treatment at 550^0C for 4h. This difference on the fatigue limit can be explained by precipitation of copper. As it mentioned before, at lower aging temperature (480^0C) with lower time (1h), there exist high number ε-cupper precipitates with smaller size. In addition, it can be also said that there exist a direct relation between hardness and fatigue limit of 15-5 PH stainless steels that are exposed to aging treatment at 480^0C for 1h and at 550^0C for 4h. According to fatigue limit calculations, changing aging treatment parameters from 550^0C for 4h to 480^0C for 1h, fatigue limit of 15-5 PH stainless steel may be increased by 15% (15 percent). In addition, if aging treatment parameters are changed to 400^0C for 70h, fatigue limit may be increased by 11% (11 percent).

In addition, hardness does not always show direct relation with fatigue strength for 15-5 PH stainless steels. Specimens, which were exposed aging treatment at temperature 400^0C for 1h, have higher hardness value compared to specimens that were exposed to aging treatment at temperature 480^0C for 1h. However, fatigue limit for these specimens is lower. This inverse relation may be explained by susceptibility

of the material against formation of fatigue crack on surface of the materials. It is known that degree of formation of surface damage depends not only on processing steps but also on strength of the material. Materials with higher strength are more susceptible to formation surface damage. It also known that in crack initiation period, fatigue is a material surface phenomenon for as machined state. Therefore, increase in susceptibility on surface defects; decreases fatigue strength of the material. This relation can be explained by Figure 65.

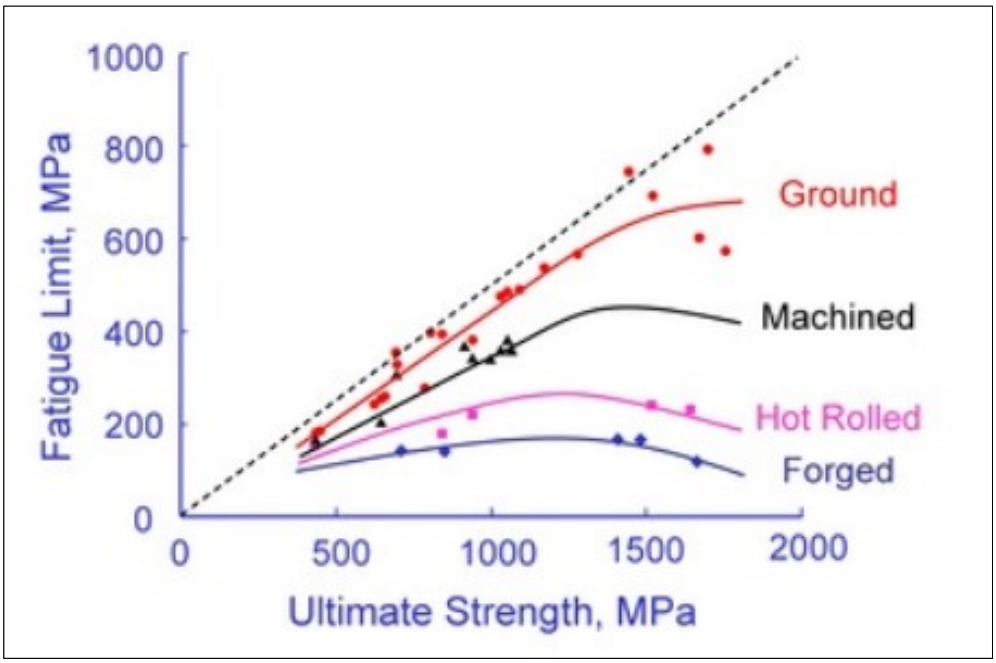

Figure 65 Relation between surface condition and ultimate tensile strength (UTS) on fatigue limit for high strength steels. [40]

4.6. FRACTURE SURFACE ANALYSIS RESULTS

Fracture surface analysis is important in order to interpret static and fatigue test results better. Therefore, fracture analysis was conducted for tensile test specimens in order to classify fracture modes and determination of crack initiation site for several fatigue tested specimens. Scanning Electron Microscopy (SEM) and Energy Dispersive X-Ray analysis (EDX) was used in order to determine the cause of failure in the microstructure.

4.6.1. FRACTURE SURFACE ANALYSIS RESULTS FOR TENSILE TEST SPECIMENS

Fracture surface analysis was conducted by scanning electron microscopy (SEM) and energy dispersive x-ray analysis (EDX).

4.6.1.1. FRACTURE SURFACE ANALYSIS RESULTS FOR GROUP-1 SPECIMENS

Ductile fracture (cup and cone) type fracture mode was observed for the specimen which is exposed to aging treatment at 550^0C for 4h. SEM analysis was also conducted for detail analysis.

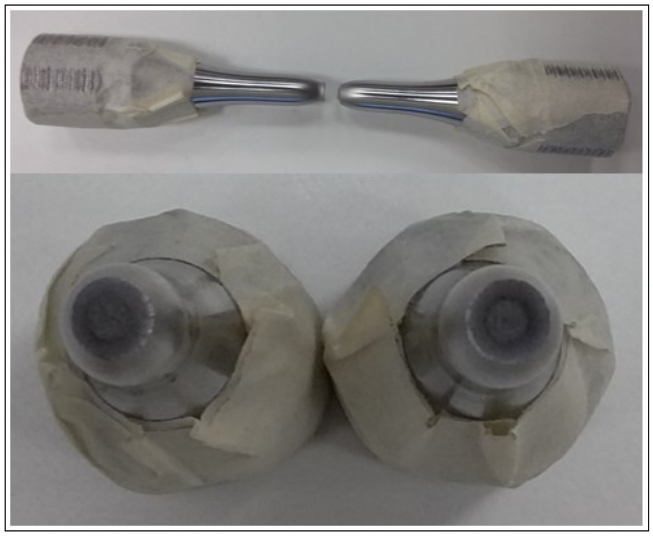

Figure 66 Cup-and-cone type fracture surface for tensile tested specimen (SP-21)

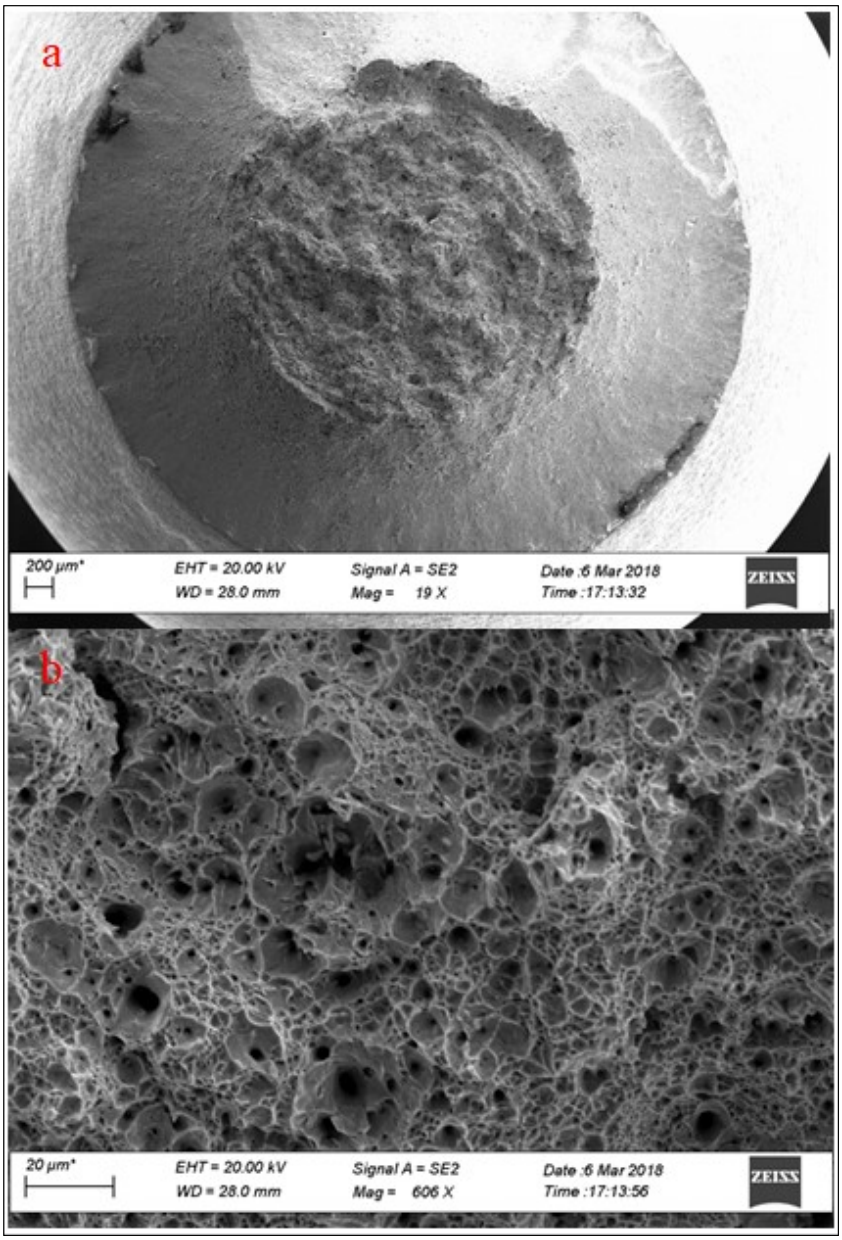

Figure 67 SEM micrograph showing (a) general view of fracture surface (b) equiaxed dimples on fracture surface of tensile tested specimen (SP-21)

According to SEM micrograph, equiaxed dimples were observed all-around of the fracture surface of the group-1 tensile test specimen.

There were some intermetallics, which may be seen in Figure 68, inside of the equaxied dimples with the size around 1µm.

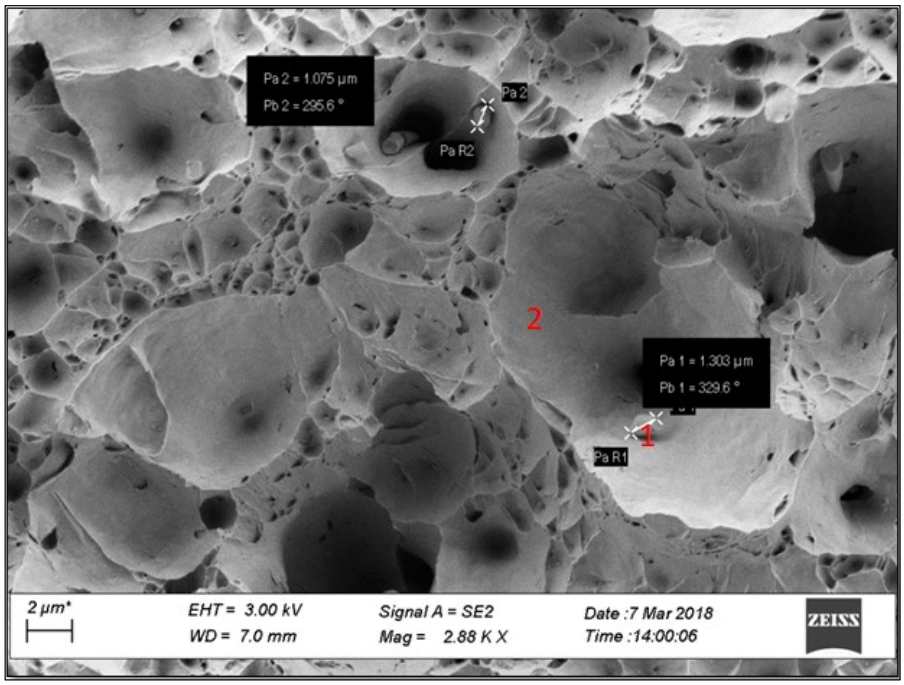

Figure 68 SEM micrograph showing equiaxed dimples with some intermetallic inside for tensile tested specimen (SP-21)

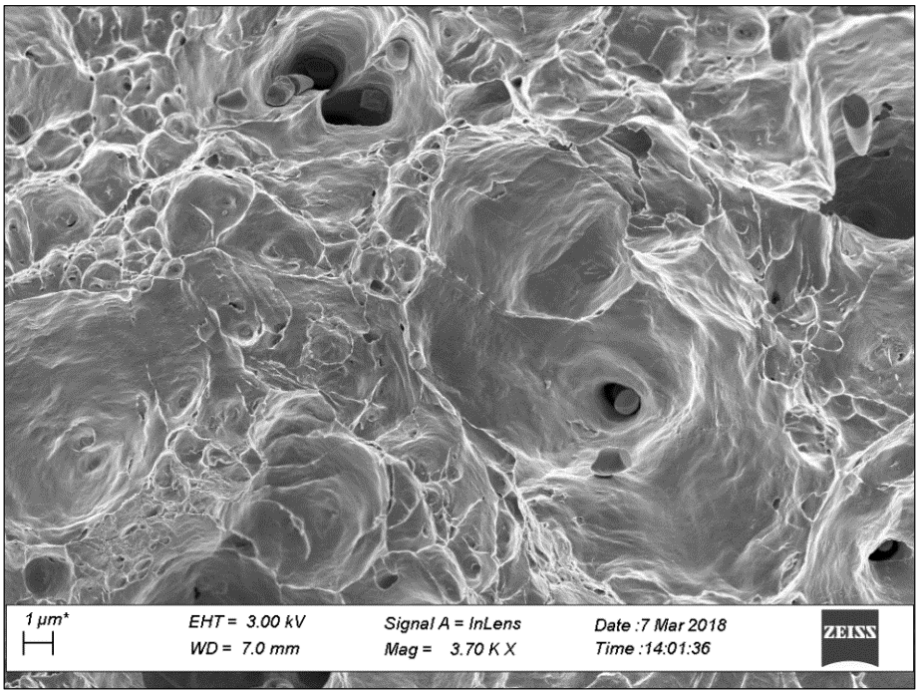

Figure 69 SEM image with in-lens detector for tensile tested specimen (SP-21)

EDX analysis was conducted for the points 1 and 2, which are shown on Figure 68, in order to determine chemical composition of the intermetallic and matrix phase.

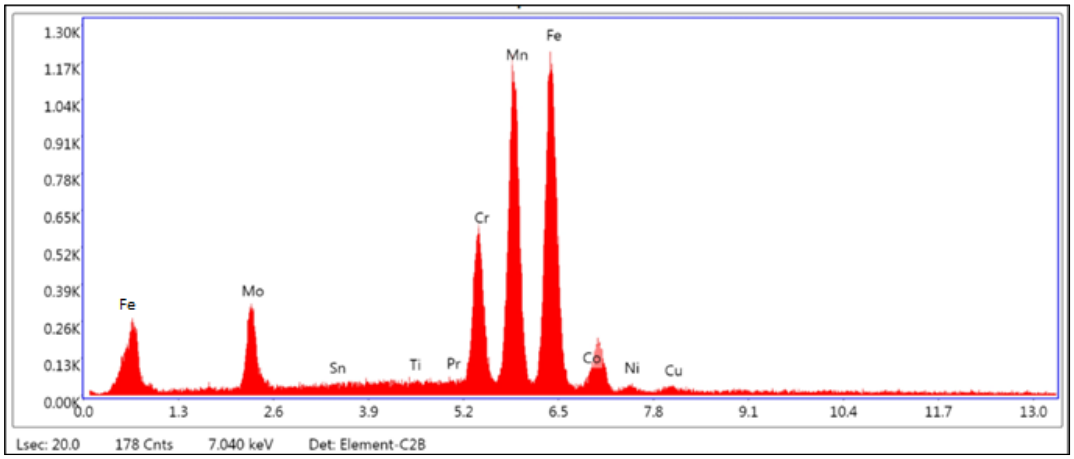

Figure 70 EDX analysis results for point-1(intermetallic)

Table 24 Quantitative elemental analysis results for point-1(intermetallic)

Quantity Analysis Results for Point-1		
Element	Weight (%)	Atomic (%)
MoL	5.85	3.52
SnL	1.04	0.51
TiK	1.04	1.26
PrL	2.79	1.14
CrK	13.84	15.36
MnK	32.65	34.28
FeK	39.26	40.55
CoK	1.58	1.54
NiK	0.86	0.85
CuK	1.10	0.99

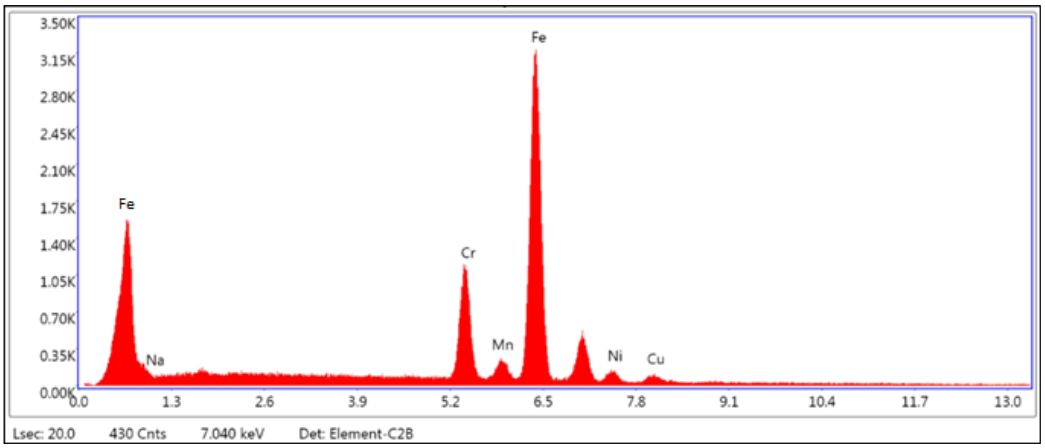

Figure 71 EDX analysis results for point- 2 (matrix phase).

Table 25 Quantitative elemental analysis results for point-2 (matrix phase).

Quantity Analysis Results for Point-2		
Element	Weight (%)	Atomic (%)
NaK	2.31	5.39
CrK	17.24	17.79
MnK	1.35	1.32
FeK	72.99	70.11
NiK	3.37	3.08
CuK	2.74	2.32

According to EDX analysis, it can be said that intermetallic may be composed by manganese and ıron. In addition, chemical composition of the matrix phase is nearly the same with the composition which is found by X-ray fluorescent (XRF) analyzers gun.

4.6.1.2. FRACTURE SURFACE ANALYSIS RESULTS FOR GROUP-2 SPECIMENS

Flat fracture surface was observed for the specimen which is exposed to aging treatment at 480^0C for 1h. SEM analysis was also conducted for fracture surfaces in order to detail investigation of the fracture surface and determine the fracture mode accurately.

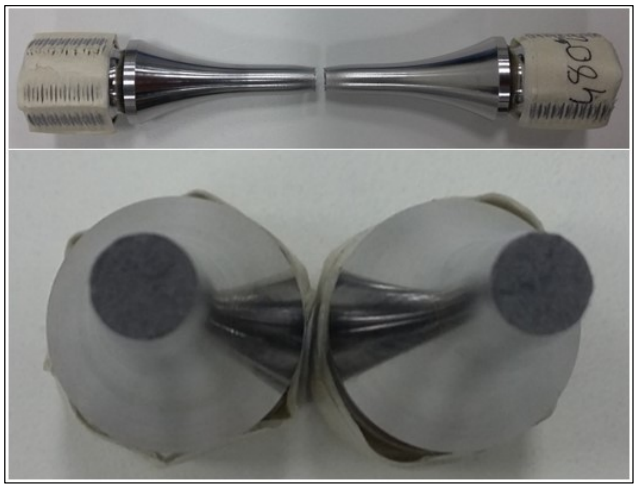

Figure 72 Brittle fracture surface for tensile tested specimen (SP-3)

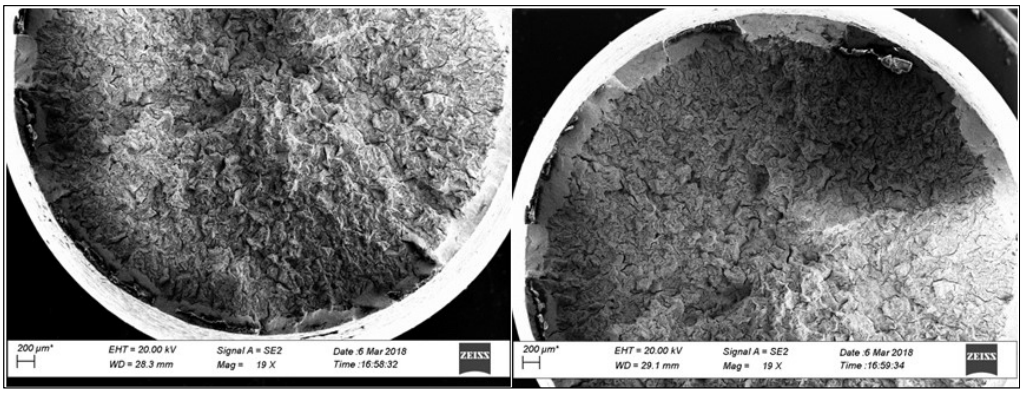

Figure 73 SEM f micrograph showing general view of brittle fracture surface of tensile tested specimen (SP-3)

Closer investigation was conducted for center and edge of the fracture surface to determine fracture mode of the specimen. According to SEM micrograph that is shown in Figure 74, both small dimples and cleavages were observed on the fracture surface. Mixed mode of fracture or quasi-cleavage fracture was observed for the specimen that is exposed to aging treatment at 4800C for 1h.

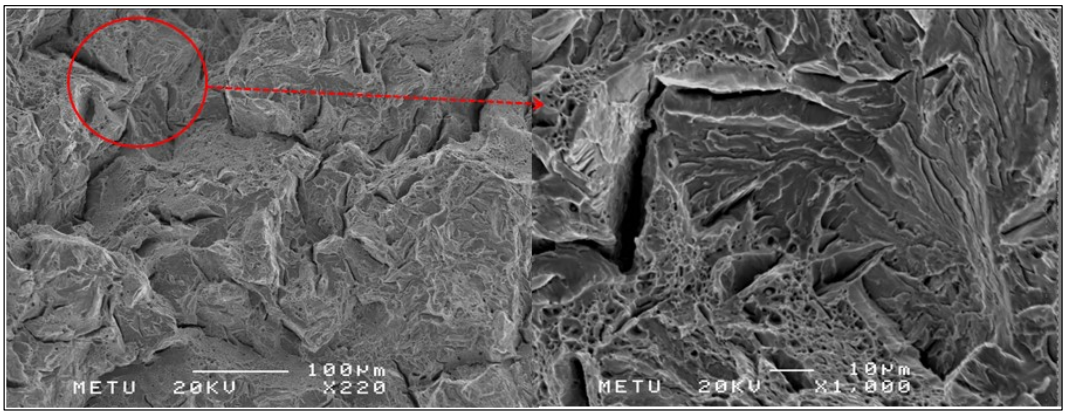

Figure 74 SEM micrograph showing dimple/voids and cleavages/facets view of fracture surface of group-2 tensile test specimen. (SP-3)

4.6.1.3. FRACTURE SURFACE ANALYSIS RESULTS FOR GROUP-3 SPECIMENS

Flat fracture surface was also observed for the specimen which is exposed to aging treatment at 400^0C for 70h. SEM analysis was also conducted for fracture surfaces in order to investigate fracture surface in detail and determine the fracture mode accurately.

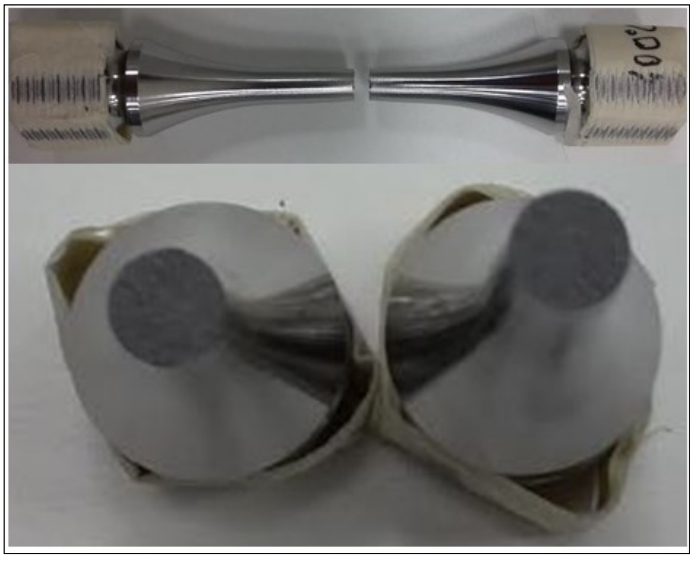

Figure 75 Brittle fracture surface for tensile tested specimen (SP-13)

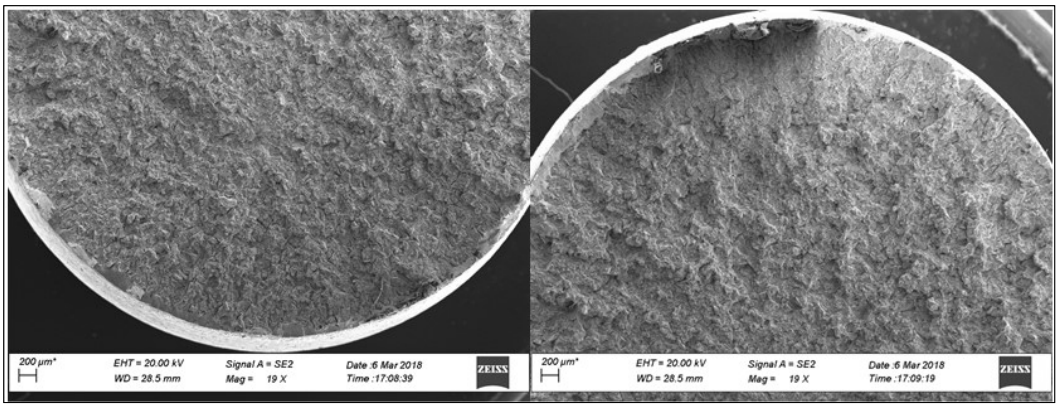

Figure 76 SEM micrograph showing general view of brittle fracture surface of tensile tested specimen. (SP-13)

Closer SEM analysis for fracture surface show that there exist both equiaxed dimples and cleavages were observed on the fracture surface. Indeed, cleavages region are larger compared to dimples area on the fracture surface. However, it can also be said that mixed mode of fracture or quasi-cleavage fracture mode was observed for the specimen that is exposed to aging treatment at 400^0C for 70h.

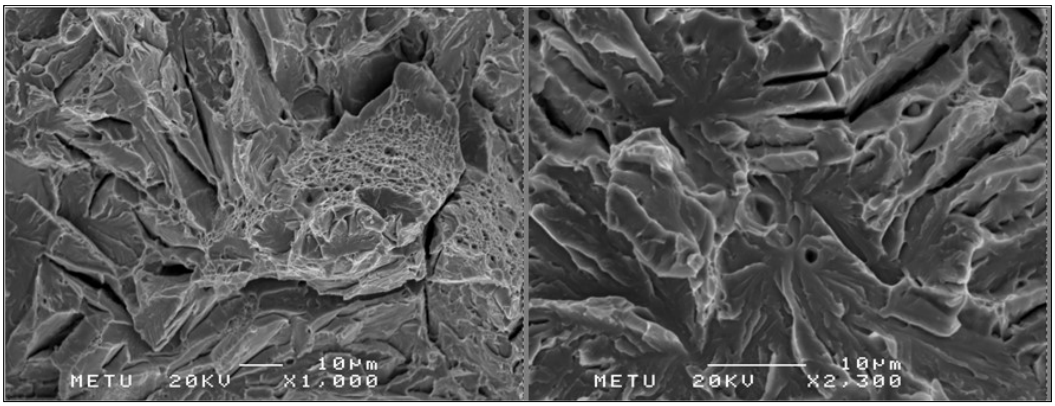

Figure 77 SEM micrograph showing dimple/voids and cleavages/facets (dominant) view of fracture surface of group-3 tensile test specimen. (SP-13)

It is known that fracture mode and surface of the materials depend on degree of plastic deformation before fracture. According to fracture surface of tensile test

results, specimen that was exposed to aging treatment at temperature 550^0C show cup and cone type fracture mode with equiaxed dimples on the surface was observed. Moreover, some intermetallics were also observed inside of the dimples. Size of these intermetallics was around 1μm. Cup and cone type fracture mode is observed as a result of microvoids coalescence that form dimples just before failure. These intermetallics cause formation of cracks due to high stress concentration around themselves which initiate cracks. After reaching critical size, grow in maximum shear stress direction.

On the other hand, specimens which were exposed to aging treatment at temperature 400^0C and 480^0C show mixed mode of fracture or quasi-cleavage fracture mode. Small dimples and cleavages were observed on the fracture surface of these specimens. However, cleavages area is larger for the specimen aged at temperature 400^0C for 1h. This difference between the fracture modes is caused by hardness of the specimens. Increase in hardness causes decrease in ductility of the specimens and amount of plastic deformation before failure. Therefore, fracture mode changes from cup and cone to quasi-cleavage fracture mode.

4.7.1. FRACTURE SURFACE ANALYSIS RESULTS FOR FATIGUE TEST SPECIMENS

Fracture surface analysis for fatigue test specimens was conducted in order to define crack initiation sites. Specimens were selected according to different stress level and different number of cycles before failure. Details of selected specimens are given in table 26.

Table 26 Selected fatigue test specimen for fracture surface analysis.

Specimen Groups	Heat Treatment Parameters	Selected Specimen		
Group-1	Hom. at 1150^0C/1hr + Sol. at 1040^0C/0.5hr + Aged at 550^0C/4hr	SP-1 (Smax= 760Mpa-N=13251)	SP-5 (Smax= 610Mpa-N=120019)	SP-13 (Smax= 460Mpa-N=10000065)
Group-2	Hom. at 1150^0C/1hr + Sol. at 1040^0C/0.5hr + Aged at 480^0C/1hr	SP-1 (Smax= 710Mpa-N=280082)	SP-5 (Smax= 560Mpa-N=10087227)	SP-9 (Smax= 510Mpa-N=4604306)
Group-3	Hom. at 1150^0C/1hr + Sol. at 1040^0C/0.5hr + Aged at 400^0C/70hr	SP-1 (Smax= 860Mpa-N=51206)	SP-4 (Smax= 560Mpa-N=7433969)	SP-7 (Smax= 510Mpa-N=1009078)

4.7.1.1. FRACTURE SURFACE ANALYSIS RESULTS FOR GROUP-1 SPECIMENS

Crack is initiated at the center of the specimen. In order to determine cause of initiation, closer examination was conducted at crack initiation point.

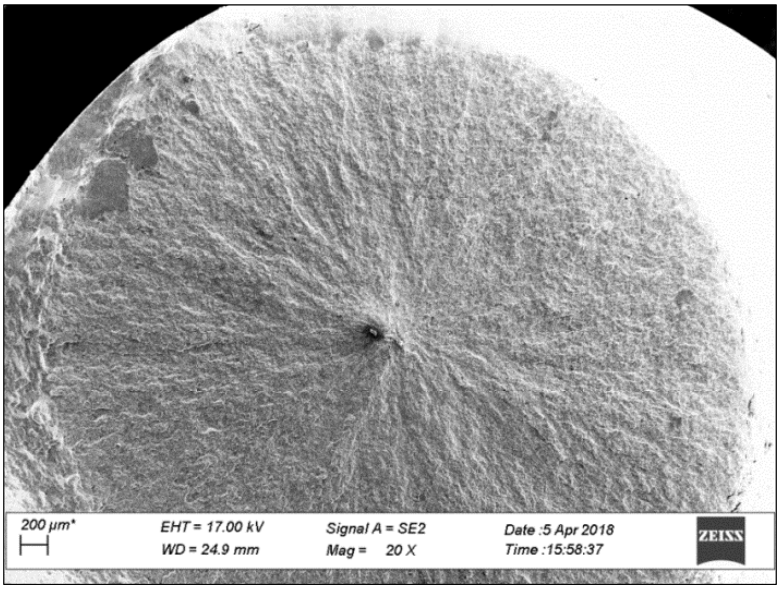

Figure 78 SEM fractograph showing general view of crack initiation site for (SP-1)

It is observed that crack is initiated from an inclusion at the center of the specimen. Size of the inclusion is around 20 to 30 µm.

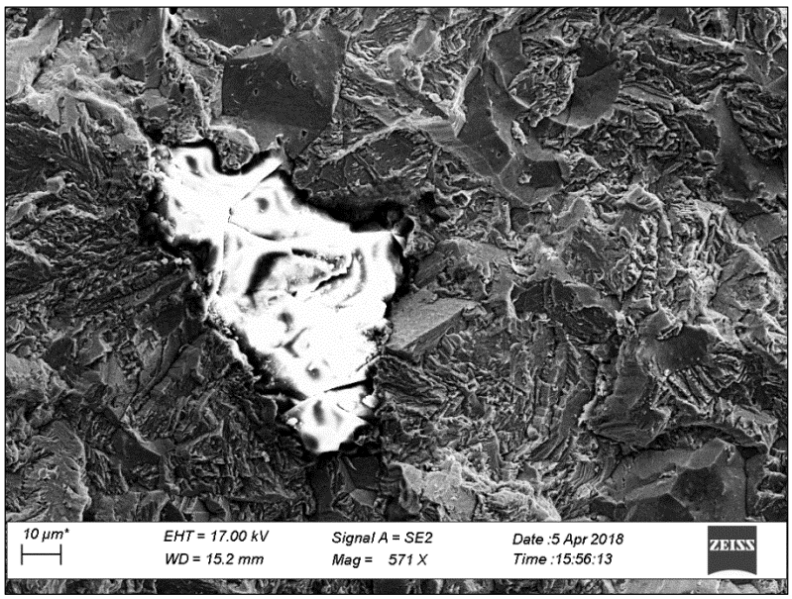

Figure 79 SEM fractograph showing crack initiation point for (SP-1)

SEM micrograph that is shown in Figure 80 show that crack initiation may also be observed at surface of the specimen.

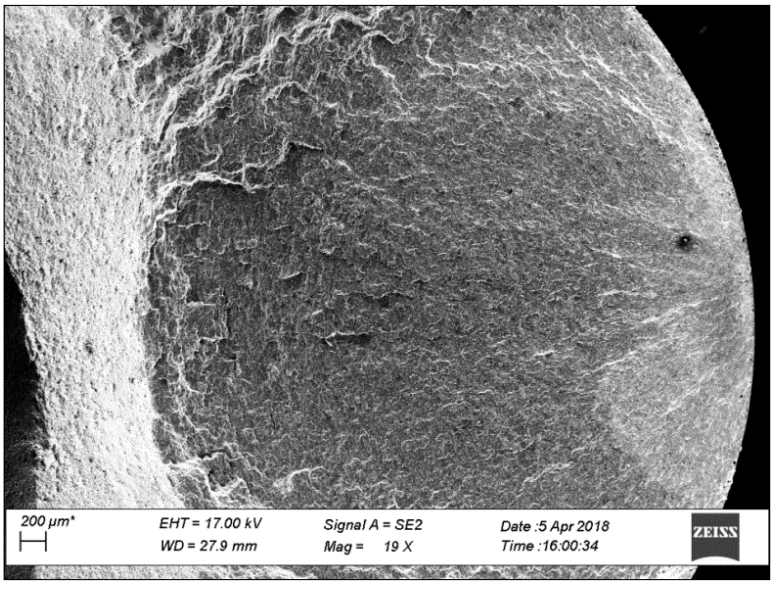

Figure 80 SEM fractograph showing general view of crack initiation site for (SP-5)

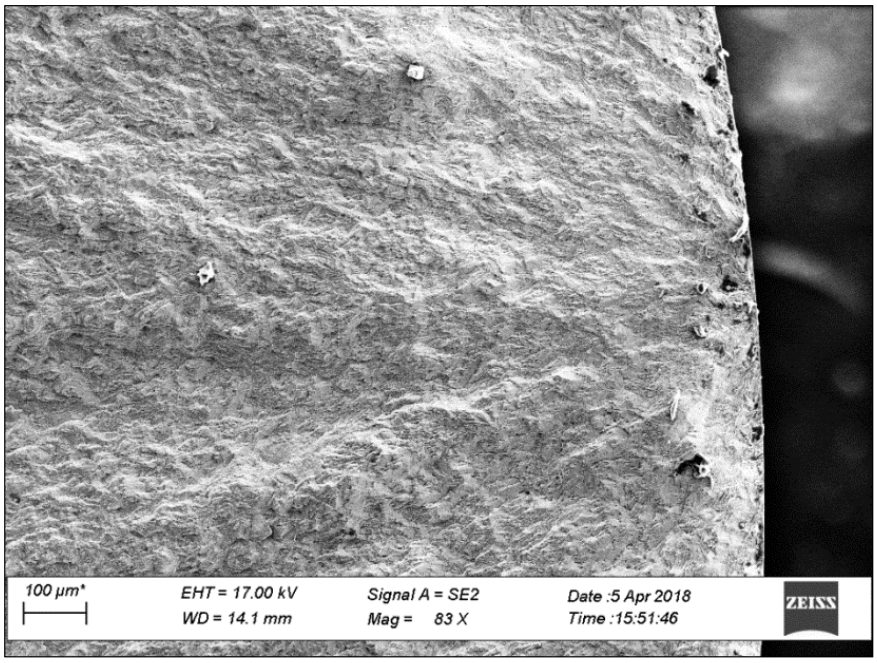

Figure 81 SEM fractograph showing crack initiation point for (SP-5)

Crack is also initiated at the center of the specimen. Closer SEM analyses show that there exists an inclusion with a size of 20 µm leads to crack initiation.

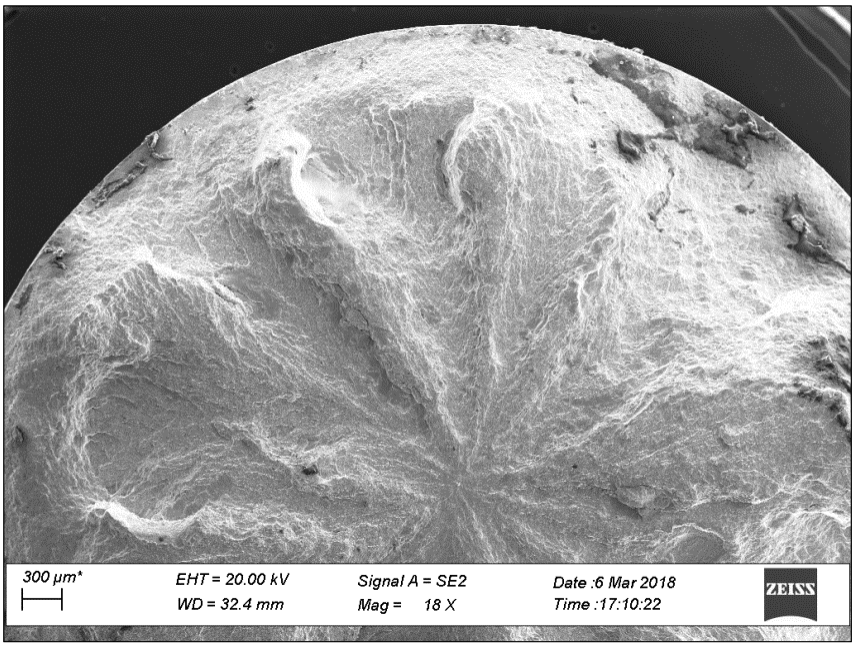

Figure 82 SEM fractograph showing general view of crack initiation site for (SP-13)

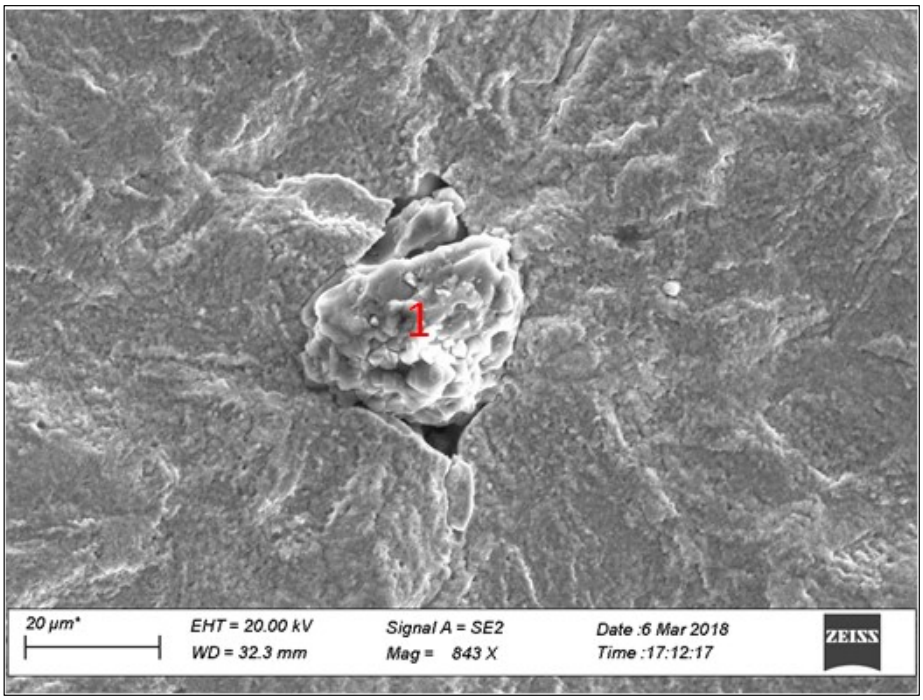

Figure 83 SEM fractograph showing crack initiation point for (SP-13)

In order to determine chemical composition of the inclusion, which cause initiation of cracks, EDX analysis was conducted on the surface of the inclusion that may be seen as point 1 in Figure 83.

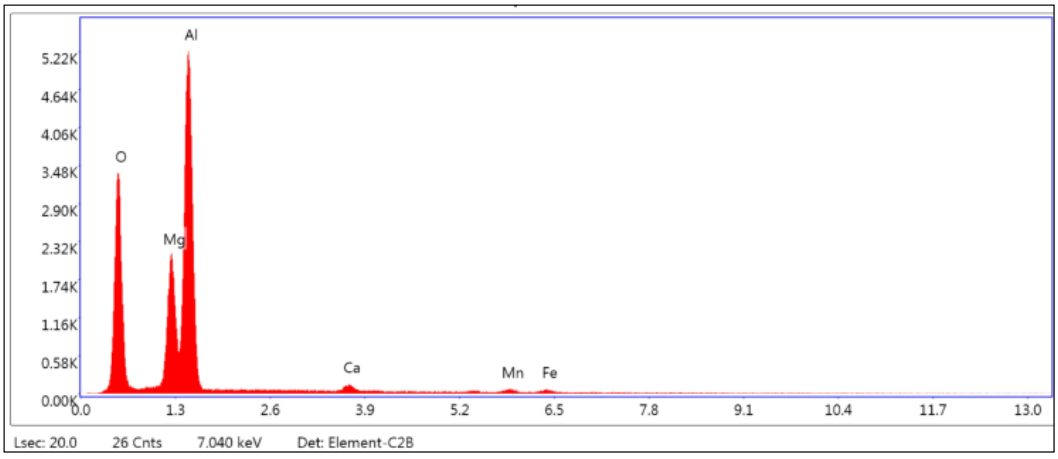

Figure 84 EDX analysis results for point- 1 in Figure 83.

Table 27 Quantitative elemental analysis results for point-1.

Quantity Analysis Results for Point-1		
Element	Weight (%)	Atomic (%)
O K	41.47	54.28
MgK	14.59	12.57
AlK	41.12	31.92
CaK	1.13	0.59
MnK	0.91	0.35
FeK	0.78	0.29

EDX analysis result shows that, inclusion is composed by oxygen. Therefore, it may be said that oxide inclusion with a size of 20 to 30 µm leads to initiation of cracks for 15-5 PH stainless steel under cyclic loading.

In order to determine crack growth direction, direction of striations was also examined. Crack growth direction may be seen in Figure 85.

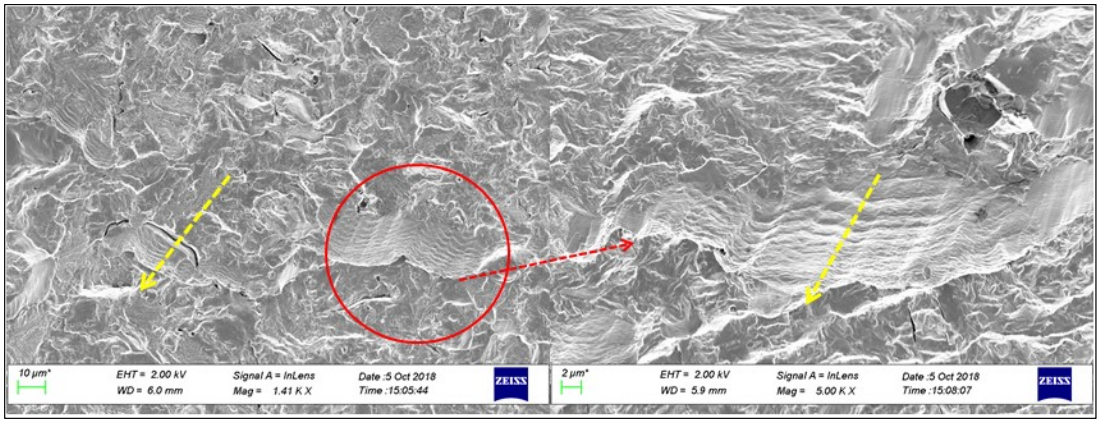

Figure 85 SEM micrograph showing fatigue striations and crack growth direction group-1 cyclic loaded specimen (SP-1)

4.7.1.2. FRACTURE SURFACE ANALYSIS RESULTS FOR GROUP-2 SPECIMENS

Crack initiation sites were also examined for group-2 fatigue test specimens ın order to see the effect of heat treatment crack initiation sites. Crack is initiated at the surface for specimen-1.

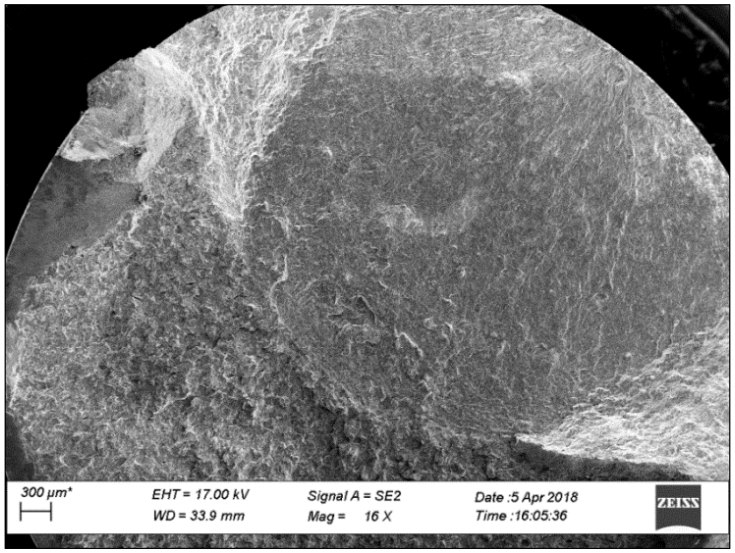

Figure 86 SEM fractograph showing general view of crack initiation site for (SP-1)

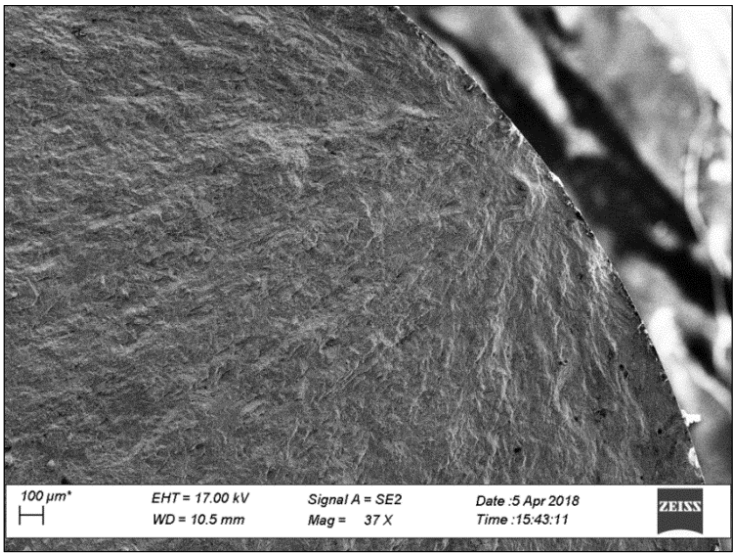

Figure 87 SEM fractograph showing crack initiation point for (SP-1)

On the contrary to SP-1, cracks were initiated at the center for the SP-5 and SP-9. In order to determine cause of initiation, closer examination was conducted at crack initiation point.

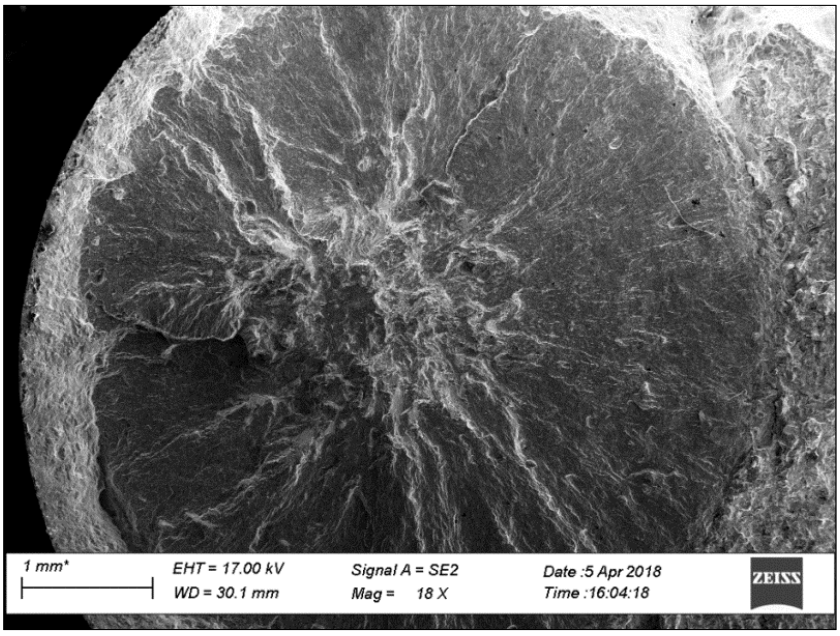

Figure 88 SEM fractograph showing general view of crack initiation site for (SP-5)

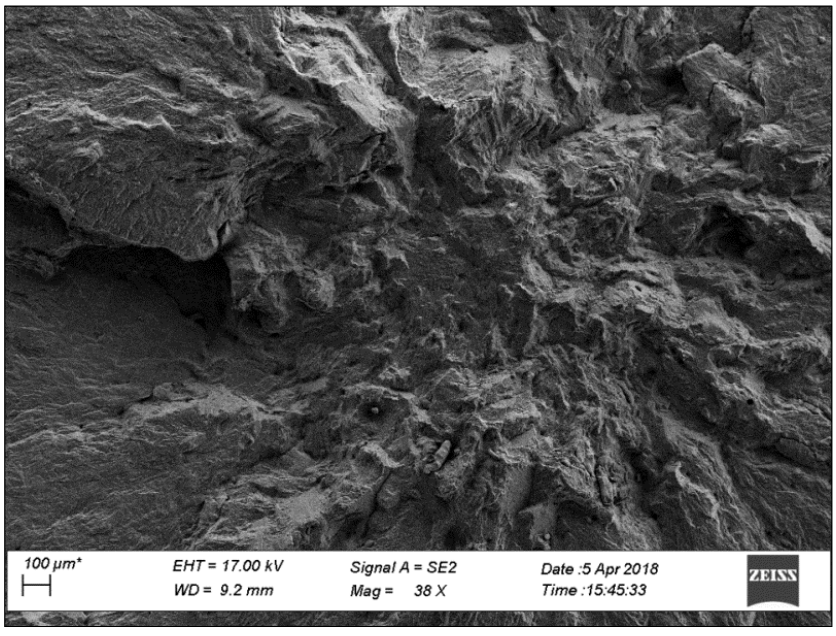

Figure 89 SEM fractograph showing crack initiation point for (SP-5)

Closer SEM micrograph shows that inclusions with 20 to 30 µm cause initiation of the cracks at the center of the specimens.

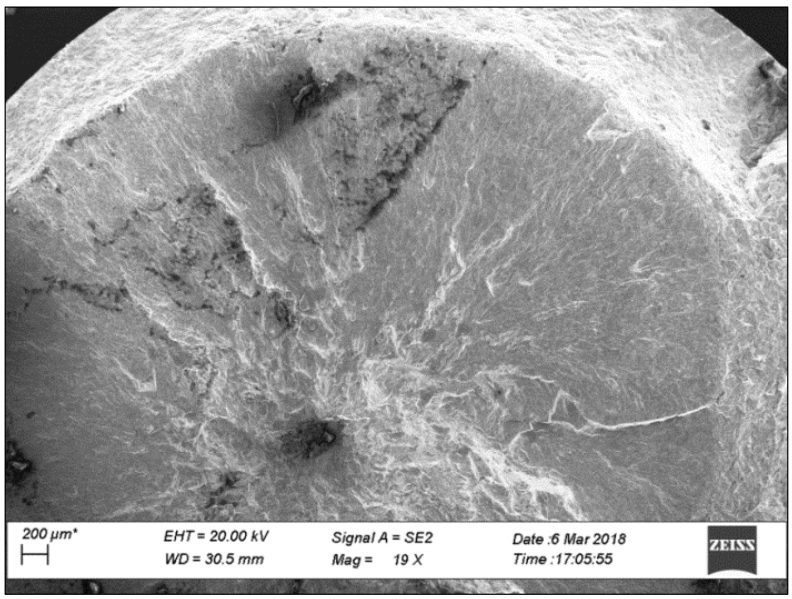

Figure 90 SEM fractograph showing general view of crack initiation site for (SP-9)

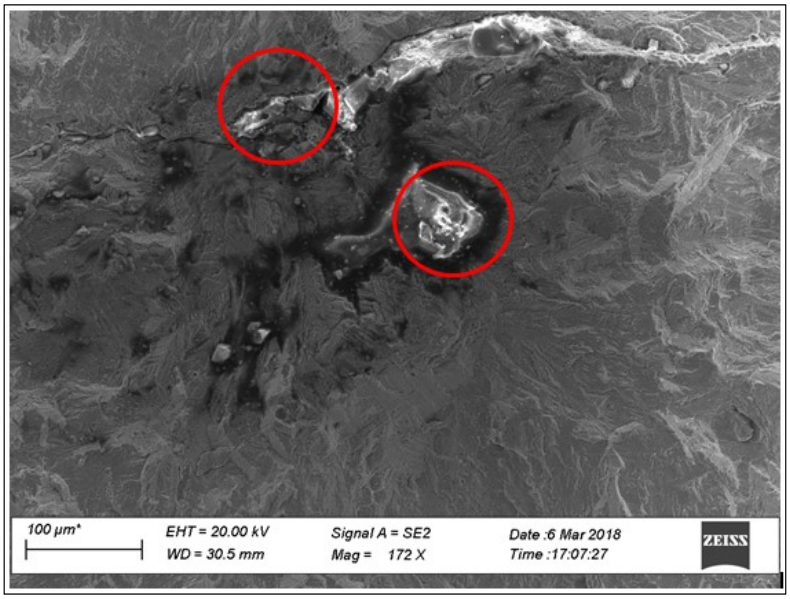

Figure 91 SEM fractograph showing crack initiation in detail for (SP-9).

Direction of fatigue striation was also examined in order to determine crack growth direction. Crack growth direction may be seen in Figure 92.

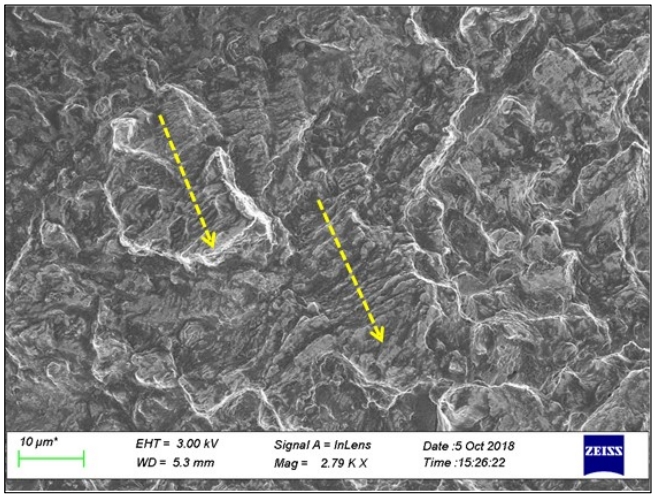

Figure 92 SEM micrograph showing fatigue striations and crack growth direction group-2 cyclic loaded specimen (SP-5)

4.7.1.3. FRACTURE SURFACE ANALYSIS RESULTS FOR GROUP-3 SPECIMENS

Crack initiation sites were also examined group-3 fatigue test specimens ın order to examine the effect heat treatment on it.

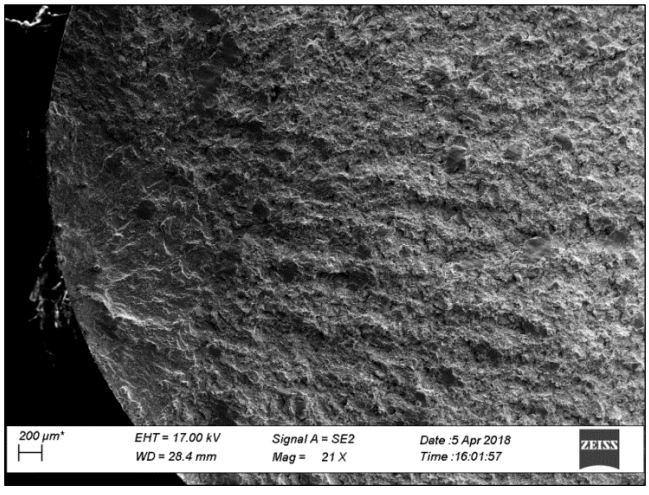

Figure 93 SEM fractograph showing general view of crack initiation site for (SP-1)

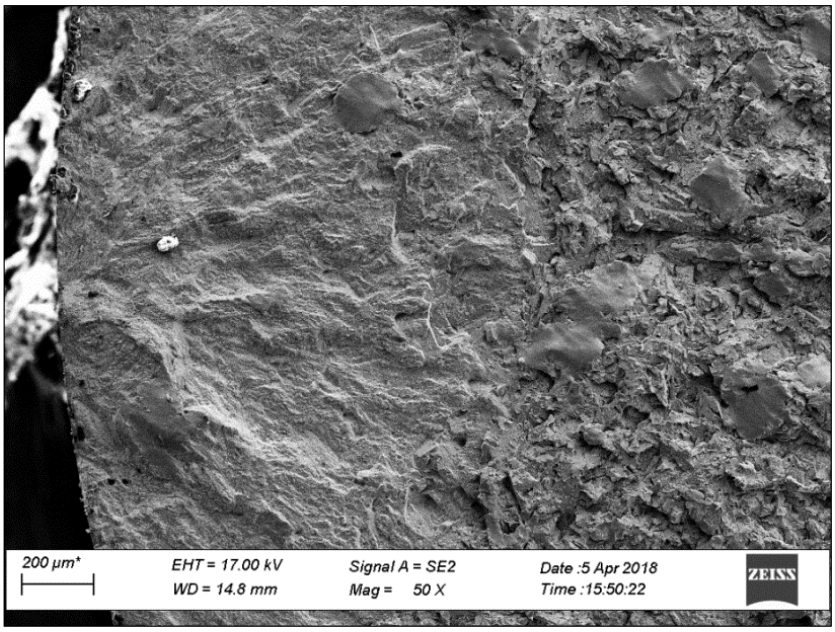

Figure 94 SEM fractograph showing crack initiation point for (SP-1)

Crack was initiated at the surface for the SP-1. However, cracks were initiated for SP-4 and SP-7. In order to find cause of crack initiation closer SEM analysis was conducted.

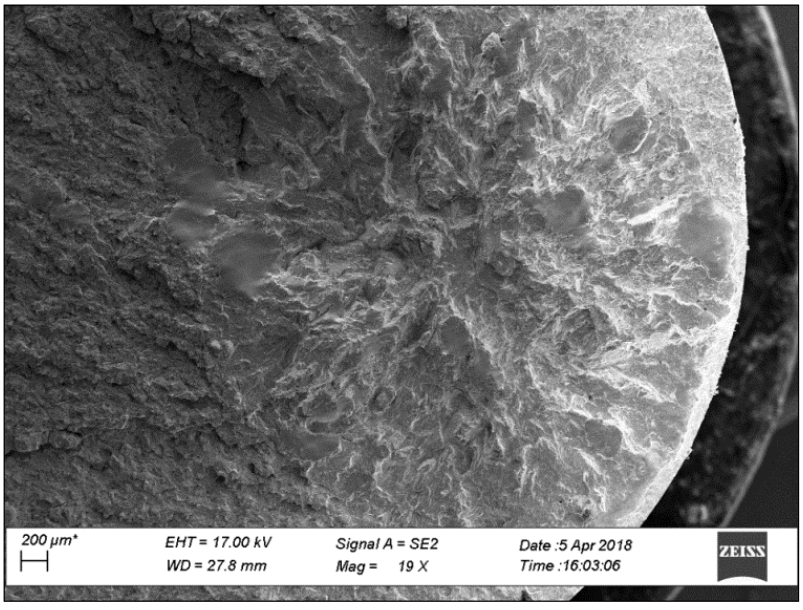

Figure 95 SEM fractograph showing general view of crack initiation site for (SP-4)

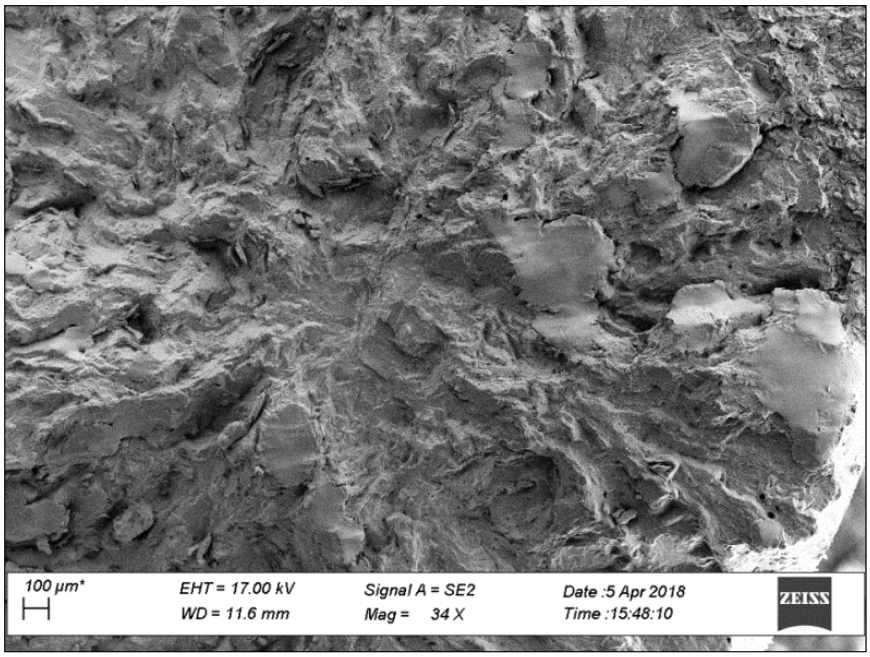

Figure 96 SEM fractograph showing crack initiation point for (SP-4)

SEM analysis show that inclusion with a size of 20-30 µm leads to initiation of cracks at inside of the specimen that may be seen in Figure 98.

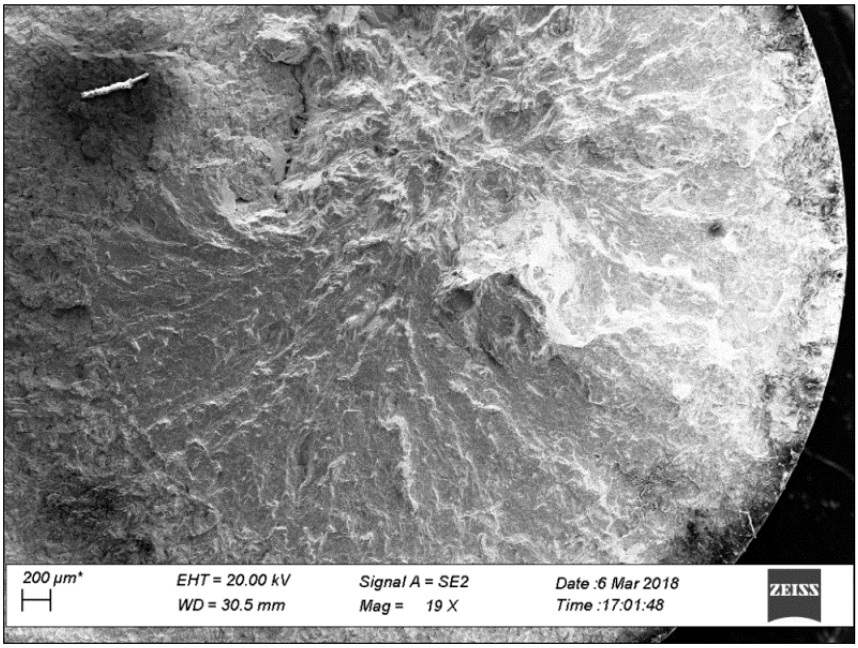

Figure 97 SEM fractograph showing general view of crack initiation site for (SP-7)

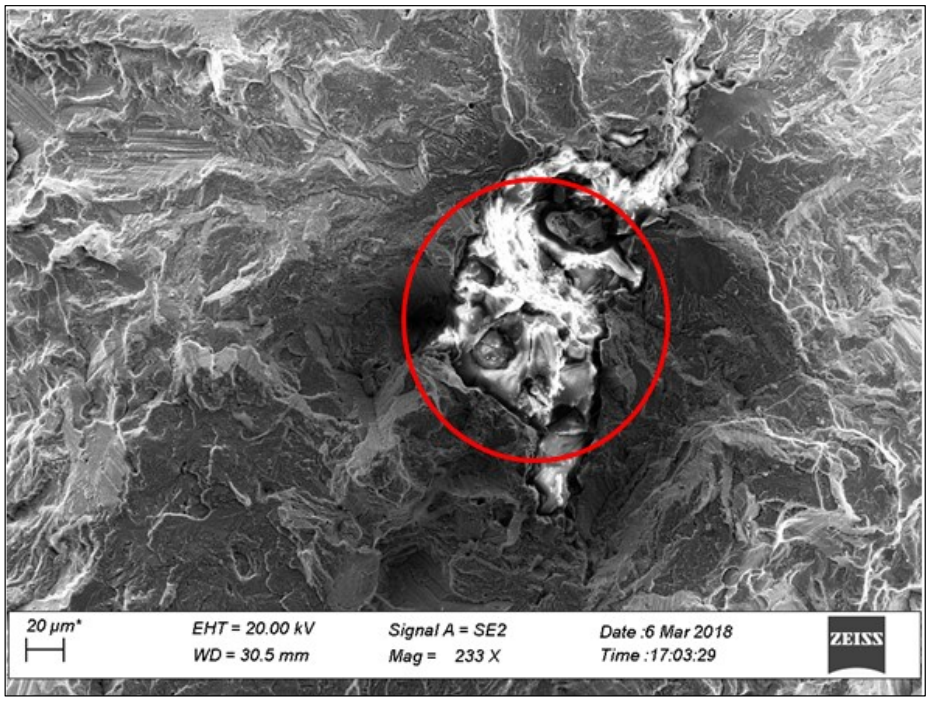

Figure 98 SEM fractograph showing crack initiation point for (SP-7)

EDX analysis was conducted for crack initiation point and show that the inclusion is composed by oxide that is shown in Figure 98.

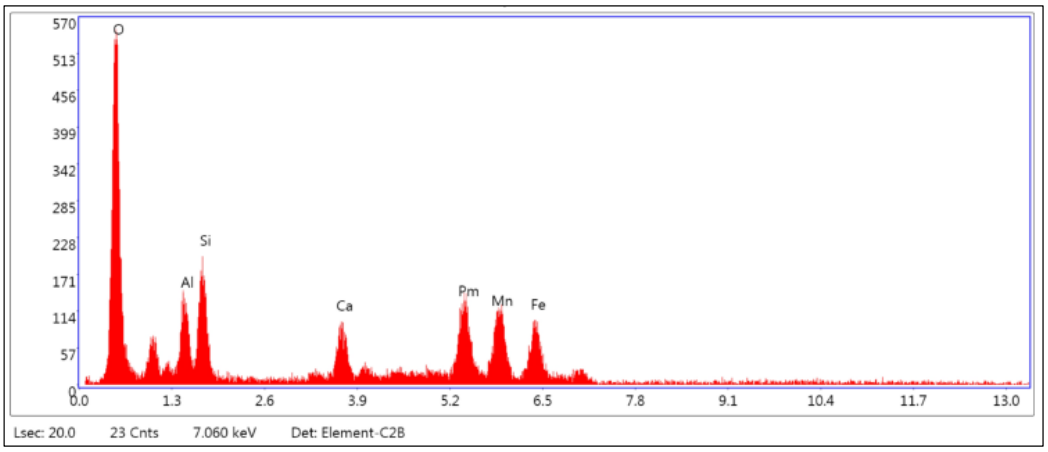

Figure 99 EDX analysis results for crack initiation point of (SP-7)

Table 28 Quantitative elemental analysis results for point-1.

Quantity Analysis Results for Point-1		
Element	Weight (%)	Atomic (%)
O K	33.13	63.94
AlK	7.19	8.23
SiK	8.21	9.03
CaK	4.99	3.84
PmL	31.77	6.77
MnK	7.62	4.28
FeK	7.08	3.91

Fatigue striations and crack growth direction was also examined for specimen-7.

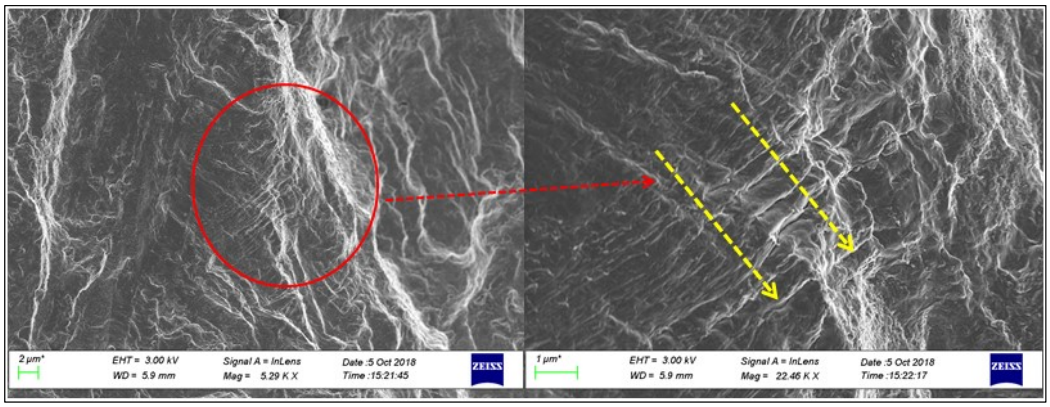

Figure 100 SEM micrograph showing fatigue striations and crack growth direction group-3 cyclic loaded specimen (SP-7)

According to scanning electron microscopy (SEM) analysis results, it is observed that crack initiation sites can be both on surface and inside for 15-5 PH stainless steels specimens after fatigue failure. There is not significant difference on crack initiation sites for different heat treatment parameters of three groups of group-5 specimens. Instead heat treatment parameters, crack initiation sites are mostly affected by applied cyclic stress.

In general, crack initiation sites were observed in the inside of the specimens which were exposed maximum stress below 560 MPa. Stress level higher than 600 MPa

causes observation of crack initiation at the surface of the specimens. Therefore, it can be said that surface defects that cause crack initiation are more sensitive at high stress level compared to interior defects.

In addition, cracks were initiated by an inclusion with a size of 20 to 30 in the inside of the specimens. In order to determine chemical composition of these inclusions, EDX analysis was performed. EDX analysis showed that these defects are composed by oxide particles according to chemical compositions. EDX analysis show that these inclusions are mostly in the form of oxide inclusions. EDX analysis was also done for matrix phase on the fracture surface for fatigue tested specimens. Results showed very similar chemical composition for 15-5 PH stainless steels that was found by XRF gun.

In order to reach general comments for crack initiation sites, fracture surface of all failed specimens were examined optically in order to see effect of heat treatment parameters and fatigue stress level on the crack initiation sites.

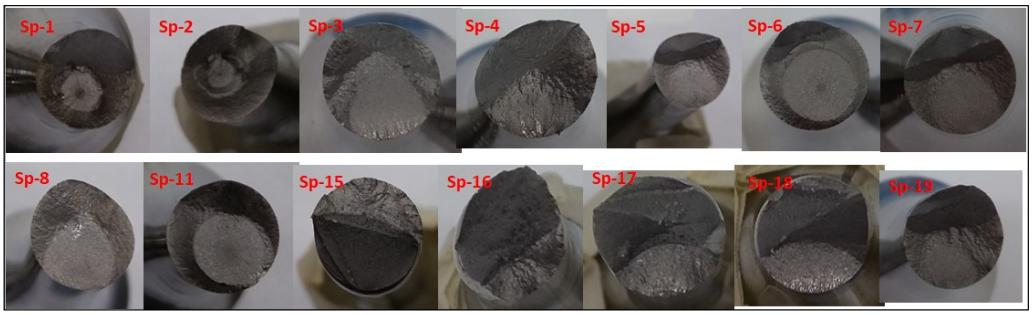

Figure 101 Optical image for fracture surface of group -1 failed specimens.

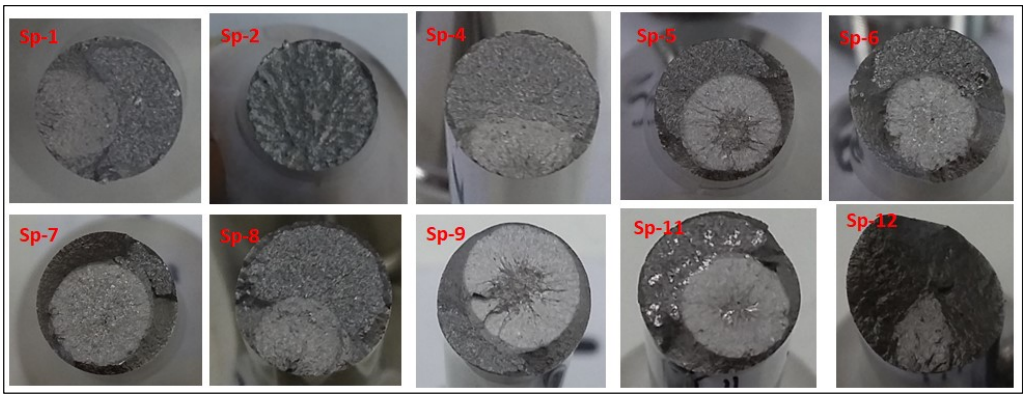

Figure 102 Optical image for fracture surface of group -2 failed specimens.

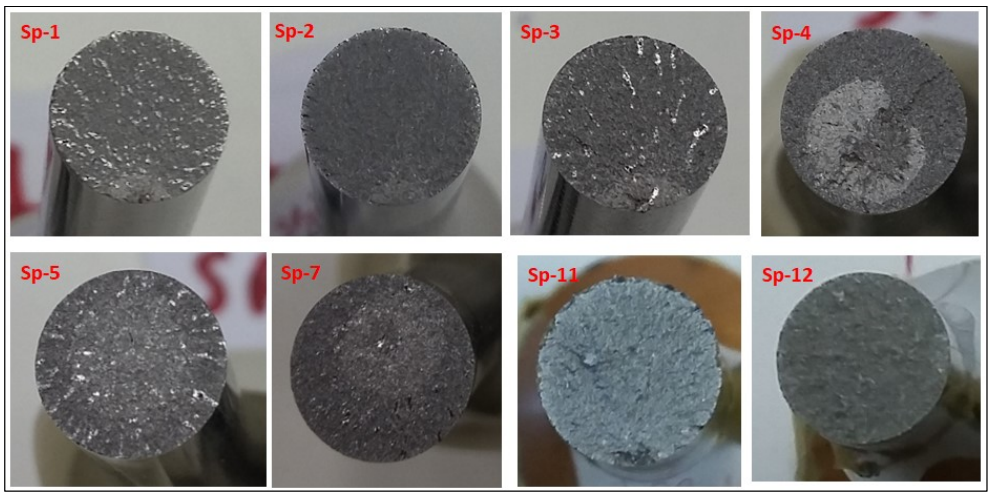

Figure 103 Optical image for fracture surface of group -3 failed specimens

According to fracture surface of all failed specimens, cracks were initiated both at surface and inside for all three groups of specimens under cyclic loading. For inside cracks there exists an optically dark area which is also mentioned at chapter 2. For ınside cracks, failure mode is usually in the form of fish- eye crack initiation type which may be seen in Figure 104.

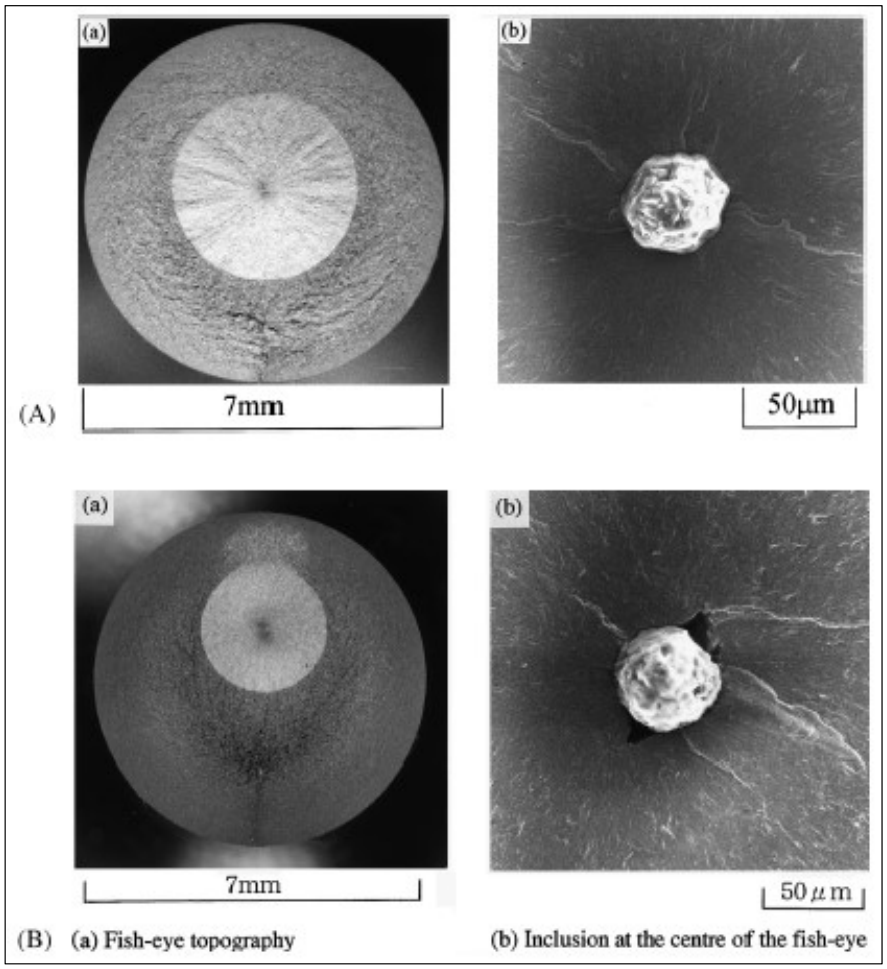

Figure 104 The inclusion at the center of the fish eye. [29]

Observation of this optically dark rough area may be caused by some environmental factor like penetration of hydrogen or oxygen during fatigue testing.

CHAPTER 5

CONCLUSION

The aim of this study is to investigate effect of the heat treatment parameters on the microstructure and mechanical properties especially hardness and fatigue strength of the AMS5659 15-5 precipitation hardenable stainless steel. In order to achieve this, heat treatment processes were applied by three different steps which were homogenization, solutionizing and aging treatment. Heat treatments were applied at different temperature and time periods. After completing the heat treatment, microstructure of the specimens was analyzed in terms of grain size. Then, hardness test was performed for all heat treated disc shaped specimens in HRC scale in order to see the effect of heat treatment parameters on hardness of the 15-5 PH stainless steels. Then, tensile and fatigue tests were conducted for selected heat treated group. Fatigue tests were conducted by servo-hydraulic and resonant fatigue testing machines at different frequency for low and high cycle region. Fatigue test results were used to construct S-N curve for three different specimen groups of group-5 specimens that were exposed to different heat treatment condition. After completing static and fatigue tests, fracture surface analysis was applied by scanning electron microscopy (SEM) and Energy Dispersive X-Ray analysis (EDX) in order to determine fracture mode for tensile test specimen and to see crack initiation sites for fatigue test specimens. Following conclusions can be drawn from this particular study:

1. Fatigue limit of the 15-5 PH stainless steel has been increased 15% (15 percent) by changing heat treatment parameter from 550^0C for 4h to 480^0C for 1h. In addition, aging treatment at 400^0C for 70h provides 11% (11 percent) increase on fatigue limit compared to aging condition at 550^0C for 4h. Increase in fatigue limit may be explained by increase in strength of material.
2. Both surface and inside cracks were observed for fatigue test specimens. Moreover, ınside cracks may be initiated from an oxide inclusion with a size of 20-30 μm for 15-5 PH stainless steel under cyclic loading.
3. Changing aging treatment from 550^0C for 4h to 480^0C for 1h, hardness of 15-5 PH stainless steel was increased by 18% (18 percent). In addition, if aging treatment parameters are changed to 400^0C for 70h, hardness has been increased by 23% (23 percent). Increase in hardness is provided by precipitation reaction during aging treatment.
4. Tensile strength of 15-5 PH stainless steel was increased 20% (20 percent) by changing heat treatment parameter from 550^0C for 4h to 480^0C for 1h. Indeed; it is also increased 27% (27 percent) by application of aging treatment at 400^0C for 70h.

REFERENCES

[1] Slunder, C. J., Hoenie, A. F., & Hall, A. M. (January 1967). Thermal and Mechanical Treatment for Precipitation- Hardening Stainless Steels. 1-192. Retrieved March 25, 2018, from http://adsbit.harvard.edu//full/1967NASSP5089

[2] History Hour: Aloha Airlines Flight 243 incident. (2017, April 28). Retrieved April 07, 2018, from https://www.aerotime.aero/en/did-you-know/18542-history-hour-aloha-airlines-flight-243-incident

[3] Herny, E. (2009). Mechanical characterization and investigation of thermal and thermomechanical aging mechanisms of martensitic stainless steel 15-5PH. International Heat Treatment and Surface Engineering,3(1-2), 65-69. doi:10.1179/174951509x466957

[4] KUMAR, A., & PRASAD, E. (2013). Indian Academy of Sciences. Indigenous development and airworthiness certification of 15–5 PH precipitation hardenable stainless steel for aircraft applications,38, 3-23. Retrieved Oct. & nov., 2016.

[5] Fakić, B., & Cubela, D. (2013). Review of The development oF Research in the Design of Semi Austenitic Stainless Steel 17-7PH. Journal of Trends in the Development of Machinery and Associated Technology,17(1), 57-60. Retrieved March 16, 2018.

[6] Research may precipitate hard results. (2006). Metal Powder Report, 61(7), 24-31. doi:10.1016/s0026-0657(06)70691-9. Retrieved March 6, 2018.

[7] Rep. No. MIL-H-6875H at 1-29 (1989). Military Specification Heat Treatment of Steel.

[8] 15- 5 PH Stainless Steel Product Data Sheet. (n.d.). Retrieved October 4, 2016, from https://www.spacematdb.com/spacemat/manudatasheets/15-5_PH_Data_Sheet.pdf.

[9] Bhambroo, R., Roychowdhury, S., & Kain, V. (2013). Effect of reverted austenite on mechanical properties of precipitation hardenable 17-4 stainles ssteel. Materials Science& Engineering A,568, 127-133. Retrieved May 6, 2017.

[10] Couturier, L., Geuser, F. D., Descoins, M., & Deschamps, A. (2016). Evolution of the microstructure of a 15-5PH martensitic stainless steel during precipitation hardening heat treatment. Materials & Design,107, 416-425. doi:10.1016/j.matdes.2016.06.068

[11] PENG, X. Y., ZHOU, X. L., & HUA, X. Z. (2015). Journal of Iron and Steel Research, International. Ffect of Aging on Hardening Behavior of 15-5 PH Stainless Steel,22(7), 607-614. Retrieved May 5, 2017.

[12] Devi, R. S., & Nath, J. S. (2013). Effect of Precipitation Hardening on Microstructural Characteristics of 15-5 Ph Steel. International Journal of Engineering Research and Development,9(1), 22-26. Retrieved March 14, 2017, from http://www.ijerd.com/paper/vol9-issue1/F09012226.pdf

[13] (Yooa, W. D., & Leeb, J. H. (2006). Solid State Phenomena. Study on the Microstructure and Mechanical Properties of 17-4 PH Stainless Steel depending on Heat Treatment and Aging Time,118, 15-20. Retrieved December 3, 2016.)

[14] (Mirzadeh, H., & Najafizadeh, A. (2009). Materials Chemistry and Physics. Aging kinetics of 17-4 PH stainless steel, 116, 119-124. Retrieved November 2, 2016.)

[15] (Hsiaoa, C. N. (2002). Materials Chemistry and Physics. Aging reactions in a 17-4 PH stainless steel, 74, 134-142. Retrieved November 2, 2016.)

[16] United States. Federal Aviation Administration. (2005). Metallic Materials Properties Development and Standardization (MMPDS): CHAPTER 2 - STEEL

ALLOYS. Retrieved October 20, 2017, from https://www.sae.org/publications/books/content/b-983/.

[17] Callister, W. D. (2007). Materials science and engineering: An introduction (7th ed.).NewYork: John Wiley & Sons. https://abmpk.files.wordpress.com/2014/02/book_maretial-science-callister.pdf

[18] Fathemi, A. (2014, June 2). Training and Seminars. Retrieved from https://www.efatigue.com/training/Chapter_4.pdf

[19] Schijve, J. (2009). Fatigue of structures and materials(2nd ed.). Berlin: Springer.

[20] Farahani, A. V. (2005). Advances in fatigue, fracture and damage assessment of materials(Vol. 1). Billerica, MA: WIT Press. doi:10.2495/1-85312-836-8/02

[21] Stress-life Diagram (s-n Diagram). (n.d.). Retrieved May 30, 2018, from https://www.semanticscholar.org/paper/Stress-life-Diagram-(s-n-Diagram)/ =abstract

[22] BOEING. (1968). Fatigue Properties of 17-4 PH and 15-5 PH Steel in the H-900 and H-1050 Condition. Retrieved April 20, 2017, from http://www.dtic.mil/dtic/tr/fulltext/u2/691794.pdf

[23] Pook, L. (2009). Metal fatigue: What it is, why it matters(Vol. 145, Ser. 1525). Dordrecht: Springer.

[24] Liard, F. (1983). Helicopter fatique design guide. Neuilly-sur-Seine: AGARD.

[25] ISO 12107: Metallic materials - fatigue testing - Statistical planning and analysis of data. (2003). Ginebra: ISO.

[26] Palanisamy, D., Senthil, P., & Senthilkumar, V. (2016). The effect of aging on machinability of 15Cr–5Ni precipitation hardened stainless steel. Archives of Civil and Mechanical Engineering,16(1), 53-63. doi:10.1016/j.acme.2015.09.004

[27] Schönbauer, B. M., Yanase, K., & Endo, M. (2017). The influence of various types of small defects on the fatigue limit of precipitation-hardened 17-4PH stainless

steel. Theoretical and Applied Fracture Mechanics,87, 35-49. doi:10.1016/j.tafmec.2016.10.003

[28] Schönbauer, B. M., Yanase, K., & Endo, M. (2016). VHCF properties and fatigue limit prediction of precipitation hardened 17-4PH stainless steel. International Journal of Fatigue,88, 205-216. doi:10.1016/j.ijfatigue.2016.03.034

[29] Murakami, Y. (2002). Effects of Nonmetallic Inclusions on Fatigue Strength. Metal Fatigue,75-127. doi:10.1016/b978-008044064-4/50006-2

[30] ASTM E466 – 15. Standard Practice for Conducting Force Controlled Constant Amplitude Axial Fatigue Tests of Metallic Materials. Retrieved October 14, 2017.

[31] ASTM E407 − 07 (Reapproved 2015) Standard Practice for Microetching Metals and Alloys. Retrieved July 2, 2017.

[32] ASTM E112 – 13. Standard Test Methods for Determining Average Grain Size. Retrieved June 25, 2017.

[33] HR-521 (L) /523 (L) Series 810-Rockwell Type Hardness Testing Machines. (n.d.). Retrieved July 11, 2018, from https://ecatalog.mitutoyo.com/HR-521-L-523-L-Series-810-Rockwell-Type-Hardness-Testing-Machines-C1334.aspx

[34] ASTM E18 – (16).Standard Test Methods for Rockwell Hardness of Metallic Materials. Retrieved October 25, 2017.

[35] GmbH, M. (n.d.). MarSurf PS 10 - Mobile roughness measuring instrument - Mahr Metrology. Retrieved July 11, 2018.

[36] 5980 Serisi Çift Kolonlu Zemin Tipi Test Sistemleri (Yüksek Kapasite). (n.d.). Retrieved July 11, 2018, from http://www.instron.com.tr/tr-tr/products/testing-systems/universal-testing-systems/electromechanical/5900/5980-floor-model

[37] (2018, July 11). Retrieved from http://www.rumul.ch/220_products.php

[38] Dericioğlu, F. A. (2018, October 17). Metallography Lecture Notes. Lecture presented at Quantitative Metallography.

[39] Inc. (n.d.). EFunda: Convert Hardness: Tensile Strength (Approx.). Retrieved July 12, 2018.

[40] Finite Element Model Stress-Life Technical Background. (n.d.). Retrieved from https://www.efatigue.com/fem/background/stresslife.html